Ionic Liquid Assisted Composite Ceramic-Polymer Electrolyte for Lithium Metal Batteries

by

Jiahua Ou

A thesis

presented to the University of Waterloo

in fulfilment of the

thesis requirement for the degree of

Master of Applied Science

in

Chemical Engineering

Waterloo, Ontario, Canada, 2020

Author's Declaration

I hereby declare that I am the sole author of this thesis. This is a true copy of the thesis, including any required final revisions, as accepted by my examiners.

I understand that my thesis may be made electronically available to the public.

Abstract

Facing demands for smaller and more powerful batteries to keep pace with technological advances, as the conventional lithium-ion battery (LIB) is reaching its inherent physicochemical limit, new electrode materials must be researched. One attractive anode material is lithium metal which has a specific energy density 11 times higher than conventional graphite anode. However, lithium metal is incompatible with conventional liquid electrolyte and leads to severe impact on cycle life and safety issues.

For lithium metal to be feasible as anode material in a secondary LIB, the electrolyte required must be thermodynamically stable against lithium metal, or can decompose and form a thin solid-electrolyte interface layer on the surface of the lithium to prevent further parasitic reactions. The electrolyte chosen must also be able to prevent or suppress the growth of lithium dendrite to avoid penetration, leading to short circuit and severe safety issues.

This thesis presents a composite ceramic-polymer electrolyte (CPE) based on solid polymer electrolyte polyethylene (PEO) containing lithium salt lithium bis(trifluoromethanesulfonyl)imide (LiTFSI). Ceramic electrolyte $Li_{1.5}Al_{0.5}Ge_{1.5}P_3O_{12}$ (LAGP) is mixed and dispersed inside the polymer to study and provide additional pathways for lithium ion conduction, which raises both ionic conductivity as well as Li^+ transference number (t_{Li+}) due to LAGP being a single-ion conductor. LAGP to PEO ratio was studied and optimized through the "bricklayer" model for ion conduction pathways. Addition of LAGP at a weight ratio of 1:1 relative to PEO (1 LAGP) allows for bulk ionic conductivity at 35°C to increase from 3.61×10^{-6} S cm^{-1} to 2.49×10^{-5} S cm^{-1}. To further improve Ionic liquid 1-ethyl-3-methylimidazolium bis(trifluoromethanesulfonyl)-imide (EMITFSI) is then added to modify the PEO further through plasticization which decreases both glass transition temperature (T_g) and melting temperature (T_m). This raises the ionic conductivity further to 6.20×10^{-5} S cm^{-1} at 35°C and 6.1×10^{-4} S cm^{-1} at 50°C. This also results in t_{Li+} = 0.72 at 50°C, which is an improvement upon PEO-LiTFSI solid polymer electrolyte of t_{Li+} = 0.46, making it more efficient. The final optimized composite electrolyte was able to initially deliver 139

mAh g^{-1} in discharge capacity and 115 mAh g^{-1} after 125 cycles at a charging rate of 0.3 C, with good rate capability of 112 mAh g^{-1} at 1C while under 50°C environment, which is reduced by 10 to 20°C compared to similar literature, providing a pathway towards a practical polymer based solid state battery with a scalable production method.

Acknowledgement

I would like to thank my supervisor Dr. Zhongwei Chen for this opportunity to work in such a diverse research group and his overall support in this new project. I also must acknowledge Dr. Eric Croiset for his support, insight, and help especially in the beginning of this project.

The technical and emotional support from my fellow graduate students and researchers have been essential during my master study. I would like to thank Dr. Wook Ahn for helping me with starting a new project in the group. I appreciate all the seemingly idle chat with other researchers which have taught and inspired me in my work. Thanks to Dr. Gaoran Li for helping me with the publishing of my first paper.

My family and friends, who have supported me financially and emotionally, have been crucial to where and who I am today. Thank you.

Finally, I would like to thank University of Waterloo, where I have had completed my undergraduate degree. Despite the ups and downs, I am grateful for my almost 9 years of experience and learning here.

TABLE OF CONTENTS

List of Figures

List of Abbreviations

CPE	Ceramic-polymer electrolyte
DEC	Diethyl carbonate
DMC	Dimethyl carbonate
EC	Ethylene carbonate
EMITFSI	1-ethyl-3-methylimidazolium bis(trifluoromethanesul-fonyl)imide
LAGP	$Li_{1.5}Al_{0.5}Ge_{1.5}P_3O_{12}$
LFP	$LiFePO_4$ Lithium iron phosphate
LIB	Lithium ion battery
LiTFSI	Lithium bis(trifluoromethanesulfonyl)imide
PC	Propylene carbonate
PEO	Polyethylene oxide
PL	PEO-LAGP
PLE	PEO-LAGP-EMITFSI
SEI	Solid-Electrolyte interface
SPE	Solid Polymer Electrolyte

Chapter 1 Introduction

1.1 Motivation

In our current information age, electronics is an integral part of our society. Despite the advances and market demand for mobile devices and vehicles, energy storage in terms of battery has not fundamentally improved or changed in the past two decades. Conventional lithium ion battery (LIB) as shown in Figure 1.1 generally consists of insertion type electrodes, a porous separator and liquid electrolytes. During charging, lithium ions at the cathode is reduced due to electrochemical potential difference and detach from the cathode, imparting one electron per atom. The lithium ion then transfers past the separator through the electrolyte and oxidizes in the anode active material. The process is then reversed upon discharging. However, LIB with an intercalation type cathode, liquid electrolyte, and graphite anode is reaching its inherent physicochemical limit in terms of capacity and power density.

New battery systems such as lithium-sulfur and lithium-air have shown to be able to drastically improve battery capacity density, where lithium metal anode has up to 11 times the gravimetric density compared to graphite. However, the conventional $LiPF_6$ salt in ethylene carbonate (EC) and dimethyl carbonate (DMC) liquid electrolyte proves detrimental to the lithium metal electrode as well as posing a serious safety concern in cases of leakage and combustion of the battery. As conventional liquid electrolyte is highly unstable under high voltage, it also limits the full use of high voltage electrodes and impedes the improvement of battery power density.

To solve the bottleneck in battery advancement, a new electrolyte which is safe, can withstand high voltage, and is stable against reactive electrodes such as lithium metal need to be developed. This is not only an advancement in terms of energy storage, but can open the gate towards new engineering fronts such as miniaturization for medical implants, flexible batteries to shatter how we think of product design, and even enabling more efficient space exploration.

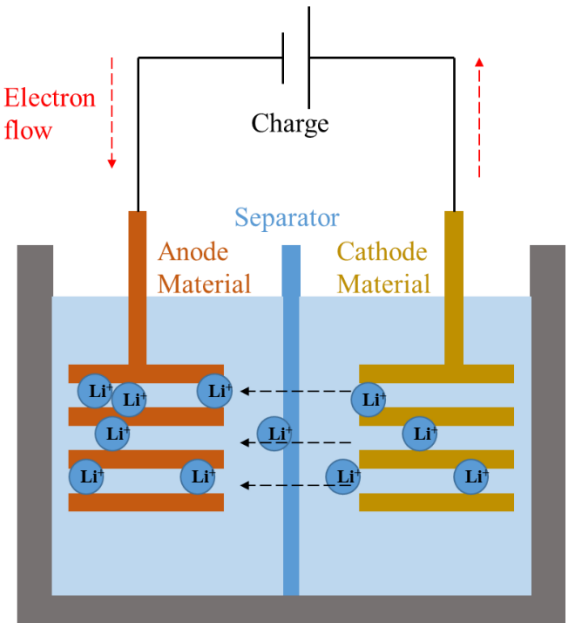

Figure 1.1 Schematic of typical intercalation type LIB during charge

1.2 Objective

Despite research on solid polymer-ceramic composite electrolytes, most focused on either having solid polymer electrolyte with low amounts of nanofillers (< 20 wt%) to improve conductivity and stability, or utilizing very high powder-ceramic electrolyte content (> 98wt%), with the least amount of polymer to act as a binder.

The first approach is limited by the low inherent ionic conductivity of solid polymer electrolytes. Nanofillers such as TiO_2, Al_2O_3 and SiO_2 have shown to be able to suppress the crystallization of polyethylene oxide (PEO) and increase ionic conductivity. However, there is a limit at around 5-20% before the nanofillers begin to congregate and raise the internal resistance of the electrolyte.

Due to the high ionic conductivity of ceramic electrolytes, the second approach of increasing the loading of ceramic electrolytes to above 98% allows for the ionic conductivity to approach sintered ceramic electrolytes. However, even at 99% $Li_{1.5}Al_{0.5}Ge_{1.5}P_3O_{12}$ (LAGP) with 1% PEO, the bulk conductivity is

reported to be roughly 14 lower than a sintered LAGP pellet[1]. This is due to the high grain boundary resistance between ceramic particles which can not be avoided unless high temperature sintering is conducted, so the return on ionic conductivity begins diminishing at extremely high LAGP loading. Furthermore, due to the high ceramic content, the electrolyte can not maintain a good contact with the electrodes without an additional PEO coating at the electrolyte-electrode surfaces.

In this thesis, an intermediate loading of LAGP in PEO will be studied. An intermediate loading of LAGP can raise the ionic conductivity as well as provide mechanical strength to the composite electrolyte. Furthermore, with an intermediate loading, there is an opportunity to improve the PEO phase. Small amounts of ionic liquid 1-ethyl-3-methylimidazolium bis(trifluoromethanesul-fonyl)imide (EMITFSI) in PEO (< 40 wt% relative to PEO) is known to have plasticizing effect on the polymer as well as improve stability against lithium anode.

The cost and energy required to synthesize LAGP is much higher than PEO with small amounts of EMITFSI. The final goal is to create a PEO_{16}LiTFSI-x LAGP-y EMITFSI composite polymer electrolyte with intermediate loading of LAGP and small amount of EMITFSI to rival or beat PEO with high LAGP loading.

Chapter 2 Background and Literature

2.1 Lithium Metal Anode

Lithium metal has been studied as anode material in energy storage cells since 1950. However, due to low reversibility, the high reactivity of lithium metal, and high cost of specialized electrolytes, it soon gave way to intercalation graphite anodes discovered by J. O. Besenhard at TU Munich in the 1970s[2][3]. However, the current intercalation type lithium-ion battery (LIB) system is reaching its theoretical physicochemical limit of volumetric and gravimetric energy densities up to 770 Wh L^{-1} and 260 Wh kg^{-1}, respectively[4]. To pave the path for future battery systems such as Li-Air, Li-Sulfur, or high voltage cathodes such as NMC, lithium metal anode is predicted to be essential as presented in Figure 2.1.

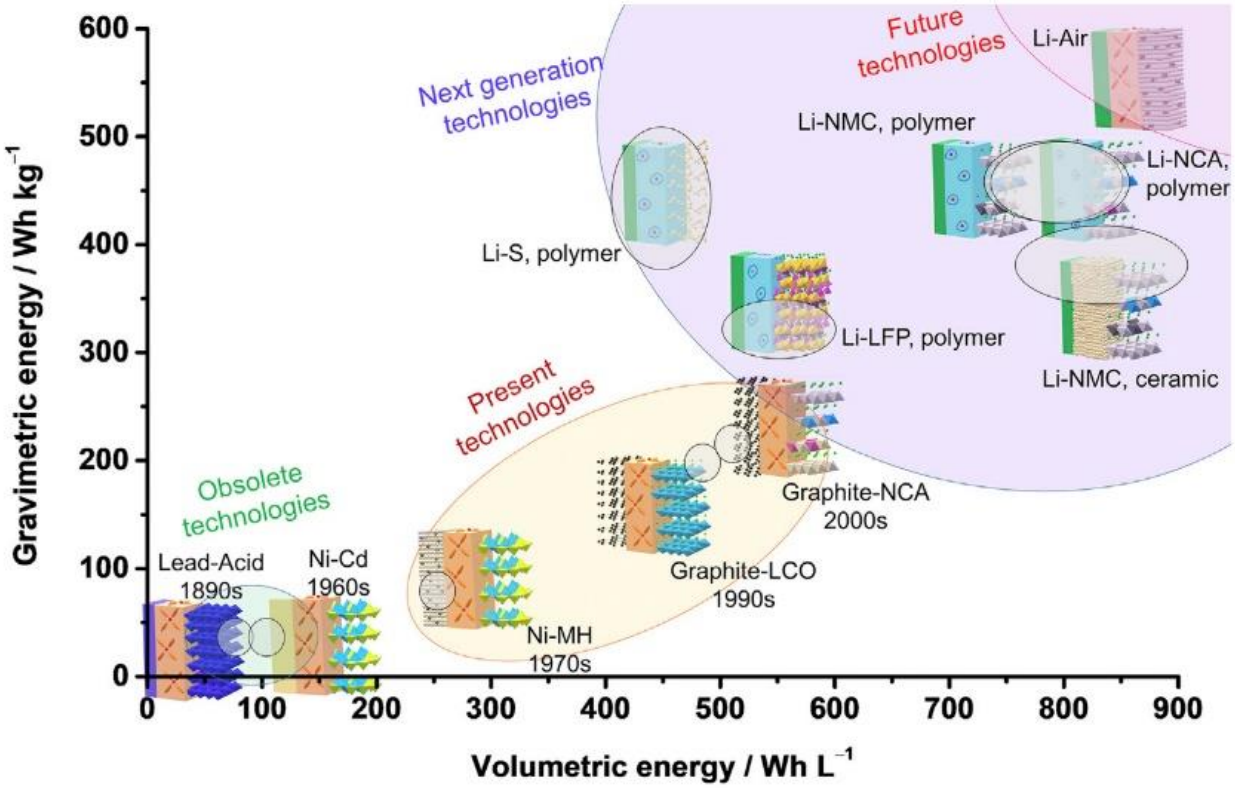

Figure 2.1 Overview of the Evolution of Battery Technologies and the Role of All Solid-State Li-Intercalation Cathode Batteries [5]

As LIB is reaching its inherent limits, more attention and work have been dedicated to revive lithium metal as anode material in secondary batteries[6][7][8][9][10]. This is attributed to the high specific capacity of lithium metal (3860 mAh g^{-1}) compared to the conventional graphite anode (372 mAh g^{-1}) which can allow for a higher energy density LIB. This is in large due to graphite anodes requiring at least 6 carbon atoms to bind 1 lithium atom[11], where as lithium anode will deposit upon the current collector and only change in size as much as the amount of lithium atom is stripped / deposited through the redox reaction of $Li^+ + e^- \Leftrightarrow Li$. Another attractive feature of lithium as anode is its low electrochemical potential of -3.04 V vs. Standard Hydrogen Electrode (SHE). Combining the two can allow for increase in both energy and power density.

However, lithium anodes have been shown to be highly incompatible with liquid electrolytes which contain organic solvents such as ethylene carbonate (EC), dimethyl carbonate (DMC) and diethyl carbonate (DEC). The presence of such organic solvents can exacerbate dendritic growth of lithium and also cause parasitic reactions with lithium metal, which consumes the electrolyte material[12][13][14][15]. This negatively impacts battery performance, lifetime and safety. In order for lithium anode to be feasible, two major problems have to be addressed:

1. Lithium dendrite growth must be controlled or suppressed.
2. Compatible electrolytes need to be selected in order to create a stable solid-electrolyte interphase (SEI).

In this work, solid polymer electrolyte polyethylene oxide (PEO) is investigated as the primary electrolyte with ionic-conductive fillers, including ceramic electrolyte and ionic liquid, forming a composite polymer electrolyte.

2.1.1 Lithium Dendrites

Dendritic penetration into the cathode leading to internal short circuit is one of the most well known reasons for catastrophic failure in lithium metal batteries. Even in cases of employing solid state electrolytes

with high shear modulus to suppress dendritic penetration, dendrite growth can still occur between the bulk lithium anode and electrolyte which decreases coulombic efficiency as well as lifetime of the battery.

A schematic in Figure 2.2 shows that an uneven surface of lithium anode can cause the flux of lithium ions to congregate at the protrusions of the anode surface during the charging phase[16][17][18]. As this process continues, the distance between the cathode and the tip of the dendrite decreases, thus lithium ions travelling through the electrolyte has to overcome less over-potential and further exacerbates dendrite growth. This will continue until either charging is stopped or dendrites reach the cathode layer and cause internal short-circuit.

In most cases, dendrite penetration into the cathode will not occur in one single charge in a battery. When discharging, lithium is stripped from the anode and may cause breaking of dendrites. With fresh lithium metal being exposed to the electrolyte, SEI layer will form around the broken lithium. However, the SEI layer is electrically insulating thus rendering the lithium electrochemically inactive, and the lithium becomes “dead”. Cross-section images of lithium plating in shown in Figure 2.3, where the dendrites have grown in a “moss-like” structure. This effect varies depending on the electrolyte composition as well as current density applied.

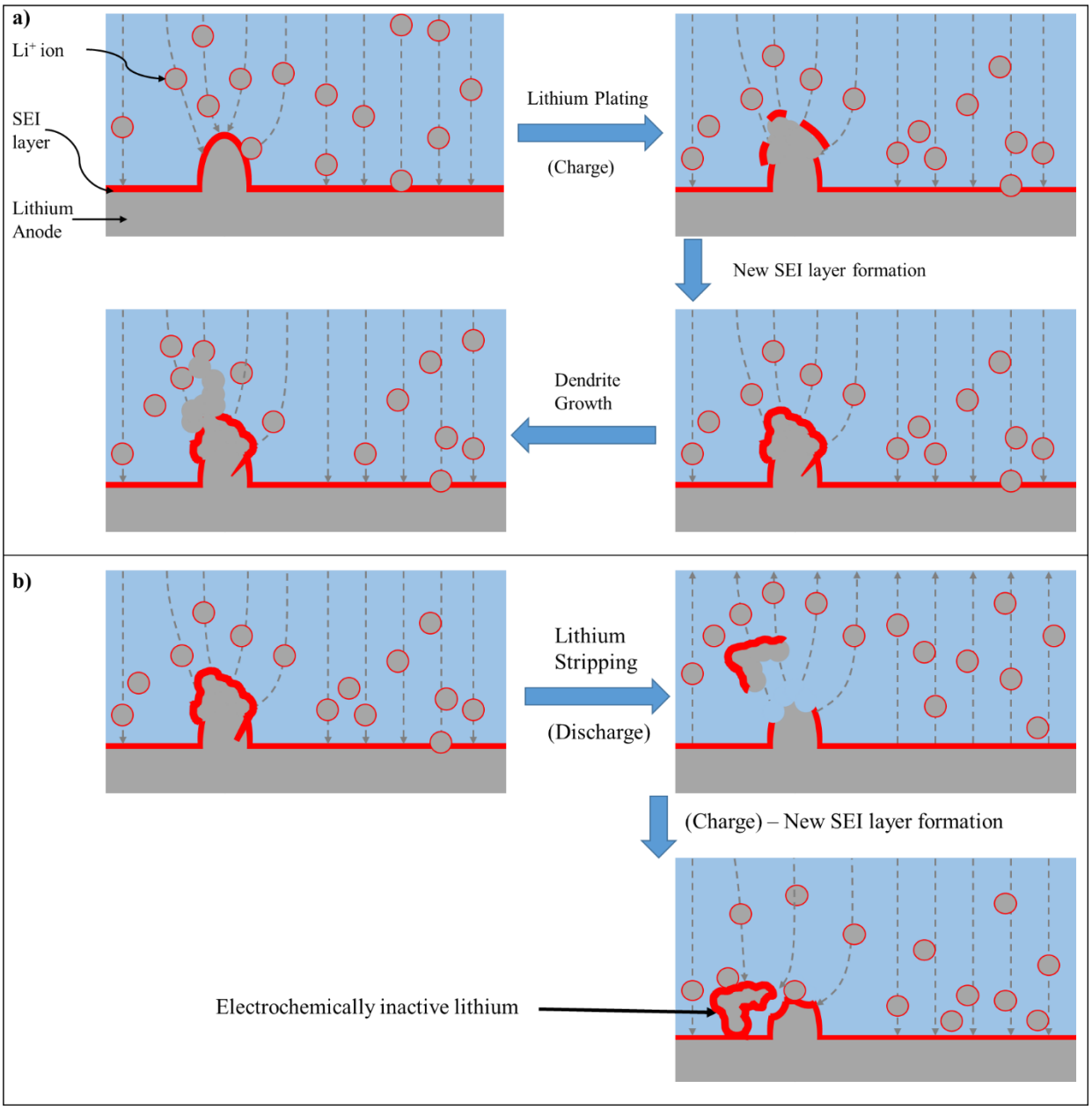

Figure 2.2 Schematic of lithium plating/striping. a) continuous lithium plating leading to dendrite growth; b) stripping of lithium causing dendrites to break and form electrochemically inactive lithium metal

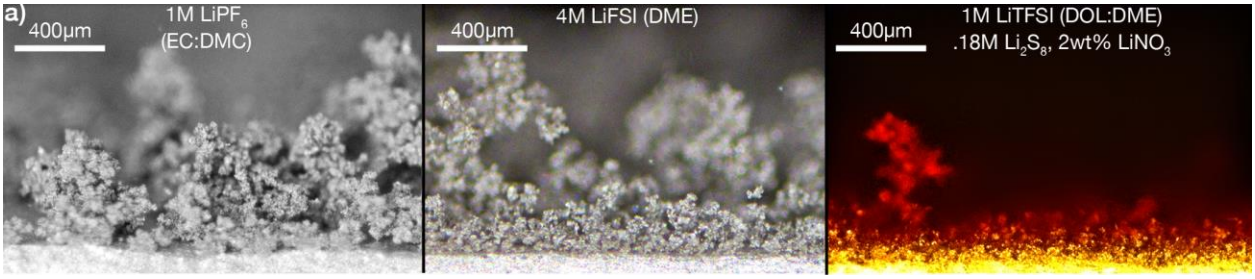

Figure 2.3 Cell images after 900 s of deposition at 5 mA cm^{-2} [15]

2.1.2 Solid-Electrolyte Interface (SEI)

Coulombic efficiency in terms of batteries can be calculated as the percentage of capacity delivered during discharge divided by the charge capacity. The cause of low coulombic efficiency is largely due to parasitic reactions occurring inside the cell[15]. The reactions generally occur at the interface between the electrode and electrolyte, forming a solid-electrolyte interface (SEI). Lithium metal anode is known to have low coulombic efficiency against liquid electrolytes due to the high reactivity, low electronegativity and unstable SEI layer which continuously exhausts electrolyte material. Most organic solvents used in liquid electrolytes are not thermodynamically stable against lithium metal and react to form a more stable SEI[19]. However, as dendrite growth occurs, fresh lithium metal is exposed to the electrolyte causing further parasitic reaction to occur every charge/discharge cycle. This will cause depletion of electrolyte material which raises internal ionic resistance and result in depreciating capacity. The exact mechanism of SEI formation is not well-known. However, stability against lithium metal can be tested and a few approaches have been proven to pacify lithium metal surface or suppress dendritic growth to some degree.

2.2 Electrolytes

Electrolyte in a battery is responsible for the shuttling of ions between the electrodes (ionically conductive) while resisting the passage of electrons (electrically insulative). In order to develop a feasible electrolyte for lithium anode, the following obstacles shown in Figure 2.4 must be overcome.

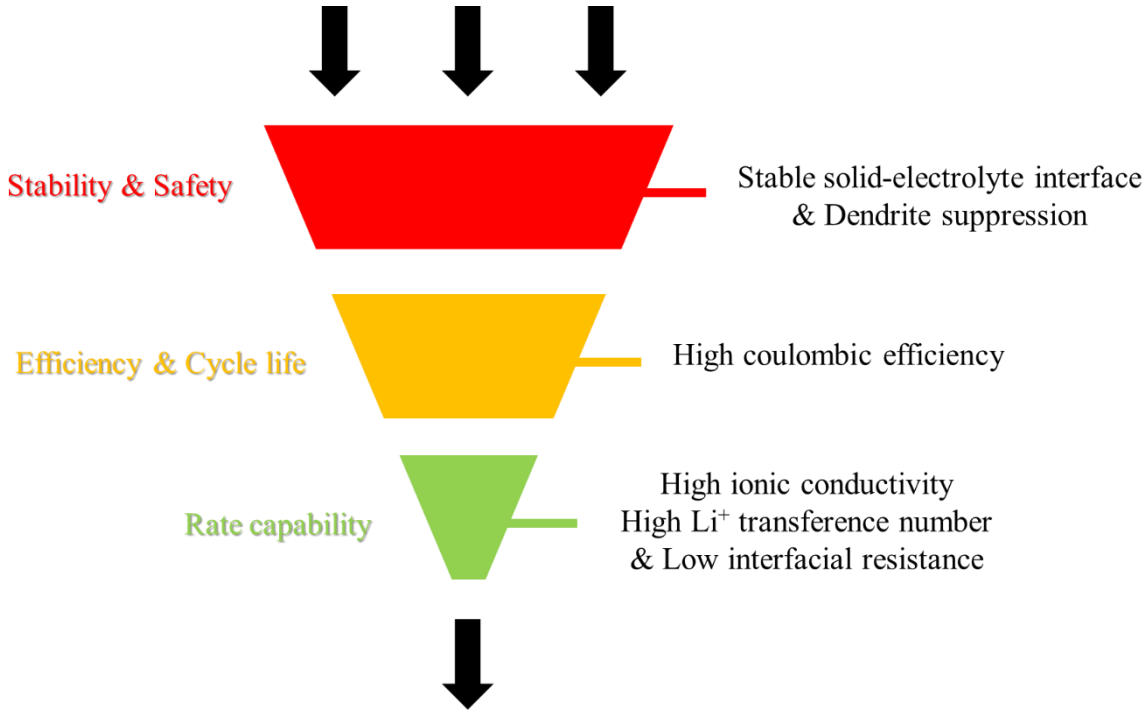

Figure 2.4 Schematic of electrolyte design for use with lithium anode

2.2.1 Liquid Electrolyte

Liquid electrolytes consist of lithium salts such as $LiPF_6$, $LiClO_4$, $LiC_2F_6NO_4S_2$ (LiTFSI) dissolved in aprotic solvents used in junction with a separator. Aprotic solvents are typically a mix of organic solvents including ethylene carbonate (EC), dimethyl carbonate (DMC), and diethyl carbonate (DEC). The organic solvents should have high ionic conductivity, low viscosity, good wettability towards the separator and electrodes, wide range of operable temperature and electrochemical stability window, and high flashpoint[20]. Thus a mixture of solvents is required to meet all the requirements. While choice of lithium

salts and their concentration can also have an impact on all the above, the cheap cost and high ionic conductivity of $LiPF_6$ has allowed it to be one of the most common lithium salts in the LIB market.

The main advantage of liquid electrolytes is its high ionic conductivity of 10^{-3} to 10^{-2} S cm^{-1}, and good contact with the electrodes, mitigating physical interfacial resistance and can accommodate volume changes in the electrodes. However, with new generations of batteries such as lithium-sulfur and lithium-air batteries, liquid electrolyte is no longer feasible as an electrolyte. Due to the high reactivity of lithium metal, organic solvents can not form a stable SEI layer and will continue to consume organic solvents and promote dendritic growth of lithium metal[7]. This will cause the internal resistance to continually increase and eventually lead to fully consuming the electrolyte material or dendrite penetration.

2.2.2 Solid Polymer Electrolyte

Solid polymer electrolytes (SPE) refer to lithium salts dissolved in solid polymer materials which have inherent abilities to conduct ions. One of the most promising material is poly(ethylene oxide) (PEO), which was the first polymer host to be introduced as an SPE with alkali metal salt[21]. The ether oxygen in the repeating ethylene oxide (EO) groups has a high donor number for Li^+ which is crucial for solvation of lithium salt. Coupled with the mobility of polymer chains and high dielectric constant, PEO is one of the most widely studied polymer host for SPE[22]. SPE have the advantage of not hosting any liquids therefore mitigating the risk of electrolyte leakage. PEO has a wide electrochemical stability window of roughly 5 V vs Li^+/Li depending on the lithium salt, which is higher than the conventional liquid electrolyte. However, the main drawback of SPE is its low conductivity, typically from 10^{-8} to 10^{-6} S cm-1 at ambient temperature depending on the molecular weight of PEO and lithium salt[23].

There exists a jump in ionic conductivity for PEO as temperature increases past its melting point (T_m). The traditional interpretation of this phenomenon assumes the crystalline phase of PEO to have lower conductivity than its amorphous counterpart due to its rigid nature. As the crystalline phase decreases with increasing temperature, the improved segmental movement of the PEO chains allow Li^+ to diffuse easier,

resulting in a jump in conductivity. However, Stoeva et al[24] demonstrated for PEO-$LiXF_6$ (X = P, As, Sb) the crystalline phase shows higher conductivity than the amorphous phase by one order of magnitude at low temperatures.. Nevertheless, the SPE crystalline phase only exhibited 6.3×10^{-8} S cm^{-1} at 28°C.

Efforts to plasticize PEO through solid fillers still proved to improve ionic conductivity. Most notably, inactive ceramic fillers such as Al_2O_3, TiO_2, $LiAlO_2$, and SiO_2 which do not conduct ions independently have shown capabilities to improve the ionic conductivity of PEO SPE at ambient temperatures as well as above T_m, suggesting the fillers play more roles than simply suppressing the recrystallization of PEO [25][26][27][28][29][30][31][32][33][34][35][36][37]. Research has demonstrated the Lewis acidic groups on the surface of the ceramic fillers can promote ion pair dissociation, weakening bonds between Li^+ and the salt anions, and the EO groups on the PEO backbone, further increasing ionic conduction even above the melting point where no crystalline PEO phase remains[38][39]. As shown in Figure 2.5, the maximum ionic conductivity can typically be achieved at around 10 wt% of ceramic filler, depending on the type, surface area, and particle size. At higher filler content, ionic conductivity begins to drop. Ceramic fillers tend to agglomerate at loadings, reducing the overall surface area of particles and thus decreasing ionic conductivity. Furthermore, as the filler content increases, the diffusion pathway of the lithium ions can become so tortuous that it decreases the ionic conductivity as well.

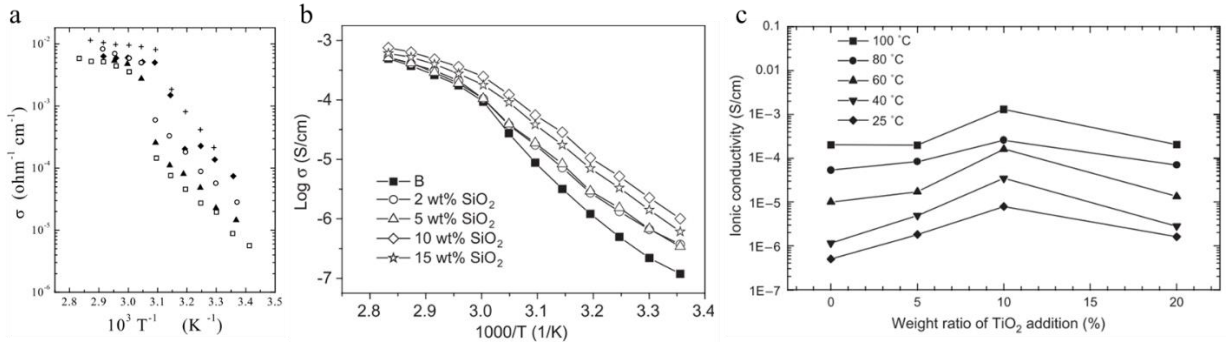

Figure 2.5 Conductivity plot of PEO electrolyte with various fillers (a) (□) PEO_8LiClO_4, (◆) PEO_8LiClO_4+5.3 wt.% of α-Al_2O_3, (+) PEO_8LiClO_4+25 wt.% of α-Al_2O_3, (○) PEO_8LiClO_4+5.3 wt.% of γ-

Al_2O_3[35], and (▲) PEO_8LiClO_4+25 wt.% of γ-Al_2O_3; (b) $(PEO)_{16}LiClO_4/SiO_2$ composite electrolytes with varying SiO_2 content[28]; (c) PEO-$LiClO_4$-TiO_2 electrolytes with varying TiO_2 content and temperature[26].

As effects of ceramic fillers benefit from high surface-to-volume ratio, recently 2D graphene oxide (GO) sheets has been studied as a new type of solid filler in PEO due to its excellent surface area[40][41][42][43][44][45]. GO filler loading optimized at 1 wt% have shown to increase ionic conductivity of PEO by two orders of magnitude, reaching 2×10^{-5} S cm^{-1} at ambient temperature as well as 260% improvement in tensile strength compared to pure PEO-$LiClO_4$[46].

Solid type fillers in SPE have the ability to disrupt recrystallization of PEO as well promote Li^+ dissociation to increase ionic conductivity and provide improvements to thermal and mechanical properties. However, as the improvement in ionic conductivity depend on surface interactions between the fillers and PEO, the benefits are limited by the maximum filler loading, after which the ionic conductivity drops due to filler agglomeration and tortuous Li^+ pathway. Further modifications to nanofillers such as surface functional groups or grafting onto PEO chains may provide satisfactory ionic conductivity.

2.2.3 Gel Polymer Electrolyte

Gel polymer electrolytes (GPE) consists of a polymer host which can absorb liquid electrolytes. It was first proposed in 1975 by G. Feuillade and Ph. Perche, utilizing polyacrylonitrile (PAN) as the polymer host[47]. The most widely studied gel polymer materials are PAN-, PEO- and PVDF-based[48]. The first commercialized LIB was produced by Sony in 1991, which employed a microporous polypropylene (PP) film as separator while flooding the electrodes with non-aqueous liquid electrolyte (Japan Patent JP8454189A). Soon after the commercialization of the first LIB, Bellcore (now Telcordia) filed a patent for a new type of GPE in 1994 (US Patent US5296318), consisting of a copolymer poly(vinylidene fluoride-co-hexafluoropropylene) (P(VDF-HFP)) containing $LiPF_6$ lithium salt dissolved in EC/DMC organic solvent. This garnered much attention in the battery industry and led to the wide-spread of lithium-polymer battery (also known as “Li-Po battery”), which most of the mobile devices currently depend on.

The main advantage of GPE is the containment of liquid electrolyte, minimizing the risk of electrolyte leakage. GPE can still maintain good physical contact against the electrodes due to the presence of liquids. By combining the function of separator and electrolyte into one, the energy density of the battery also improved[49]. Since then, the main focus of GPE research has been improving the ionic conductivity, liquid uptake and strength of the polymer.

However, the use of organic solvents is still incompatible with lithium anode. There has recently been increased effort into researching replacing the solvents with compatible fluids such as room temperature ionic liquid (RTIL)[50]. RTILs are salts that exist in liquid form in near room temperature. RTILs can have very high ionic conductivities, from 10^{-3} to 10^{-1} S cm^{-1} at room temperature. While this is an attractive feature in supercapacitors, the high mobility of cations can The drawback is the low Li^+ transference number (t_{Li+}) of roughly 0.4 – 0.6[51]. This implies both cations and anions contribute almost equally towards charge transport and can cause high inefficiencies.

2.2.4 Inorganic Solid Electrolyte

Inorganic solid electrolytes, often referred to as "ceramic electrolytes" encompass crystalline, partial crystalline (glass-ceramics), and amorphous glasses which have the ability to conduct Li^+. Inorganic solid electrolytes are known to have high thermal stability and ionic conductivity amongst solid electrolytes. Inorganic solid electrolytes have the distinctive feature of being single-ion conductors, where lithium ions lithium transference number is near unity except halides. Compared to liquid electrolytes where dissolved ions move in a solvent, ceramic electrolytes conduct ions through vacancies or interstitial sites which involves periodic bottlenecks in energy as shown in Figure 2.6.

Most inorganic solid electrolytes can generally be divided into oxides and sulfides. Lesser studied inorganic solid electrolytes such as Li-hydrides ($LiBH_4$, Li_3AlH_6, $Li_2BH_4NH_2$, etc)[52][53][54][55][56], and Li-halides ($Li_{1.8}N_{0.4}Cl_{0.6}$, Li_2CdCl_4, Li_3YCl_6, $Li_3InBr_3Cl_3$, etc)[57][58][59] are currently viewed as

inferior due to disadvantages such as instability against cathode materials or low ionic conductivity as summarized in Figure 2.7.

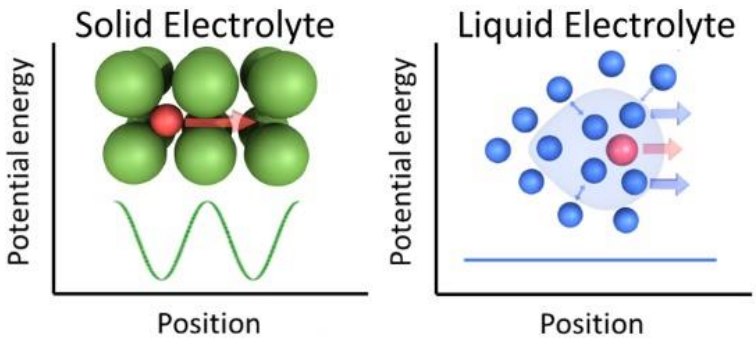

Figure 2.6 Potential energy of migration in liquid electrolytes of a charged species in red with a solvation shell of electrolyte molecules (highlighted in blue) and an interstitial mobile ion in a crystalline solid, respectively. [60]

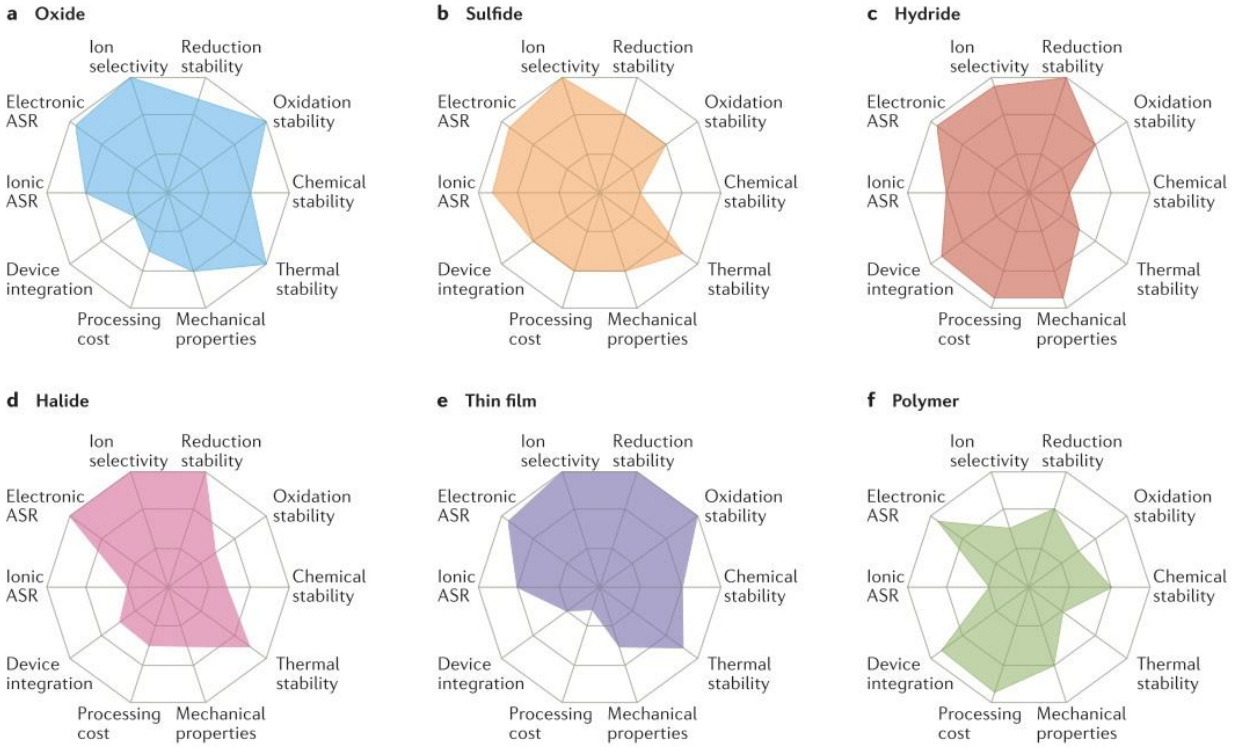

Figure 2.7 Performance of different solid electrolyte materials [61]

A crucial property of inorganic solid electrolyte is its electrochemical stability. Unstable electrolytes can lead to decomposition of electrolyte, dendrite penetration, and overall low cyclability of the cell. Most inorganic solid electrolytes despite showing wide electrochemical stability window of 0 – 5V, are not truly thermodynamically stable as shown below in Figure 2.8. Decomposition of the electrolyte at the electrolyte-electrode interface forms a passivating layer known as the solid-electrolyte-interface (SEI) layer which has a higher stability thus extending the electrochemical stability window. The SEI layer is often the cause of cell aging due to its higher ionic resistivity and uneven formation. The exact mechanisms are widely unknown and is an intensely researched topic.

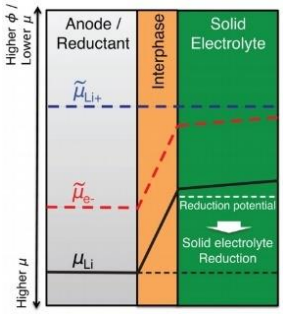

	reduction potential (V)	phase equilibria at the reduction potential	oxidation potential (V)	phase equilibria at the oxidation potential
Li_2S	-	Li_2S (stable at 0 V)	2.01	S
LGPS	1.71	P, Li_4GeS_4, Li_2S	2.14	Li_3PS_4, GeS_2, S
$Li_{3.25}Ge_{0.25}P_{0.75}S_4$	1.71	P, Li_4GeS_4, Li_2S	2.14	Li_3PS_4, GeS_2, S
Li_3PS_4	1.71	P, Li_2S	2.31	S, P_2S_5
Li_4GeS_4	1.62	Li_2S, Ge	2.14	GeS_2, S
$Li_7P_3S_{11}$	2.28	Li_3PS_4, P_4S_9	2.31	S, P_2S_5
Li_6PS_5Cl	1.71	P, Li_2S, LiCl	2.01	Li_3PS_4, LiCl, S
$Li_7P_2S_8I$	1.71	P, Li_2S, LiI	2.31	LiI, S, P_2S_5
LiPON	0.68	Li_3P, $LiPN_2$, Li_2O	2.63	P_3N_5, $Li_4P_2O_7$, N_2
LLZO	0.05	Zr_3O, La_2O_3, Li_2O	2.91	Li_2O_2, La_2O_3, $Li_6Zr_2O_7$
LLTO	1.75	$Li_4Ti_5O_{12}$, $Li_{7/6}Ti_{11/6}O_4$, $La_2Ti_2O_7$	3.71	O_2, TiO_2, $La_2Ti_2O_7$
LATP	2.17	P, $LiTiPO_5$, $AlPO_4$, Li_3PO_4	4.21	O_2, $LiTi_2(PO_4)_3$, $Li_4P_2O_7$, $AlPO_4$
LAGP	2.70	Ge, GeO_2, $Li_4P_2O_7$, $AlPO_4$	4.27	O_2, $Ge_5O(PO_4)_6$, $Li_4P_2O_7$, $AlPO_4$
LISICON	1.44	Zn, Li_4GeO_4	3.39	Li_2ZnGeO_4, Li_2GeO_3, O_2

Figure 2.8. (a) Schematic diagram about the change of Li chemical potentials μLi (black line), the electrochemical potential $\tilde{\mu}_{Li+}$ (blue dashed line), and $\tilde{\mu}_{e-}$ (red dashed line) across the interface between the anode and the solid electrolyte. (b) Electrochemical window and phase equilibria at the reduction and oxidation potentials of the solid electrolyte materials [62]

2.2.4.1 Oxide Solid Electrolyte

The most well-rounded type of inorganic solid electrolyte may be the oxide solid electrolytes. With its higher stability against ambient air and high temperature, manufacturing such material is viewed to be most realistic in scaling up for industrial applications. Oxide solid electrolytes can be mainly separated into perovskite, NASICON-type, LISICON-type, garnet and LiPON groups with corresponding structure as listed in Table 2.1 showing their respective total ionic conductivity and activation energy.

Table 2.1. Selected oxide solid electrolytes grouped by electrolyte type. *RT (Room temperature).

Electrolyte Compounds	Electrolyte Type	Structure	Synthesis Method*	Total Conductivity (S cm^{-1})	T (°C)	Activation Energy (eV)	Ref

$Li_{0.34}La_{0.51}TiO_{2.94}$	Perovskite	Crystalline	Solid-State	7.00×10^{-5}	RT	0.40	[63]
$Li_{0.75}La_{0.5}TiO_3$	Perovskite	Thin film glass	Atomic-Layer Deposition	9.40×10^{-7}	RT	/	[64]
$(Li_{0.33}La_{0.56})_{1.005}Ti_{0.99}Al_{0.01}O_3$	Perovskite	Crystalline	Citrate sol-gel synthesis	3.17×10^{-4}	RT	0.36	[65]
$Li_{1.3}Al_{0.3}Ti_{1.7}(PO_4)_3$	NASICON	Crystalline	Solid-State	7.00×10^{-4}	25	/	[66]
$Li_{1.3}Al_{0.3}Ti_{1.7}(PO_4)_3$	NASICON	Crystalline	Citrate sol-gel	7.80×10^{-5}	RT	0.40	[67]
$Li_{1.5}Al_{0.5}Ge_{1.5}(PO_4)_3$	NASICON	Crystalline	Solid-State, Thermal quenching	4.22×10^{-3}	27	0.61	[68]
$Li_7La_3Zr_2O_{12}$	Garnet	Crystalline (tetragonal)	Solid-State	4.16×10^{-7}	RT	0.54	[69]
$Li_7La_3Zr_2O_{12}$	Garnet	Crystalline (cubic)	Solid-State	2.44×10^{-4}	25	0.34	[70]
$Li_{6.55}La_3Zr_2Ga_{0.45}O_{12}$	Garnet	Crystalline (cubic)	Citrate sol-gel	1.30×10^{-3}	24	0.30	[71]
$Li_{3.25}Si_{0.25}P_{0.75}O_4$	LISICON	Crystalline	Solid-State	1.00×10^{-6}	30	0.44	[72]
$Li_{2.8}Zn_{0.6}GeO_4$	LISICON	Crystalline	Solid-State	1.00×10^{-4}	50	/	[73]
$Li_{3.6}Ge_{0.8}S_{0.2}O_4$	LISICON	Crystalline	Solid-State, Spark Plasma Sintering	2.00×10^{-5}	RT	/	[74]
$Li_{3.6}Ge_{0.8}S_{0.2}O_4$	LISICON	Crystalline	Solid-State	1.00×10^{-5}	27	0.5	[75]
$Li_{2.9}PO_{3.3}N_{0.46}$ (LiPON)	Oxynitride	Thin film glass	RF magnetron sputtering	3.30×10^{-6}	25	0.54	[76]
LiPON	Oxynitride	Thin film glass	MOCVD	5.90×10^{-6}	RT	/	[77]

2.2.4.1.1 Perovskite

One of the most well-researched perovskite type (ABO_3) solid electrolyte is the $Li_{3x}La_{2/3-x}TiO_3$ (LLTO). This is largely due to its high room temperature bulk ionic conductivity of 1×10^{-3} S cm^{-1} with x = 0.1[78]. The conduction mechanism depends on the A-site vacancy and thus the value of x plays a large

role in ionic conductivity[79]. However, the high grain boundary resistance which can up be to two orders of magnitude higher than bulk resistance, remains a major bottleneck for achieving high total ionic conductivity. Studies on sintering conditions and elemental doping has yielded some favourable results, increasing the total ionic conductivity up to 3.17×10^{-4} S cm^{-1} at 25°C[65]. Furthermore, due to LLTO's instability against lithium metal or intercalated electrodes with cathodic potential above 2.8V, the Ti^{4+} can be reduced to Ti^{3+} which grants the electrolyte electronic conductivity, leading to decomposition of the electrolyte and short-circuiting of the cell[80].

2.2.4.1.2 NASICON-type

NASICON was originally named as sodium super ionic conductor, with the general structure of $AM_2(BO_4)_3$ first coined by Goodenough and Hong et. al. for their work on $Na_{1+x}Zr_2P_{3-x}Si_xO_{12}$ in 1976[81]. Lithium-containing NASICON-type electrolytes can be obtained by substituting Na^+ with Li^+ in the A-site and utilized as high ion conducting lithium solid electrolytes. Such electrolyte gain traction when $Li_{1+x}M_xTi_{2-x}(PO_4)_3$ system was discovered to exhibit high ionic conductivity, with Al^{3+} substitution for M at x = 0.3 (LATP), yielding total ionic conductivity of 7×10^{-4} S cm^{-1} at 25°C[66]. However, LATP suffers from the same Ti^{4+} reduction issue as LLTO and requires a lithium protective layer to be utilized practically as an electrolyte. A more recent NASICON-type electrolyte was found to exhibit room temperature ionic conductivities between 7.5×10^{-5} and 5×10^{-4} S cm^{-1} [82][83][84]. Though reduction of Ge^{4+} to Ge^{3+} can still occur against lithium metal, LAGP exhibits a more stable interface than LATP with electrochemical stability up to 6 V versus Li/Li^+[82][85].

2.2.4.1.3 LISICON-type

LISICON (Lithium super ionic conductor)-type structure include Li_4SiO_4 and γ-Li_3PO_4 with XO_4-based (X = Al, S, Si, Ge, Ti, or P) tetrahedral units, and Li−O polyhedrals. The first LISICON-type electrolyte was discovered by Hong et. al. with the general structure of $Li_{16-2x}D_x(TO_4)_4$, where D = Mg^{2+} or Zn^{2+}, and T = Si^{4+} or Ge^{4+}. Ionic conductivity of 1.3×10^{-1} S cm^{-1} was achieved at 300°C with the $Li_{14}Zn(GeO_4)_4$ composition[86]. LISICON-type electrolytes generally exhibit ionic conductivity of

roughly 10^{-5} S cm^{-1} at room temperature which is amongst the lower range of oxide solid electrolytes. LISICON-type electrolytes show high stability even in moist air, allowing for ease of manufacturing and handling. However, stability against lithium metal is relatively poor.

2.2.4.1.4 Garnet

Ideal Garnets have a general formula of $A_3B_2(CO_4)_3$ with cubic phase ($la\bar{3}d$ space group), where A = Ca, La, Mg, Y, or rare earth elements; B = Al, Fe, Ga, Ge, Mn, Ni, or V; C = Al, As, Fe, Ge, or Si[87][88]. The first discovery of garnet-type lithium electrolyte is $Li_5La_3M_2O_{12}$ (M=Nb, Ta) by Thangadurai, where $Li_5La_3Ta_2O_{12}$ achieved total ionic conductivity of 3.4×10^{-6} S cm^{-1} at 25°C [89]. Garnet-type solid electrolytes show exceptional stability against lithium metal anodes, with electrochemical stability ≥ 6 V vs Li^+/Li at room temperature[90]. Notably, $Li_7La_3Zr_2O_{12}$ (LLZO) have been shown to stable against molten lithium metal and exhibits ionic conductivity of 3×10^{-4} S cm^{-1} at 25°C [70]. Due to the high stability and promising ionic conductivity of $Li_7La_3Zr_2O_{12}$, much work has been done in elemental doping to further improve the performance of LLZO in terms of improving ionic conductivity, and lowering sintering temperature and activation energy.

2.2.4.1.5 LiPON

Lithium phosphorous oxide nitride (LiPON) is an amorphous phase solid electrolyte. The first LiPON electrolyte was fabricated through d.c. magnetron sputtering with a Li_3PO_4 target in N_2 gas, which yielded $Li_{2.9}PO_{3.3}N_{0.46}$ with 3.3×10^{-6} S cm^{-1} at 25°C. Due to its high stability against lithium metal up to 5.5 V, it has been a popular solid electrolyte[91][92][93]. However, limited by its low conductivity, it has often been utilized as a lithium protective layer due to sputtering techniques being able to control the thickness to under 1 μm[94].

2.2.4.2 Sulfide Solid Electrolyte

Sulfide solid electrolytes generally show higher ionic conductivity as presented in Figure 2.8, where $Li_{10}GeP_2S_{12}$ is able to compete with liquid electrolyte with above 10^{-2} S cm^{-1} conductivity at room

temperature. The improvement over oxide electrolyte is attributed to the lower electronegativity of S compared to O. Li^+ less strongly bonded to S result in higher ionic conductivity for sulfide electrolytes.

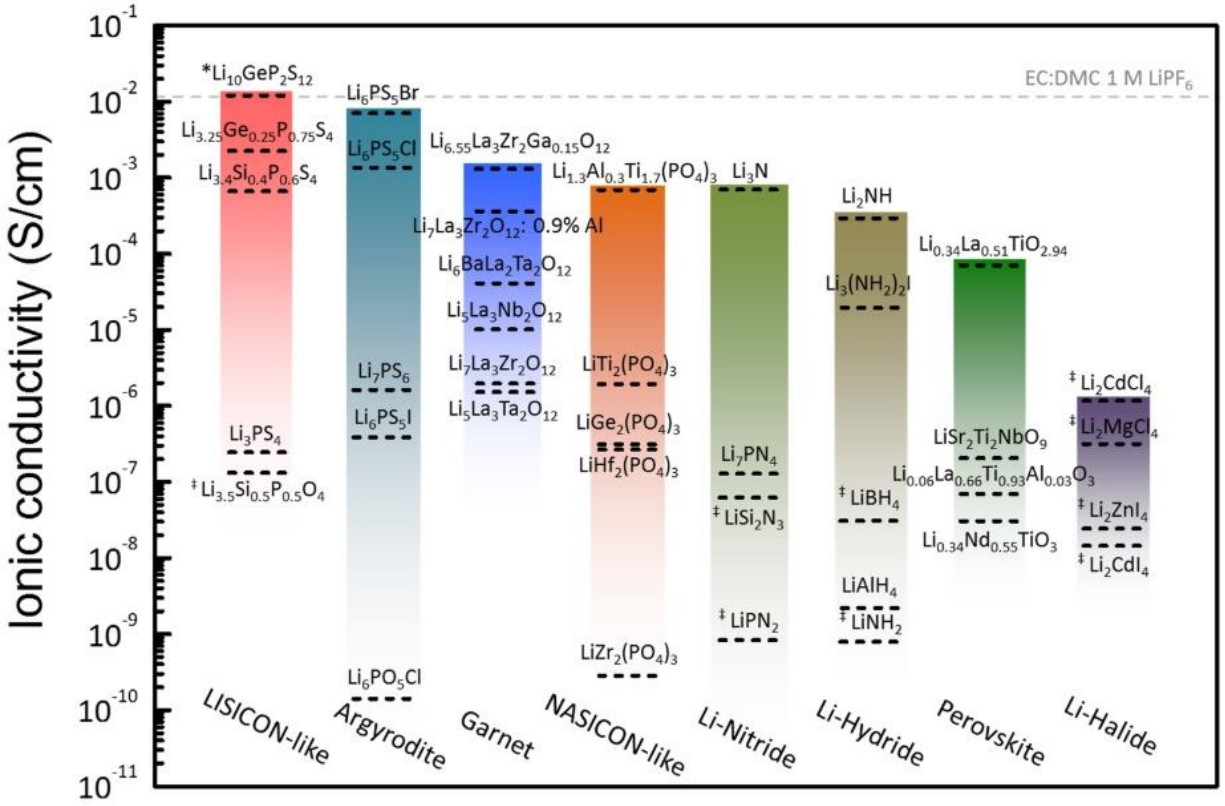

Figure 2.8 Reported total ionic conductivity of solid-state lithium-ion conductors at room temperature [60]

The flexible nature of glassy type sulfide electrolytes allows for better conformant to the volume change of the electrode materials. However, the conforming effect is still shown to be limited as studied with NCM-811 cathode material and β-Li_3PS_4 electrolyte in Figure 2.9, where visible gaps form between the solid electrolyte and active material. Furthermore, the formation of a resistive layer formed by oxidation of the sulfide electrolyte in the cathode along with gap formation result in the common irreversible capacity loss after the first cycle. Due to the narrow electrochemical stability window of most sulfide electrolytes as shown in Figure 2.9, and. The main drawback of sulfide electrolytes is its sensitivity towards moisture and oxygen, limiting production and handling of sulfide electrolytes to inert gas environments.

Due to the complications and production limitation of sulfide based solid electrolytes, this research will focus on oxide based solid electrolytes.

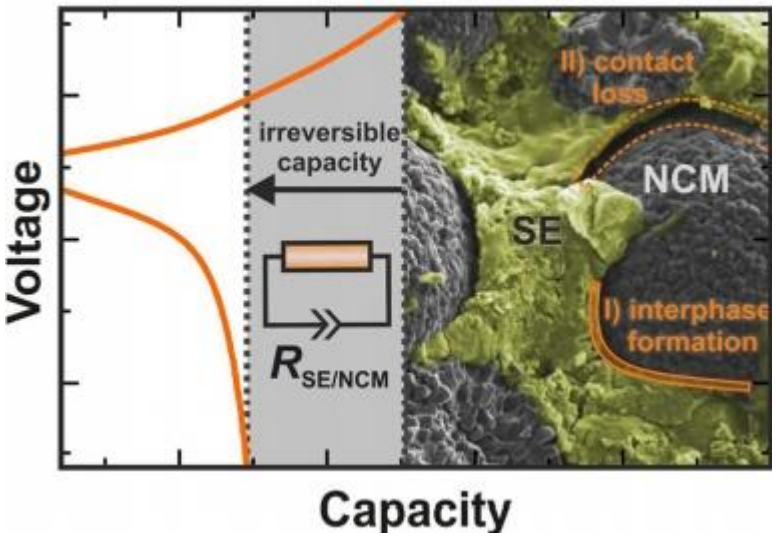

Figure 2.9 Schematic of capacity loss and SEM image of β-Li_3PS_4 solid electrolyte and NCM-811 cathode material after cycling [95]

2.2.5 Composite Polymer Electrolyte

Given the distinct advantages and disadvantages of the various types of solid electrolytes listed in Table 2.2, one approach to combine the electrolyte in different configurations to achieve a balanced and high performing composite electrolyte.

Table 2.2 Advantage and disadvantage comparison of electrolyte types

Electrolyte Type	Advantages	Disadvantage
Solid Polymer	• Flexible and low interfacial resistance • Cheap • Wide electrochemical stability window	• Low ionic conductivity • Low lithium transference number

	• Can incorporate various fillers to tailor specific properties	
Ceramic	• High ionic conductivity • Ideal lithium transference number ($t_+ = 1$)	• High interfacial resistance

2.2.5.1 Polymer-Ceramic-Polymer Layered Structure

One of the earliest methods of utilizing composite electrolytes is a layered structure, where solid polymer electrolyte is sandwiched on both sides of a dense ceramic electrolyte. As ceramic electrolytes garnered heavy interest due to their exceptional ionic conductivity amongst solid electrolytes such as the perovskite LLTO, two major bottlenecks were quickly discovered. The first is the nature of contact between two rigid solid phases between the electrode and the ceramic electrolyte causing voids to form which was not impacting a liquid electrolyte system. The second is the electrochemical instability of most ceramic electrolytes against lithium metal. By introducing a solid polymer electrolyte interphase, it takes advantage of the malleability of solid polymer electrolyte to decrease the high interfacial resistance of ceramic electrolytes and prevent reactions based on incompatibility between electrodes and ceramic electrolytes as represented in Figure 2.10.

However, this approach poses limitations on the thickness of the composite electrolyte layer. Given that solid electrolytes generally have sub par ionic conductivity compared to its commercial liquid counter-part, the target thickness of solid electrolytes is generally < 100 μm in order to have commercial success. The thickness is important due to internal resistance of the electrolyte scaling linearly with thickness. For a ceramic pellet to be formed at less than 100 μm including the polymer layer, manufacturing cost as well as fragility of the electrolyte are major concerns at this point in time until much improvement is made in terms of solid electrolyte conductivity.

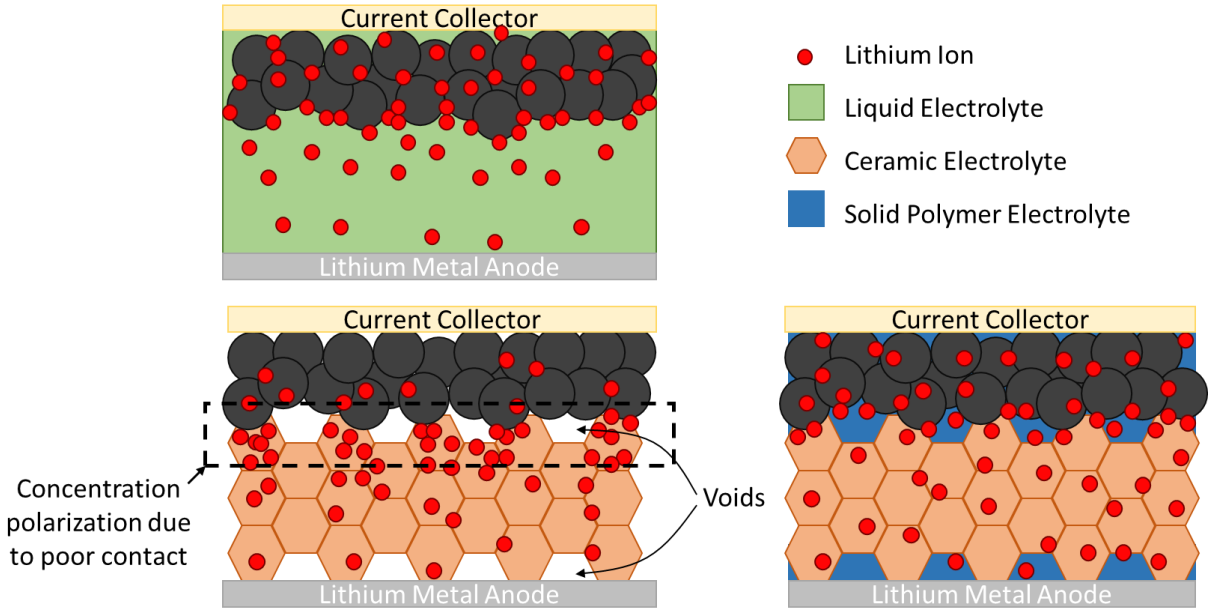

Figure 2.10 Schematics illustrating the impact of solid polymer electrolyte interface layer and Li anode for solid-state Li metal batteries

2.2.5.2 Powder Ceramic in Polymer

One of the simplest methods of fabricating polymer-ceramic composite electrolyte is by dispersing low weight loading of fine active ceramic powder into a polymer matrix. By simply dispersing ceramic electrolyte in a polymer host, a synergistic effect can be achieved. The ceramic electrolyte can provide lithium ion transport pathways with high conductivity as well as plasticizing the polymer host by disrupting the nucleation process and lowering the crystallinity of the polymer electrolyte to further improve ionic conductivity.

However, this method has certain limitations. As the ionic conductivity of such composite electrolyte does not form a linear relationship with the weight loading of the ceramic electrolyte, many studies have been performed to unravel the ionic transport mechanism in such composite electrolyte.

Various papers have measured the ionic conductivity of the composite electrolyte in relation to their active ceramic electrolyte loading as shown in Figure 2.11 with the optimal ceramic loading varying anywhere from 10 – 70%.

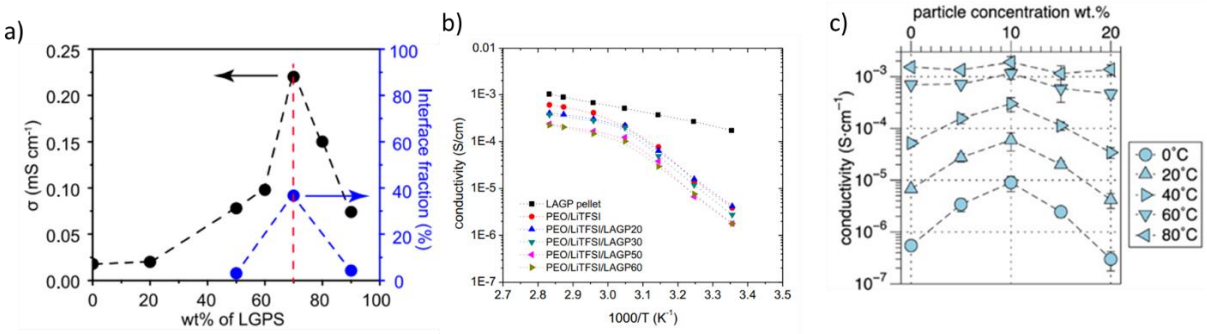

Figure 2.11. Relation between total ionic conductivity and their respective active ceramic electrolyte loading in PEO where a), b), and c) are LGPS [96], LAGP [97], and LATP [98] respectively in a PEO matrix.

Various contributing factors have been speculated and tested in order to optimize the performance of such composite electrolytes. The exact optimal loading can be influenced by the particle size, surface functional groups, the molecular weight of the PEO matrix, as well as the type of salt and salt concentration in PEO. Hence research groups such as J. Zheng and S. Bonizzoni have attempted to pin point through nuclear magnetic resonance (NMR) the mechanism of lithium transportation in composite electrolyte. As shown in Figure 2.12[99], the proposed transport mechanism can change due to ceramic loading as well as PEO property change. At low (<20%) loading, the main effect of LLZO ceramic is simply to plasticize the PEO phase, allowing for higher ionic conductivity in the PEO phase without utilizing the channels within the LLZO particles. This is due to the energy barrier required to cross from multiple PEO-LLZO boundaries in order to utilize transport pathways in LLZO. As LLZO reaches 50 wt%, the tortuous pathways in PEO due to blockage by the LLZO particles forces more lithium ion to travel through the LLZO particles instead, resulting in a lowered conductivity as seen in Figure 2.12 b. This theory is further supported by the addition of PEO plastcizer tetraethylene glycol dimethyl ether (TEGDME), resulting in a drastically increased ionic conductivity. By lowering the resistance of the PEO pathways, both the LLZO, LLZO-PEO interphase, and PEO can compete equally for ion transport even at a higher LLZO loading.

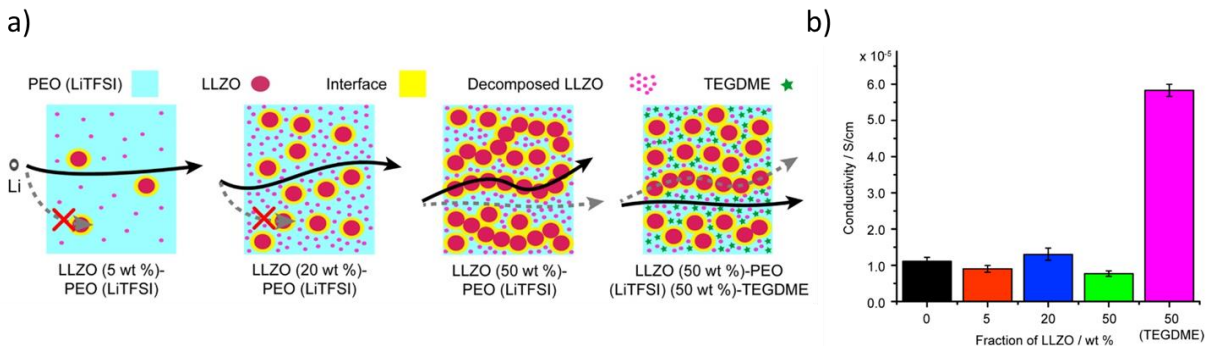

Figure 2.12 Schematic of Li-ion pathways within LLZO (5 wt %)−PEO (LiTFSI), LLZO (20 wt %)−PEO (LiTFSI), LLZO (50 wt %)−PEO(LiTFSI), and LLZO (50 wt %)−PEO (LiTFSI) (50 wt %)−TEGDME composite electrolytes [99]

2.2.5.3 Continuous Ceramic Structure in Polymer

Advanced continuous ceramic structure in polymer electrolyte is gaining more attention due to its attractive feature of allowing continuous ionic transport along a fixed pathway. Compared to its particle-in-polymer counterpart, ion transport would require much less energy due to no longer requiring crossing ceramic-polymer boundaries. The two main methods of production include electrospun ceramic fibre imbedded in ceramic and in-situ formation of porous ceramic structure allowing for infiltration of polymer electrolyte as shown below in Figure 2.13 and Figure 2.14 respectively.

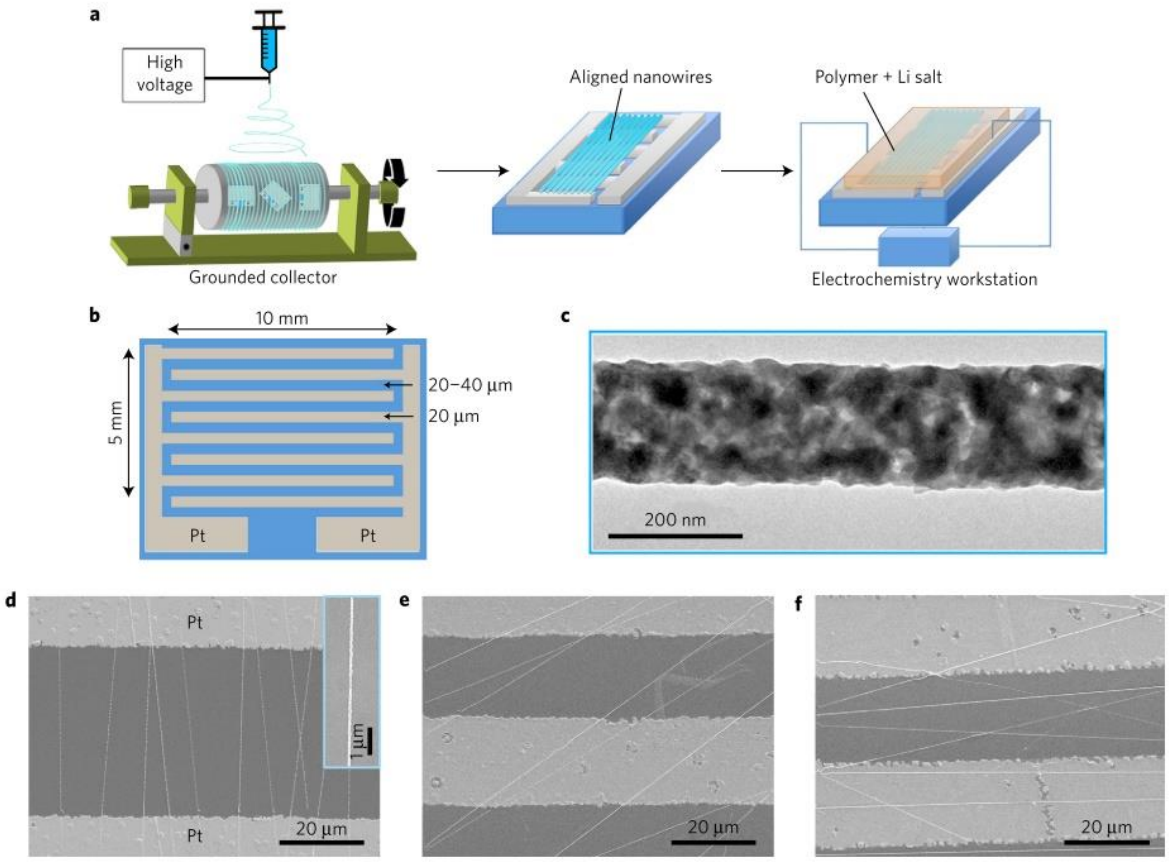

Figure 2.13 Synthesis procedure and morphologies for the composite polymer electrolyte with aligned nanowires (a) Synthesis procedure for the composite polymer electrolyte with aligned nanowires together with illustration of the electrode configuration for the a.c.-impedance spectroscopy measurement. The quartz substrates with Pt electrodes are placed at three different orientations on the rotating drum collector during electrospinning. (b) Interdigital Pt electrode. (c) TEM images of the LLTO nanowire calcined at 800 ◦C. (d–f), SEM images of the aligned nanowires at orientations of 0 ◦ (d), 45 ◦ (e) and 90 ◦ (f). The inset in figure d is a SEM image at high magnification for the aligned nanowires [100]

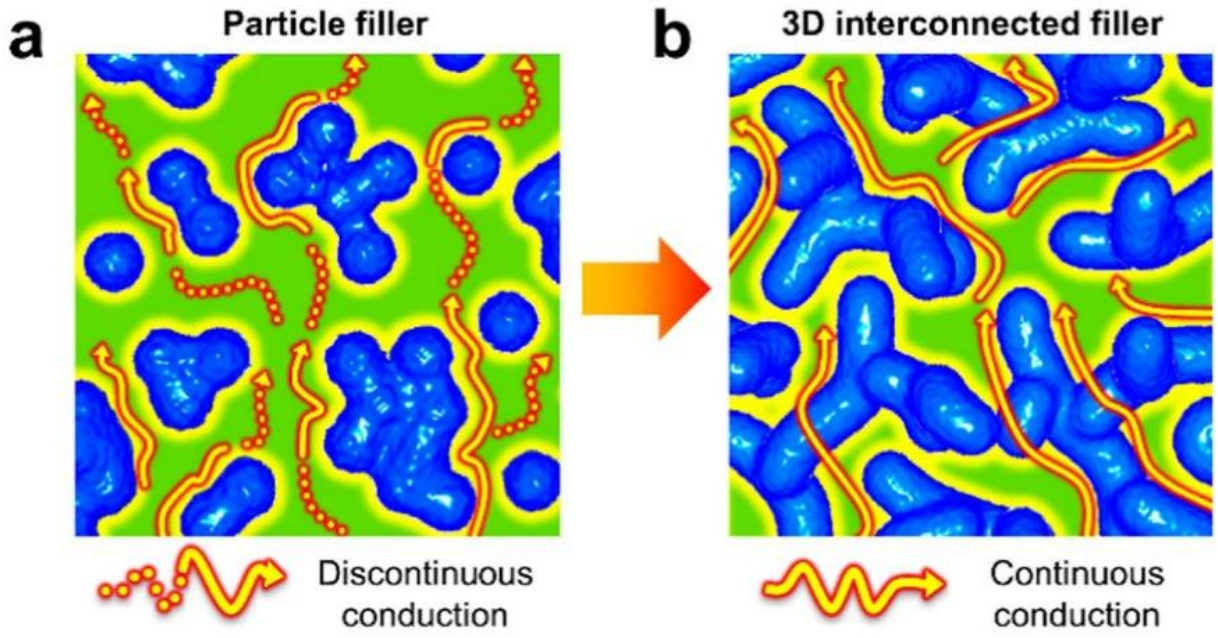

Figure 2.14 Schematic of ionic conduction mechanism in composite polymer electrolytes: (a) conventional discontinuous particle filler and (b) 3D interconnected LLZO [101].

Advanced ceramic structure has additional advantages such as minimizing the conglomeration of ceramic particles, higher ionic conductivity and generally higher mechanical structure compared to powder-in-polymer composite electrolytes. However, the methods to produce them are not well-suited for mass-production and are energy intensive.

Chapter 3 Materials and Methods

3.1 Materials

Polyethylene oxide (PEO, avg M_w = 400,000), lithium bis(trifluoromethanesulfonyl)imide (LiTFSI, 99.95%), and Lithium iron phosphate ($LiFePO_4$, <5 μm dia., 97%) are purchased from Sigma-Aldrich Inc. $Li_{1.5}Al_{0.5}Ge_{1.5}P_3O_{12}$ nanoparticles (LAGP, 500 nm average dia., 99.99%) is purchased from MTI Corp. 1-ethyl-3-methylimidazolium bis(trifluoromethanesul-fonyl)imide (EMITFSI, 97.5%), and "Super P" conductive carbon black (99%) are purchased from Alfa Aesar.

PEO was dried in a vacuum oven at 50°C for 24 hr while LiTFSI, $LiFePO_4$ and LAGP were dried in a vacuum oven at 80°C for 24 hr before use.

3.2 Experimental

3.2.1 Electrode and Electrolyte Slurry Preparation

The procedure to fabricate electrode and electrolyte is shown in Figure 3.1. PEO is first measured into a glass vial and then transferred into an Ar-glovebox, where LiTFSI is weighed at molecular ratio of [EO]:[Li] = 16:1 and added to the vial. Ionic liquid EMITFSI is added with relative weight to PEO. Acetonitrile is then added to the vial at roughly 10 times the weight amount of PEO to dissolve the mixture. Finally, the PEO_{16}LiTFSI-EMITFSI slurry is stirred at 50°C for 24 hr.

Active cathode material $LiFePO_4$ and conductive carbon Super P are weighed and is mixed in acetonitrile through stirring and ultrasonication to form a cathode slurry. PEO_{16}LiTFSI-EMITFSI is added to the cathode slurry to achieve the following weight ratio. $LiFePO_4$: Super P : PEO_{16}LiTFSI-EMITFSI = 5 : 1 : 4 (weight ratio)

The content of the vial is then stirred on a magnetic hot plate at 50°C for 48 hr to form a composite cathode.

To complete the electrolyte slurry, LAGP is added to the PEO_{16}LiTFSI-EMITFSI mixture at a weight ratio relative to PEO. The slurry is then stirred at 50°C for 24 hr with intermittent sonication.

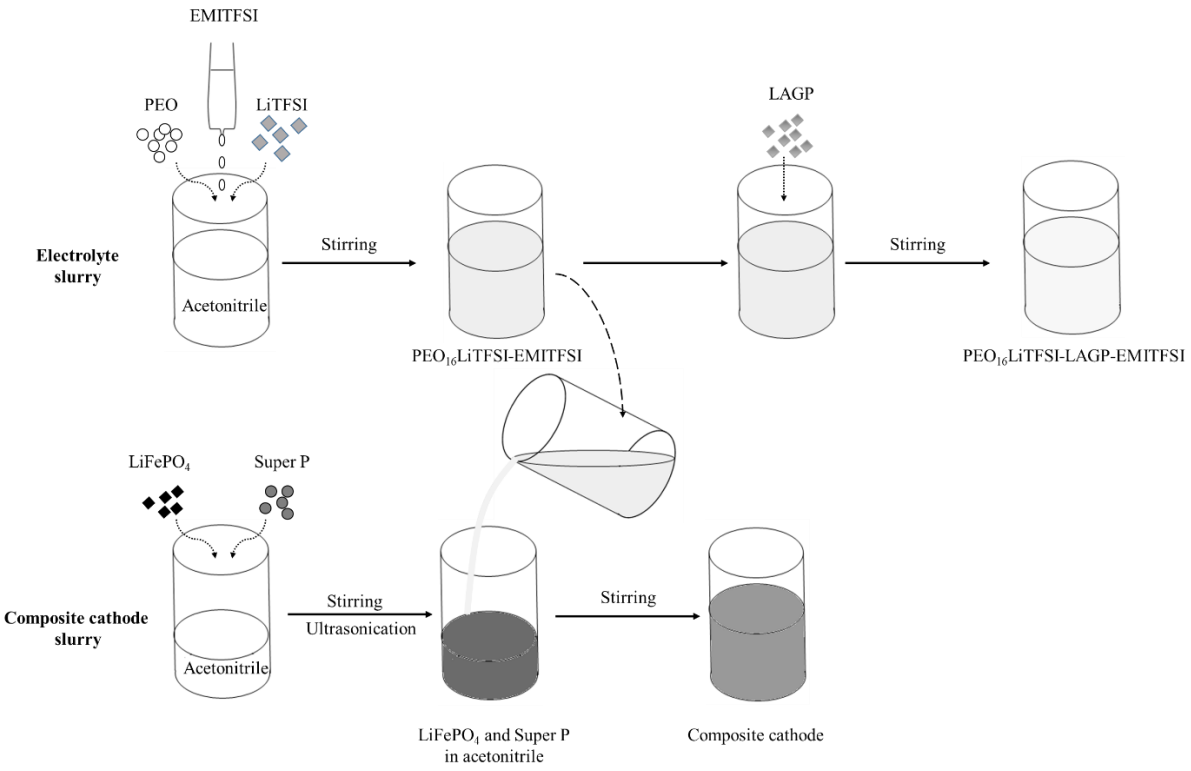

Figure 3.1 Schematic of electrode and electrolyte slurry preparation

3.2.2 Electrode and Electrolyte Slurry Casting

The composite electrode slurry is cast on an aluminum sheet current collector through tape casting as seen in Figure 3.2 c). After casting, the samples are allowed to dry in air for 30 min before transferring a vacuum oven, where the samples are dried at room temperature under vacuum for 24 hrs.

The composite ceramic-polymer electrolyte slurry is then cast on varying substrates for testing through tape casting. Such substrates include the surface of cast cathode layer to construct $LiFePO_4$|CPE|Li full cell as shown in Figure 3.2 d), or aluminum (Al) for Al|CPE|Li cells, or on a dish lined with polyethylene film to later peel off and cut as a stand-alone electrolyte film as shown in Figure 3.2 b). Before

the electrolyte slurry is cast on top of the cathode, the cathode sheet is cut down to circles with diameter of 15 mm and weighed to obtain the weight of $LiFePO_4$ by subtracting the weight of the aluminum sheet and multiplied by the ratio of $LiFePO_4$. After casting, the samples are allowed to dry in air for 30 min before transferring a vacuum oven, where the samples are dried at room temperature under vacuum for 24 hrs.

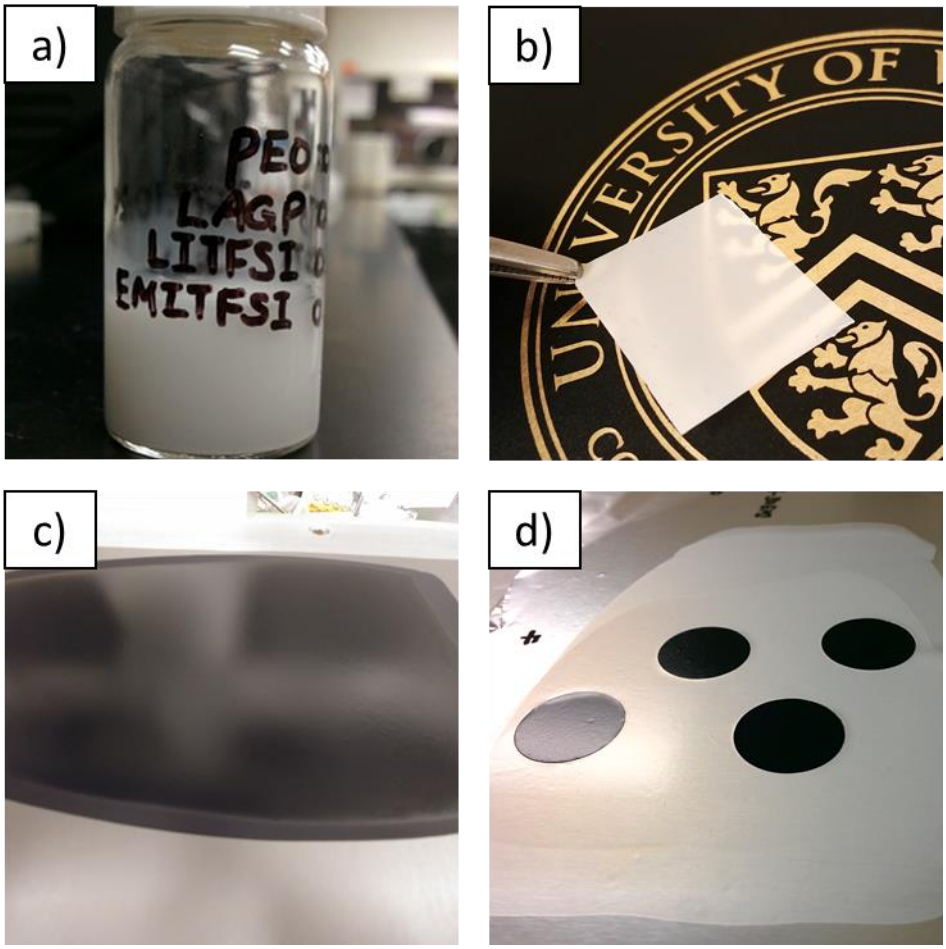

Figure 3.2 Photo of battery component coating. a) Composite polymer electrolyte slurry, b) Stand-alone composite polymer electrolyte film, c) Cathode layer cast on current collector, d) Composite polymer electrolyte cast on top of cathode layer

3.2.3 Cell Fabrication

All cells are fabricated inside an Ar-Glovebox using commercial 2032 coin cells. Samples are first dried in vacuum ovens then transferred into the glovebox and left for at least 12 hr to remove residual moisture and oxygen before cell assembly. Lithium metal is used as electrode material by being attached to the electrolyte layer to construct SS|CPE|Li and $LiFePO_4$|CPE|Li cells in 2032 coin cells. A configuration summary is as shown in the Figure 3.3.

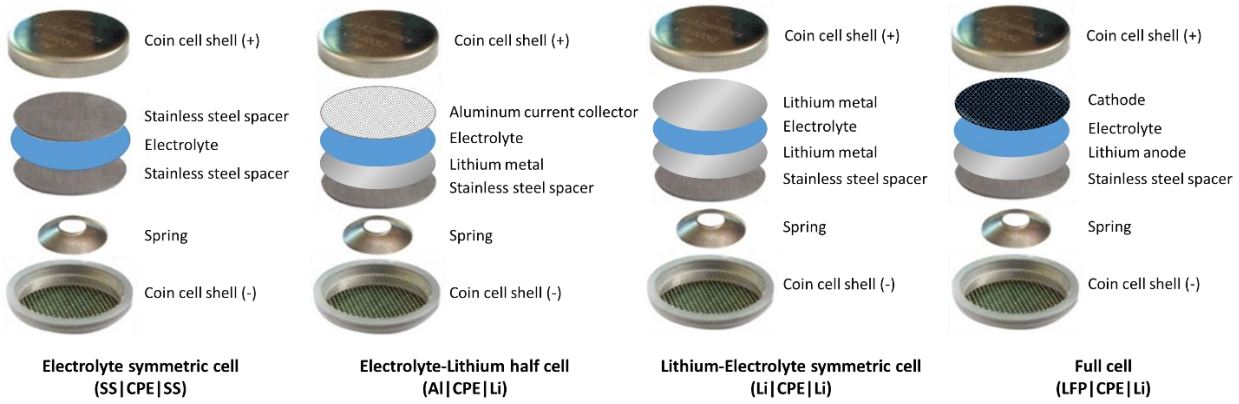

Figure 3.3. Coin cell assembly configurations.

3.3 Characterization and Equipment

The X-ray diffraction patterns of the electrolytes are obtained through X-ray diffraction (XRD) at 2° min^{-1}. The ceramic LAGP powder is scattered onto the sample holder while the CPE are cast onto the sample holder with a doctor blade and allowed to fully dry.

Thermal properties are characterized by TA Instruments Q2000 differential scanning calorimeter (DSC) by scanning at 10°C min^{-1} from -80 to 95°C. One heating/cooling cycle is first performed on the samples to remove thermomechanical history before collecting data on the following heating segment.

Morphology and elemental mapping are obtained through Zeiss Leo 1530 scanning electron microscope (SEM) and the on-board energy-dispersive X-ray spectroscopy (EDS).

The electrochemical stability window of the composite polymer electrolytes is measured through linear sweeping voltammetry (LSV) at 0.1 mV s^{-1} at room temperature where the cell is constructed as Al|CPE|Li in a coin cell.

Long term full cell cycling is performed using the LAND2001A battery testing station. The cells are kept in a Yamato DVS402C oven to ensure consistent environmental temperature during testing.

Ionic conductivity (σ) is measured by electrochemical impedance spectroscopy (EIS) in symmetric SS|CPE|SS coin cells, from 35°C to 60°C. The scans are carried out from 1 MHz to 0.1 Hz with ac amplitude of 10 mV. The ionic conductivity is then calculated as shown in Equation (1), where L is the thickness of the CPE, R_B is the bulk ionic conductivity, and A is the area of the interface between the SS electrode and CPE.

$$\sigma = \frac{L}{R_B A} \tag{1}$$

To obtain the cation transference number (t_+) of the CPE, Li/CPE/Li coin cells are fabricated and tested at 50°C. EIS is first conducted from 1MHz to 1 Hz at 10 mV. The cells are then polarized by applying a constant voltage of 10 mV for 5 hours, until the current has reached steady state. EIS is then performed again after polarization to obtain cell resistance. By applying Bruce and Vincent's work on transference number, steady state cation transference number can be calculated through Equation (2). In this case, ΔV refers to applied potential, I_o and I_{SS} are measured currents at the beginning and steady state value during polarization, and $R_{B,O}$ and $R_{B,SS}$ are bulk resistances of the composite polymer electrolytes measured through EIS before and post-polarization.

$$t_+ = \frac{I_{SS}\,(\Delta V - I_o R_{B,O})}{I_o(\Delta V - I_{SS} R_{B,SS})} \tag{2}$$

Chapter 4 Polymer-Ceramic Composite Electrolyte

The subject of "ceramic-in-polymer" electrolyte has been widely studied as a model candidate for composite electrolyte. The "ceramic-in-polymer" electrolyte consists of only the ceramic electrolyte LAGP, solid polymer electrolyte PEO, and lithium salt LiTFSI to facilitate ionic transport in the bulk PEO phase. The simplicity in manufacturing as well as the seemingly straightforward benefits of increase in ionic conductivity, mechanical strength, and in some cases electrochemical stability compared to pure polymer electrolytes. Two of the most contested areas for such CPE is the optimal ceramic loading and its ion diffusion pathway, which this chapter will attempt to clarify.

4.1 Composite Electrolyte and Electrode Preparation

As a baseline comparison, LAGP pellets were prepared by pressing LAGP powder in a steel die at 9 MPa and sintered in air at 850°C for 5 hours. $PEO_{16}LiTFSI$ – x LAGP electrolyte was prepared through slurry casting with doctor blade as described in the experimental section to obtain stand alone films as shown below in Figure 4.1.

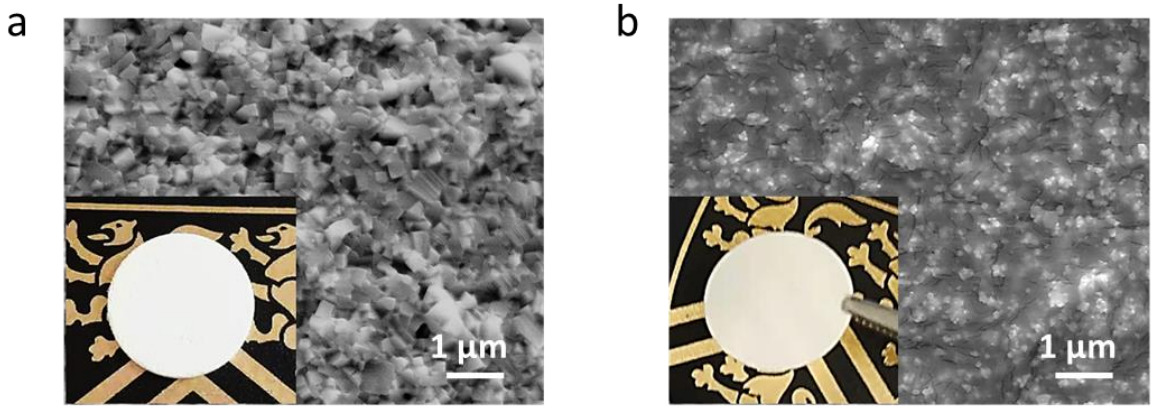

Figure 4.1. Photo and SEM image of a) LAGP pellet cross-section; b) $PEO_{16}LiTFSI$ with LAGP powder at LAGP:PEO = 1:1 weight ratio

$LiFePO_4$ active cathode material is prepared with $PEO_{16}LiTFSI$ as the binder as described in experimental section to facilitate ion transfer in the cathode layer in place of conventional PVDF or P(VDF-

HFP) which have poor ionic conductivity without liquid electrolyte. This will also provide a continuous ion transport pathway from cathode layer to bulk electrolyte region by eliminating the inert PVDF binder. SEM image of the cross section of LFP|PEO_{16}LiTFSI-LAGP is as shown in Figure 4.3, where no gaps can be observed at the cathode-electrolyte interface. To verify even distribution of cathode material, top view of the bare cathode layer and EDS mapping for Fe is as shown in Figure 4.2a-b. Cross section EDS mapping were performed as shown in Figure 4.2c-e. No agglomeration was observed and the cathode-electrolyte interface clearly shows elemental separation of cathode layer and bulk electrolyte, indicating no diffusion of electrolyte or cathode into each other.

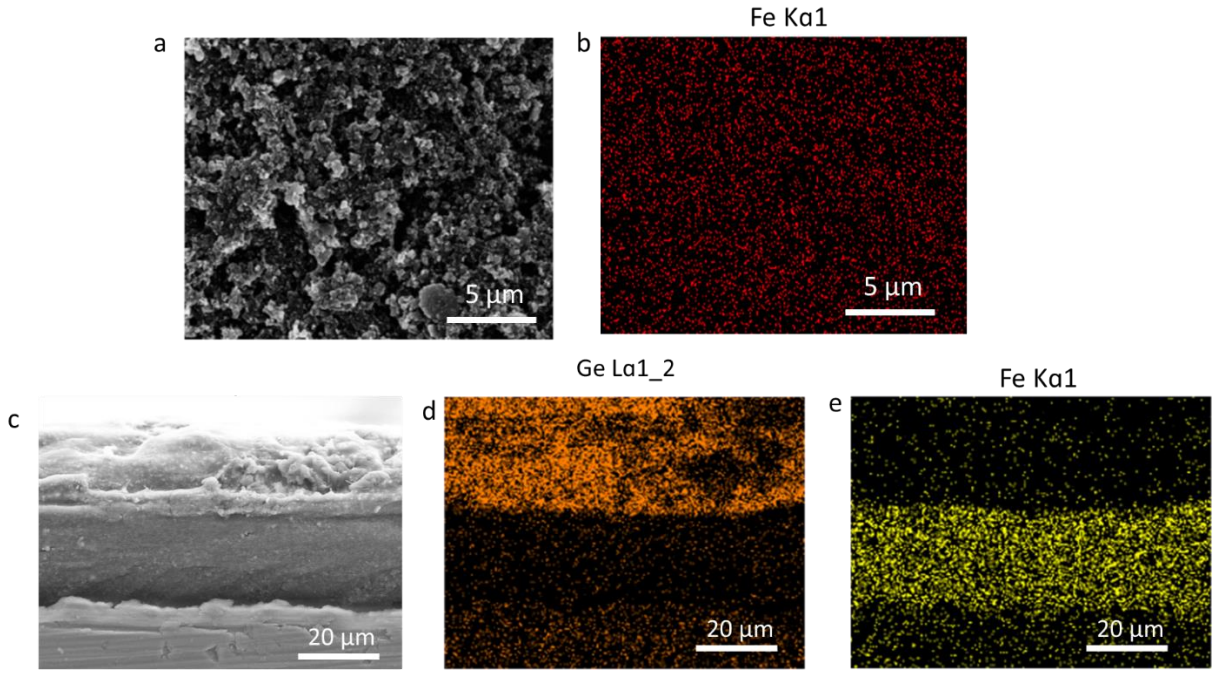

Figure 4.2. a) Top view SEM image of LFP composite cathode, b) EDS mapping of Fe; c) Cross section SEM image of LFP|PEO_{16}LiTFSI-LAGP, and EDS mapping of d) Ge; e) Fe

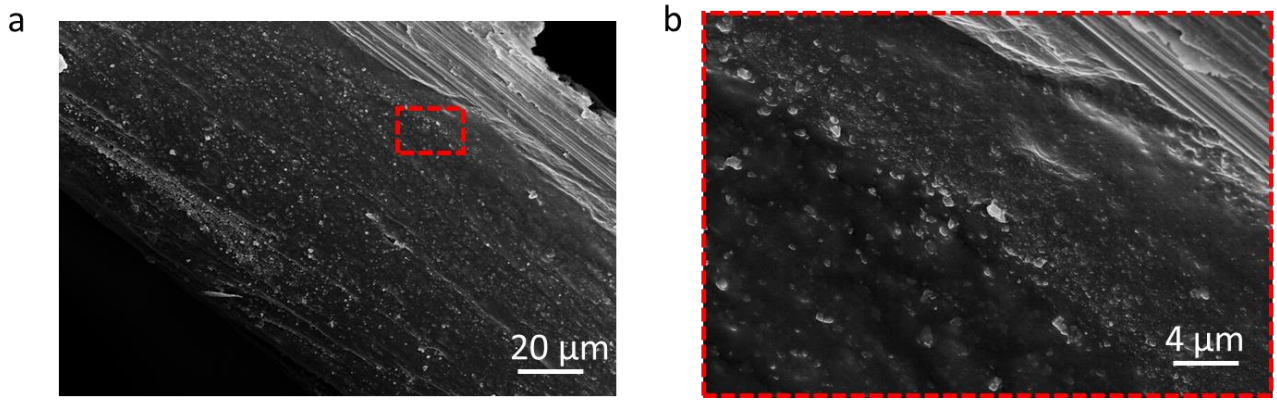

Figure 4.3. Cross section SEM image of LFP|PEO_{16}LiTFSI-LAGP

4.2 Ionic Conductivity – "Brick layer" Model

To determine the optimal LAGP loading in PEO, impedance testing was first conducted on composite polymer electrolytes PEO_{16}LiTFSI – x LAGP ($x = m_{LAGP}/m_{PEO}$) with varying LAGP weight content at varying temperatures. To meaningfully study the impedance results of the composite electrolyte, the "brick layer" model is used to quantify the origins of the internal impedances[102][103][104]. The basis of the "bricklayer" model stems from the assumption of 3 different ionic pathways in a ceramic-polymer composite electrolyte as shown in Figure 4.4. The path of least resistance is provided by the bulk LAGP, where ions can travel inside the crystalline structure of LAGP. The path of highest resistance is through the bulk PEO phase, where ionic conduction is slow due to the low ionic conductivity of pure PEO-lithium salt solid polymer electrolyte. Where the LAGP is in contact with the PEO, exists a grain boundary region which has slightly improved ionic conductivity compared to bulk PEO due to the interference of LAGP on the local crystalline structure of PEO, allowing a thin region of amorphous PEO to exist. To further modify the model, as LAGP content increases, the amount of LAGP-electrode contact surface increases which is detrimental to ionic transport at the interface, thus introducing interfacial resistance. The Nyquist plots with experimental data and fitted lines, along with equivalent circuit proposed is as shown in Figure 4.5**.** The high frequency interception at the x-axis represents the impedance of ion conduction in the bulk LAGP phase (σ_{LAGP}) as represented in Figure 4.5d. The first depressed semi-circle has been proposed to be

competition between polymer electrolyte phase conduction (σ_{PE}) and grain-boundary conduction (σ_{GB}) and referred to as $\sigma_{PE/GB}$ through the "brick layer" model. At high LAGP content, a second semi-circle appears at lower frequency, signifying the interfacial resistance.

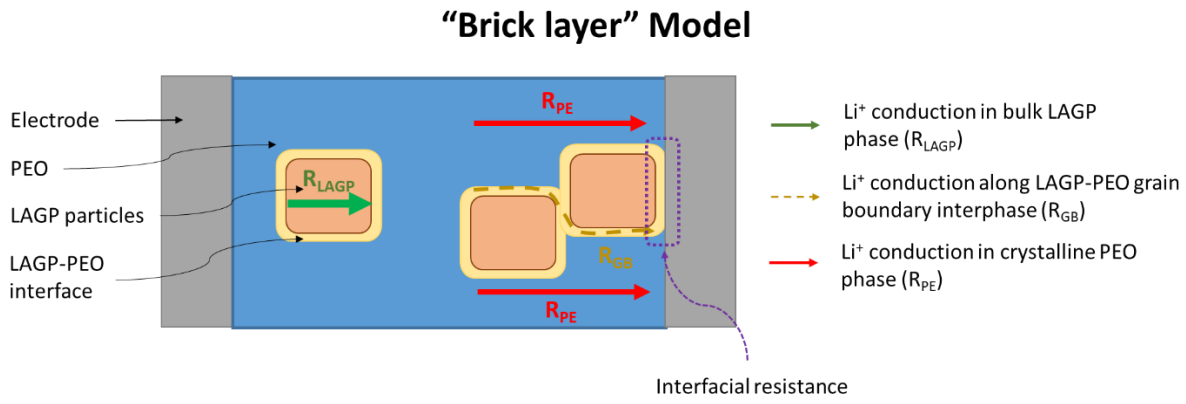

Figure 4.4. Schematic of "Brick layer" Model

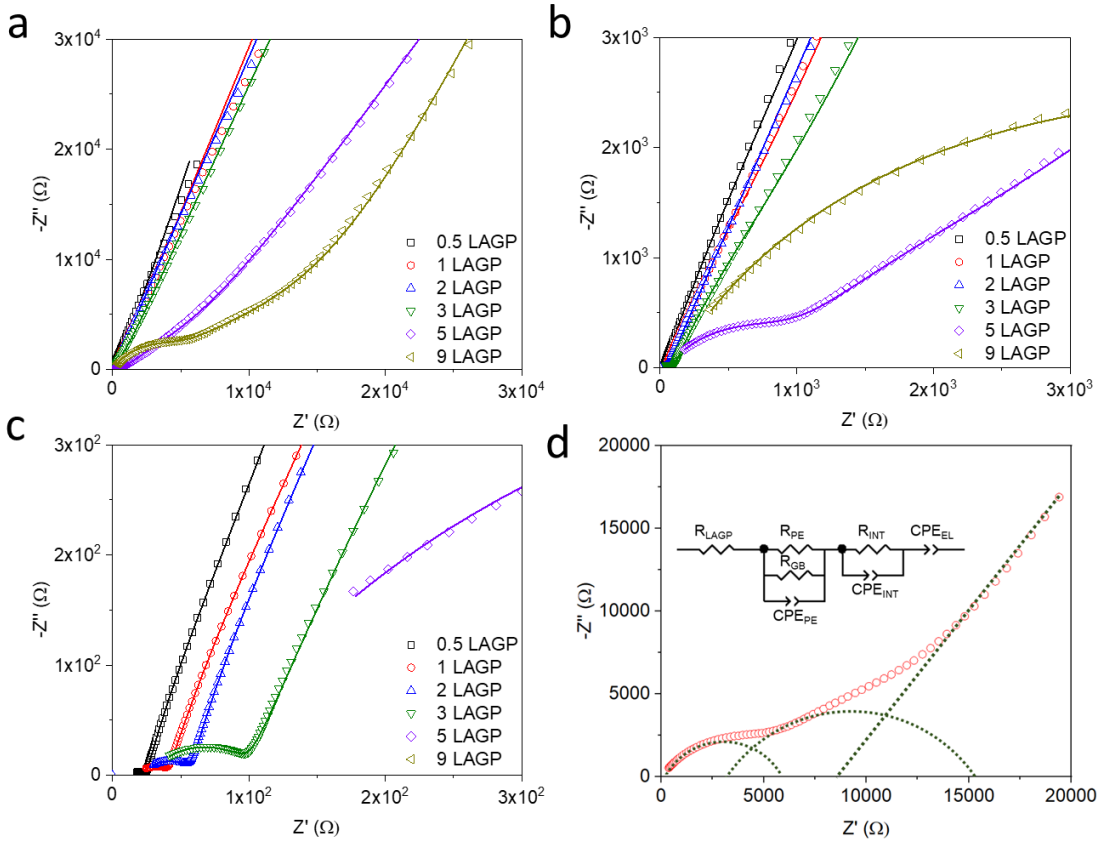

Figure 4.5. Nyquist plot and equivalent circuit of $PEO_{16}LiTFSI$ - xLAGP composite electrolyte at 35°C

By separating the LAGP and PEO conduction, the bulk LAPG conduction (σ_{LAGP}) and bulk polymer with grain boundary conduction ($\sigma_{PE/GB}$) can be plotted on an Arrhenius plot as shown in Figure 4.6. σ_{LAGP} shows a mostly linear trend across all LAGP loading in Figure 4.6a, in-line with a conventional ceramic electrolyte such as LAGP agreeing with "bricklayer" model. While $\sigma_{PE/GB}$ in Figure 4.6b shows a less regular pattern, the general pattern following a Vogel-Tamman-Fulcher (VTF) relation for a single-ion polymer electrolyte[105]. With the ionic pathway separated more clearly, it can be seen that at low temperatures, the polymer phase conduction is severely lacking. However, for LAGP loading at x = 3 and below, σ_{LAGP} eventually becomes over taken by $\sigma_{PE/GB}$ as temperature increases.

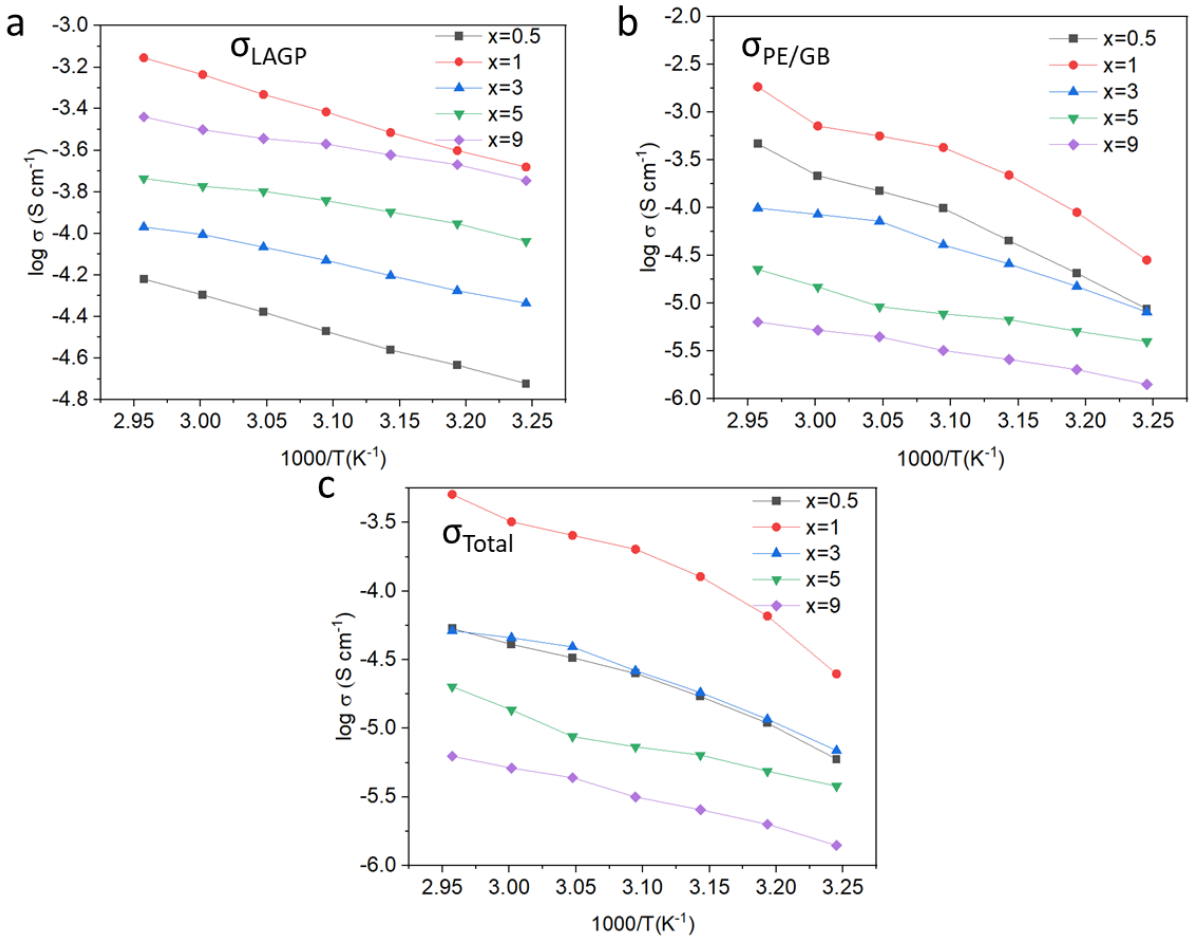

Figure 4.6. Arrhenius plot of $PEO_{16}LiTFSI$ - xLAGP, separated into a) bulk LAGP conductivity; b) bulk polymer electrolyte and grain boundary; c) total conductivity

Hence, σ_{LAGP}, $\sigma_{PE/GB,}$ along with the total bulk conductivity (σ_{Total}) of the CPE tested at 35°C is compiled in Figure 4.7a. There exists a local minima of σ_{LAGP} and maxima of $\sigma_{PE/GB}$ at LAGP:PEO = 3:1 (3 LAGP). This is due to the effect of LAGP particles on the lithium ion transference pathways in the composite polymer electrolytes. The lithium ion transport pathways in polymer-ceramic composite polymer electrolytes have been shown to be very complex[99]. As illustrated in Figure 4.7c, low LAGP content ($x \leq 1$) serves to lower the overall crystallinity of the polymer by disrupting the nucleation of PEO crystals while the majority of the lithium conduction occur in the bulk PEO phase[106]. As LAGP content increases to an intermediate level ($x = 1$), the total bulk ionic conductivity reached its maxima due to the low impedance ion pathway provided by the additional bulk LAGP as well as its plasticizing effect on the polymer phase. At an intermediate-high LAGP loading ($1 < x \leq 3$), ion mobility begins to be constricted in the PEO phase due to blockage by the LAGP, forcing lithium ions to travel in tortuous pathways thus decreasing $\sigma_{PE/GB}$. Utilization of the bulk LAGP phase likely declined (decrease in σ_{LAGP}) as the energy required to cross the increased number of PEO-LAGP boundaries is less favourable than the tortuous polymer phase pathway. Finally, as LAGP content increases further to $3 < x \leq 9$, the increasingly tortuous ion pathway in the polymer phase along with the increase in PEO-LAGP interfaces continues to cause a decrease in $\sigma_{PE/GB}$. Possibly due to the extremely low conduction in polymer phase, the bulk ionic pathway is instead forcing higher utilization of the bulk LAGP phase, causing an increase in σ_{LAGP} instead. However, the total conductivity is still mostly constricted by the polymer phase, yielding the lowest σ_{Total}. Although the ionic conductivity of the composite polymer electrolytes has the potential to keep increasing as LAGP to PEO ratio is further increased past 9:1 as demonstrated by Wang et al.[1], it is ultimately constrained by grain boundary resistance of un-sintered LAGP particles and loses the flexibility advantage of a CPE.

In the lower temperature range, an incomplete semi-circle can also be observed in the lower frequency corresponding to interfacial resistance against the electrode and is easier observed in high LAGP loading samples. The interfacial resistance of PEO_{16}LiTFSI – x LAGP is shown in Figure 4.7b. As expected, at higher LAGP, more LAGP particles come in contact with the stainless steel electrode and interfacial

resistance becomes higher. At 35°C, the interfacial of 9 LAGP is 425 times that of 1 LAGP, while the interfacial resistance of 1 LAGP effectively disappears at > 50°C. The composite polymer electrolytes from here-on uses LAGP:PEO = 1:1 (x = 1) and are also denoted as PEO_{16}LiTFSI-LAGP (PL).

However, the ionic conductivity of PEO_{16}LiTFSI-xLAGP is still not satisfactory. Comparison with pure LAGP phase and pure solid PEO phase ionic conduction is carried out by measuring dense LAGP pellet and PEO_{16}LiTFSI casted film. As compared in Figure 4.8, the bulk ionic conductivity of the sintered LAGP pellet at 35°C is an order of magnitude higher than PEO_{16}LiTFSI-LAGP, which is in turn an order of magnitude higher than PEO_{16}LiTFSI solid polymer electrolyte. Given the bottleneck in ion conduction being the polymer phase especially in near room temperature, there is room to further improve the ionic conductivity of PEO_{16}LiTFSI-LAGP by modifying the solid polymer phase.

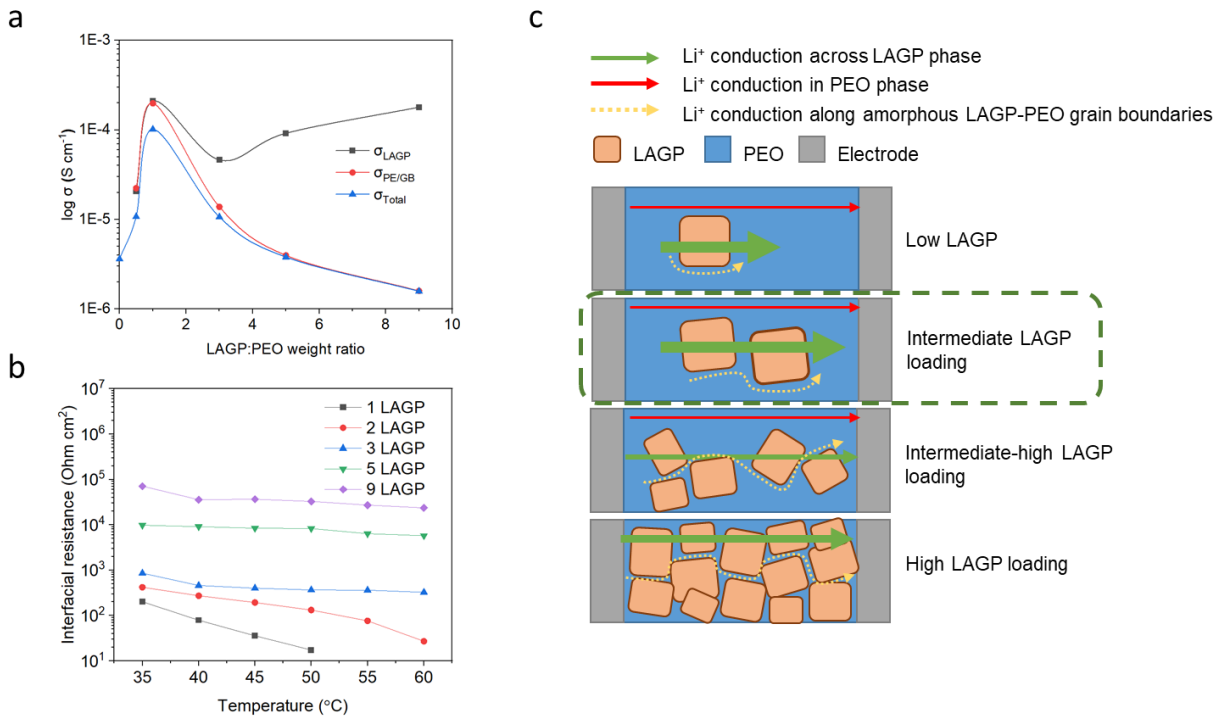

Figure 4.7 a) Ionic conductivity of PEO_{16}LiTFSI - x LAGP at 35°C separated into LAGP phase conduction, parallel PE/GB conduction, and the total bulk conductivity. b) Interfacial resistance of PEO_{16}LiTFSI - x LAGP electrolyte from 35 to 60°C with varying LAGP loading. c) Schematic of ionic conduction pathway changes in relation to LAGP loading.

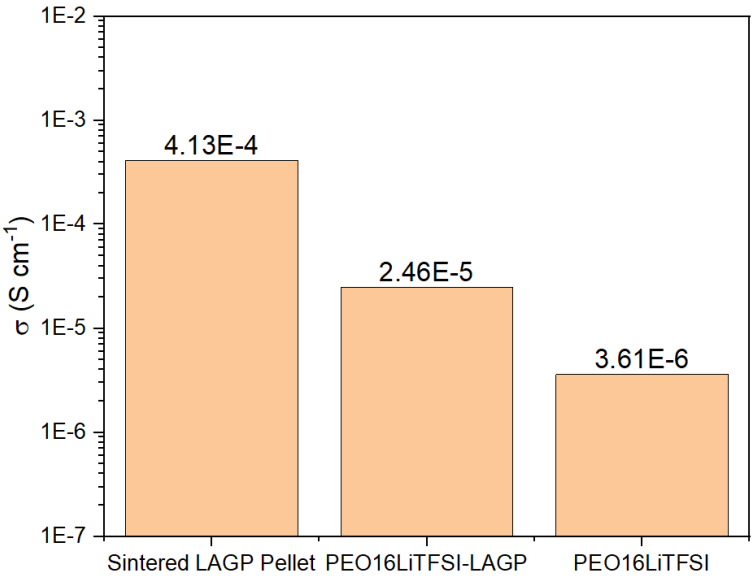

Figure 4.8 Ionic conductivity comparison of sintered LAGP pellet, PEO_{16}LiTFSI-LAGP and PEO_{16}LiTFSI at 35°C

4.3 Stability testing and Galvanic Cycling

Given the high reactivity of lithium metal anode, linear sweep voltammetry is crucial in determining suitable electrolytes. Al|PEO_{16}LiTFSI – x LAGP|Li coin cells were assembled for x = 0, 1, 3, and 9 due to their ionic conductivity characteristics from the previous section. LSV scans were carried out in room temperature, at a scan rate of 1 mV s^{-1} from OCV to 6.5 V vs Li/Li^+ as compiled below in Figure 4.9. 0 LAGP represents a solid polymer (PEO) electrolyte with lithium salt, which shows an upper electrochemical stability limit of 4.1 V vs Li/Li^+ due to oxidation of $TFSI^-$ anion. As LAGP loading increased to x = 1, the limit is increased to 4.25 V. This phenomenon has been explained as the surface interaction of LAGP particles and $TFSI^-$, causing an immobilization the anions and as a result, widening of the electrochemical stability window[107]. As LAGP loading further increased to x = 3 and 5, the upper limit decreased to 4.1 and 3.9 V respectively. This is due to the oxidation nature of LAGP against bare lithium metal as less PEO is available to protect the LAGP particles. It has been reported that the SEI layer formation created between LAGP and lithium metal can eventually pacify the interface up to 6 V[108]. However, given the same condition, 1 LAGP appears to the most compatible with lithium metal anode.

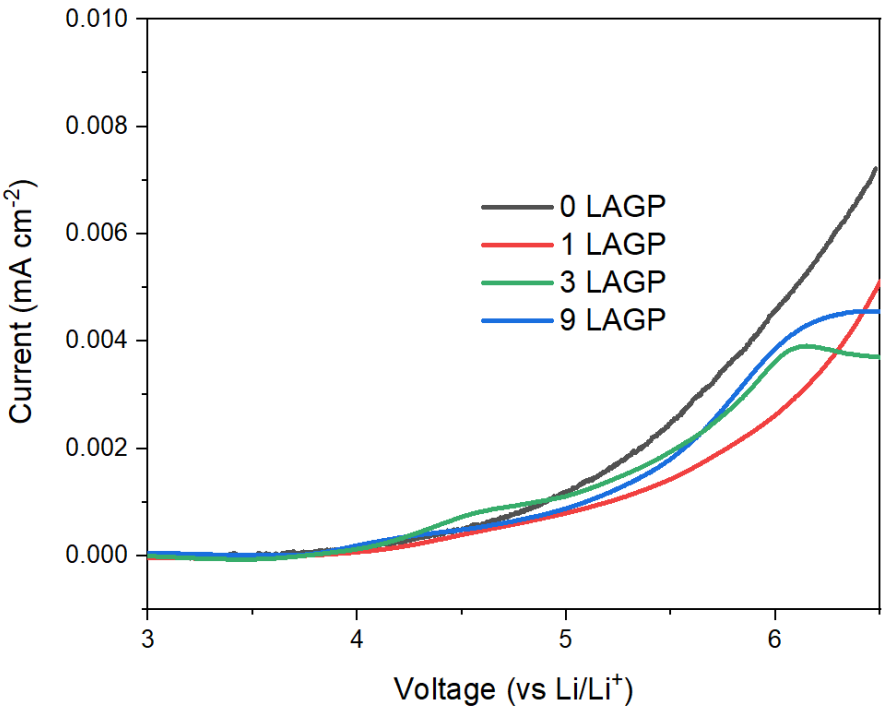

Figure 4.9. LSV scan of Al|PEO_{16}LiTFSI - x LAGP |Li for x = 0, 1, 3, and 9 at room temperature

LFP|PEO_{16}LiTFSI – x LAGP|Li batteries were then constructed into coin cells and cycled at temperature of 50°C and charge rate of 0.3 C as summarized in Figure 4.10. With no LAGP present (0 LAGP), the solid polymer electrolyte cell performed as expected compared to similar solid PEO-lithium salt batteries[43][109]. The discharge capacity delivered by the solid polymer electrolyte increases for the 10 first cycles, reaching 104 mAh g^{-1} before quickly depreciating after. This phenomenon is most likely due to the continuous oxidation of $TFSI^-$ as reflected previously in the LSV results. 1 LAGP showed a relatively consistent discharge profile, with initial capacity of 98 mAh g^{-1} and 9.4% depreciation over 45 cycles. For 3 and 9 LAGP, the capacity trends are both highly unstable as well as decreased capacity with higher LAGP loading. From SEM images it can be seen that gaps exist between PEO and LAGP particles which is exacerbated with higher LAGP loading, which can contribute to unstable performance. The

decreased capacity with increasing LAGP can be speculated to be the extremely high interfacial resistance of 367 and 32824 Ω that exist for 3 and 9 LAGP respectively even at 50°C.

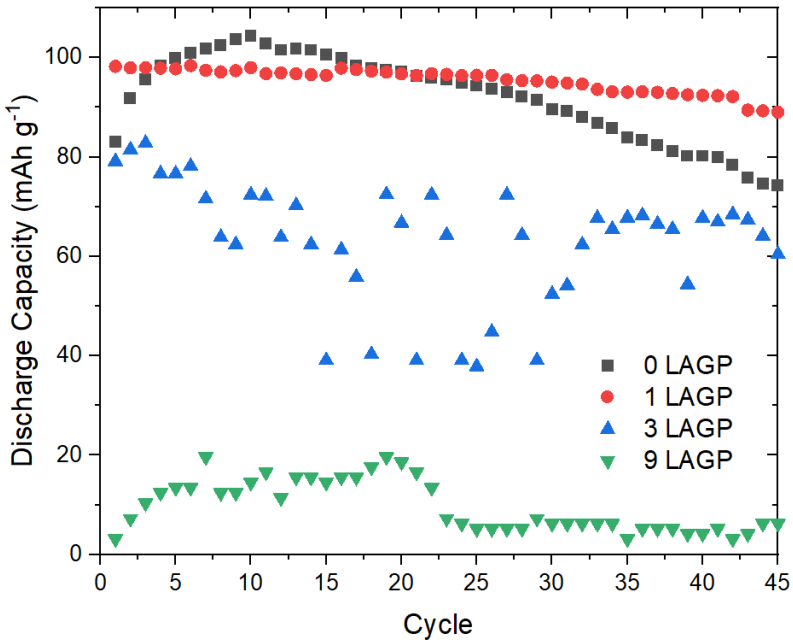

Figure 4.10. Full cell galvanic cycling of LFP|PEO_{16}LiTFSI - x LAGP|Li in 50°C and 0.3 C, where x = 0, 1, 3, and 9.

4.4 Conclusion

Active ceramic filler LAGP in solid polymer electrolyte PEO has been studied in terms of electrochemical performance, as well as investigation into ion transport mechanism through electrical impedance spectroscopy. EIS revealed the optimal loading of LAGP in PEO to be 1:1 weight ratio with ionic conductivity of 2.46×10^{-5} S cm^{-1} at 35°C and 2.02×10^{-4} S cm^{-1} at 50°C. Full cells constructed with PEO as the cathode binder allowed for a continuous ionic pathway across the cathode-electrolyte interface in lieu of liquid electrolyte and is visualized through SEM imaging of the cross section. Galvanic cycling yielded discharge capacity of 98 mAh g^{-1} with 9.4% depreciation over 45 cycles in 50°C and at a charge rate of 0.3 C. The separation of σ_{LAGP} and $\sigma_{PE/GB}$ through the "brick layer" model allowed for a better understanding of the overall ionic transport and quantified the resistance along both the bulk LAGP as well

as the polymer phase pathways, where the polymer phase is found to be a major bottleneck especially at lower temperatures. This allows for strategic targeting of near-room-temperature improvement of the polymer phase to advance this composite electrolyte towards being more practical.

Chapter 5 Ionic Liquid EMITFSI Modified PEO-LAGP Electrolyte

Given the poor ionic conductivity in the polymer phase in a PEO-LAGP electrolyte, as studied in previous chapter, a strong candidate for plasticizing the PEO phase without further increasing the tortuosity of the ionic pathway in order to increase its ionic conductivity is ionic liquid EMITFSI to form PEO-LAGP-yEMITFSI (PLE, where $y=m_{EMITFSI}/m_{PEO}\times100\%$). The ionic liquid functions as plasticizer by locally disrupting the crystalline formation of PEO as shown below in Figure 5.1, as well as weakening the O-Li bond on the PEO chains to decrease binding energy. Both of these effect culminate in an increased ionic conductivity. By plasticizing PEO, the voids between PEO and LAGP will decrease, increasing wetting and achieving higher over all conductivity as well as represented in Figure 5.2. Herein, by introducing ionic liquid EMITFSI, this chapter will explore the effects on the ceramic-polymer electrolyte by studying the physical and electrochemical properties of a polymer-ceramic-ionic liquid composite electrolyte.

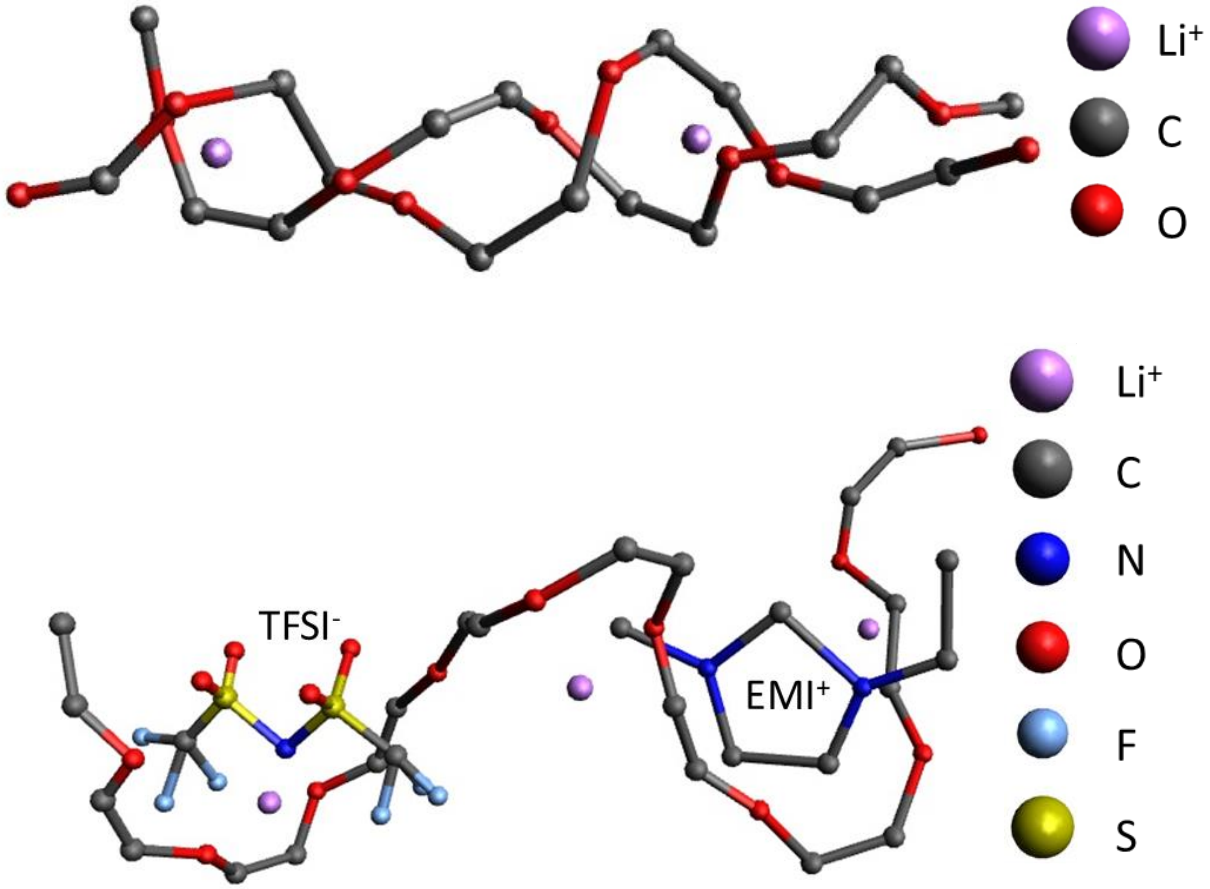

Figure 5.1 Crystalline PEO chains in double helix structure with lithium ions, and amorphous PEO chains being disrupted by EMITFSI

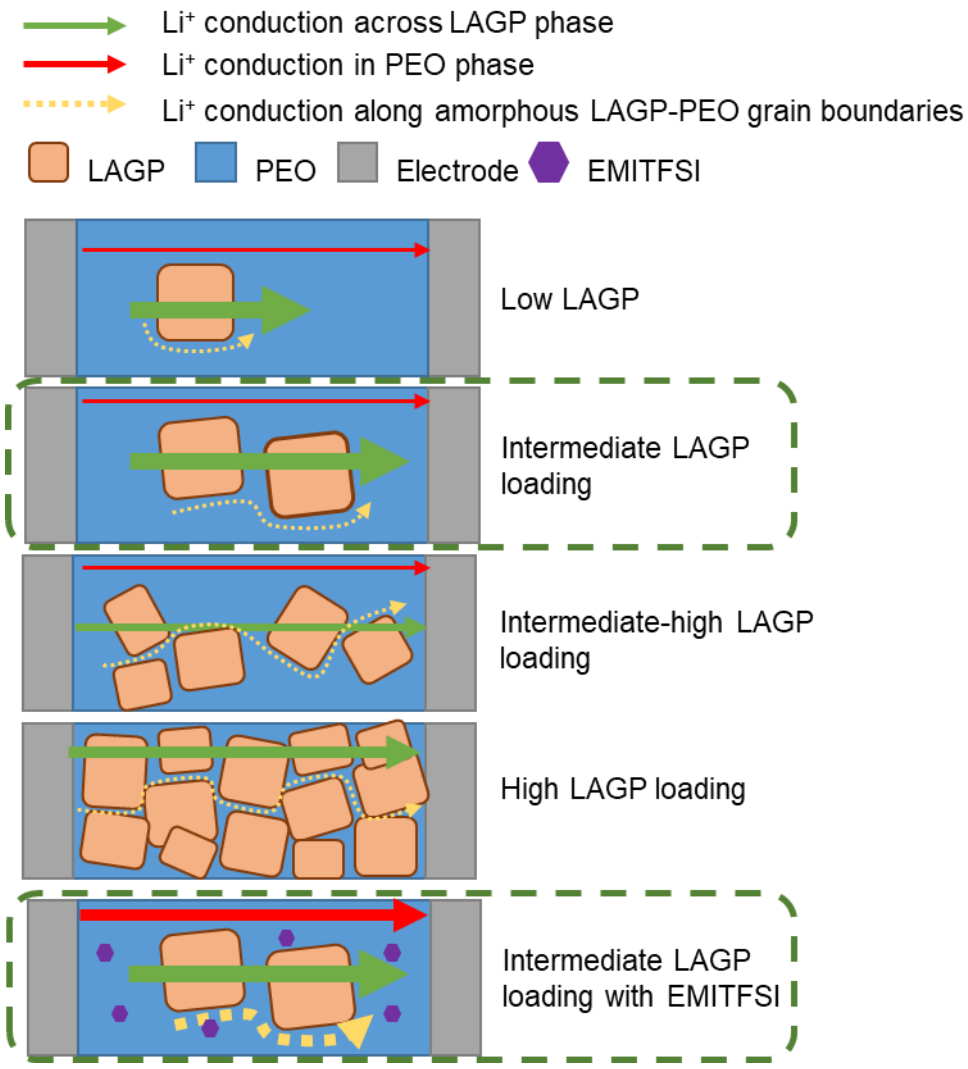

Figure 5.2 Schematic of ion transport pathways with EMITFSI modification

5.1 Physical Characterization (XRD, DSC, SEM)

5.1.1 X-ray Diffraction (XRD)

XRD patterns for LAGP powder, PEO_{16}LiTFSI, PEO_{16}LiTFSI-LAGP, and PEO_{16}LiTFSI-LAGP with varying EMITFSI content (0-40%) are presented in Figure 5.3**.** Peaks at $2\theta = 19°$ and 23° are assigned to the crystalline phase of PEO. As ionic liquid content increases, the peaks are less prominent, indicating the decrease of PEO's crystalline phase. This is consistent with reports of EMITFSI's ability to plasticize PEO.

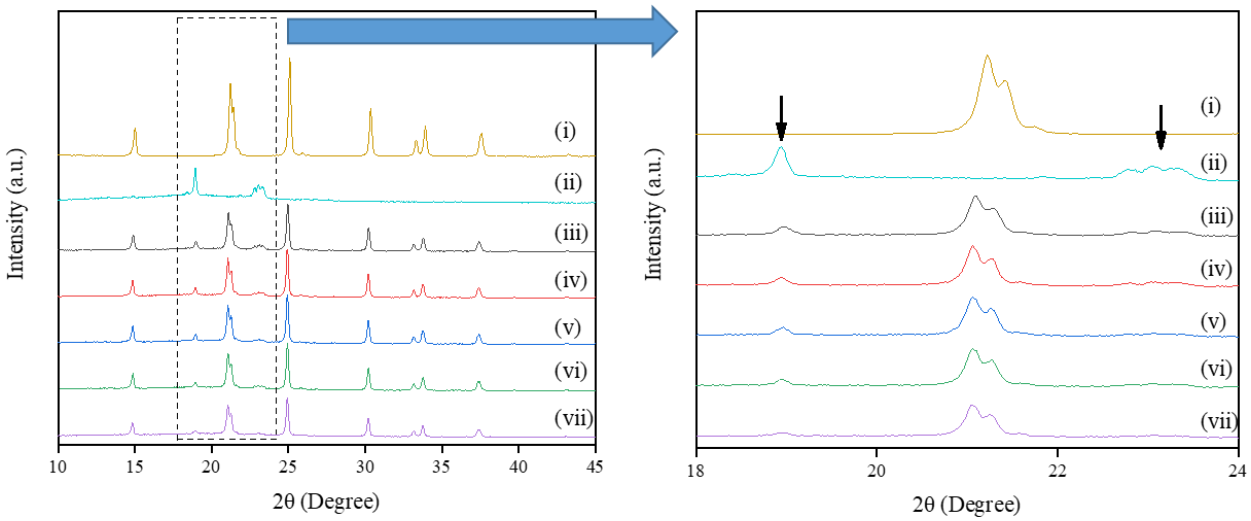

Figure 5.3 XRD patterns of electrolytes. (i) LAGP powder. (ii) $PEO_{16}LiTFSI$. (iii)-(vii) $PEO_{16}LiTFSI$-LAGP with 0%, 10%, 20%, 30%, and 40% EMITFSI respectively. Reproduced with permission from *J. Electrochem. Soc*., 166, H205 (2019). Copyright 2019, The Electrochemical Society [110].

5.1.2 Differential scanning calorimetry (DSC)

PLE electrolyte with varying EMITFSI content are analyzed through DSC to investigate their glass transition temperature (T_g) and melting temperature (T_m). The DSC thermograms are shown in Figure 5.4 from -80°C to 90°C with arbitrary heat flow units, normalized to the mass of each sample.

T_g is the transition point at which the crystalline polymer begins to convert to amorphous glass phase at temperatures above T_g. It is indicative of the polymer chains' microscopic viscosity and mobility. It is generally accepted that ion conduction practically starts at above T_g, so it is beneficial for ionic conductivity to have a lower T_g value[111][112][113].

Temperatures above T_m indicates complete melting of the polymer. The melted phase of PEO can allow for a much higher ionic conductivity due to the lowered viscosity and increased polymer chain movement. However, structural integrity can be become an issue if operation temperature is much higher than the melting point, at which point the viscosity of PEO can be too low to act as a separator.

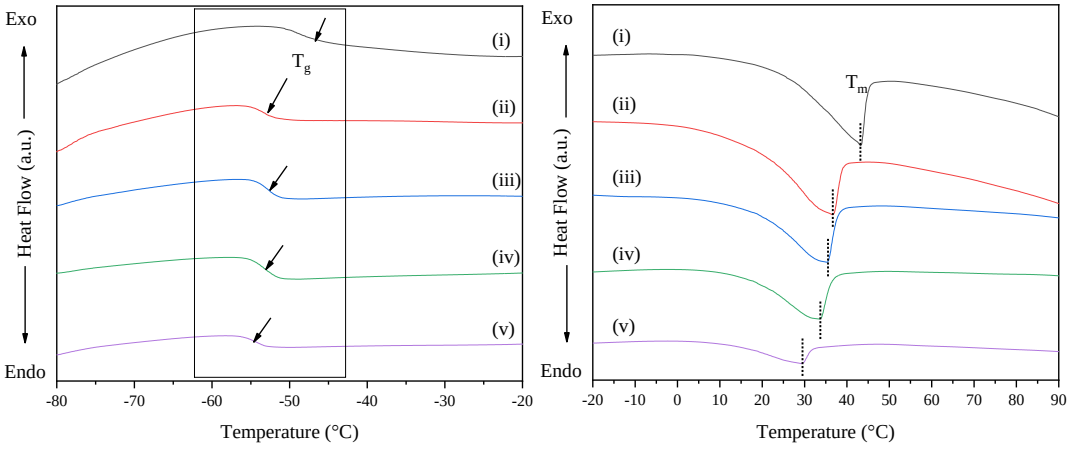

Figure 5.4 DSC thermograms of PEO_{16}LiTFSI-LAGP electrolyte with (i) 0% EMITFSI, (ii) 10% EMITFSI, (iii) 20% EMITFSI, (iv) 30% EMITFSI, and (v) 40% EMITFSI. Reproduced with permission from *J. Electrochem. Soc*., 166, H205 (2019). Copyright 2019, The Electrochemical Society [110].

The tabulated data of T_g and T_m are summarized below in Table 5.1. The melting enthalpy (ΔH_m), and relative degree of crystallinity (X_c) values of different samples are calculated, where X_c is calculated based on the melting enthalpy of 100% crystalline PEO (203.0 J g^{-1}).

The T_g values drop by 4.7 degrees at 10% EMITFSI followed by a slight increase with 20% and 30% EMITFSI and finally drops further to -54.5°C with 40% EMITFSI. T_m on the other hand shows consistent decrease with increasing EMITFSI content. On the other hand, T_m continuously decreases with increasing EMITFSI. It can also be seen from Figure 5.4 the dip in heat flow during the melting phase decreases with increasing EMITFSI content. Given that more energy is required to melt polymer containing more crystalline phase, the amount of crystalline phase (X_c) can be calculated by the percentage of actual melting enthalpy divided by 203.0 J g^{-1}, resulting in decreasing degree of crystallinity with addition of ionic liquid, down to X_c=12.4% at 40% EMITFSI loading. This is consistent with the XRD results.

Table 5.1. T_g, T_m, ΔH_m, and X_c of composite polymer electrolytes obtained from DSC thermogram

Ionic Liquid Content	T_g (°C)	T_m (°C)	ΔH_m (J/g)	X_c (%)
0% EMITFSI	-49.3	43.2	90.8	42.5
10% EMITFSI	-54.3	36.5	80.8	37.8
20% EMITFSI	-53.5	35.2	71.4	33.4
30% EMITFSI	-53.2	33.5	58.0	27.2
40% EMITFSI	-54.3	29.2	26.4	12.4

The change in morphology is subtle but under SEM imaging as shown in Figure 5.5. Due to the rigid powdery nature, the stacking of LAGP particles contributes to a rugged pellet surface, resulting in serious ion transfer barriers at the electrode/electrolyte interface and sluggish battery electrochemistry. By contrast, the PLE electrolyte membrane shows much smoother surface with LAGP homogeneously embedded within the PEO matrix This further supports the improvement in electrolyte performance with EMITFSI. The obtained electrolyte membrane delivers strong structural integrity and good flexibility in comparison with LAGP pellet and PL electrolyte membrane as shown in Figure 5.5(insets). This solution-based preparation is facile and efficient, which is highly favorable for large-scale fabrication.

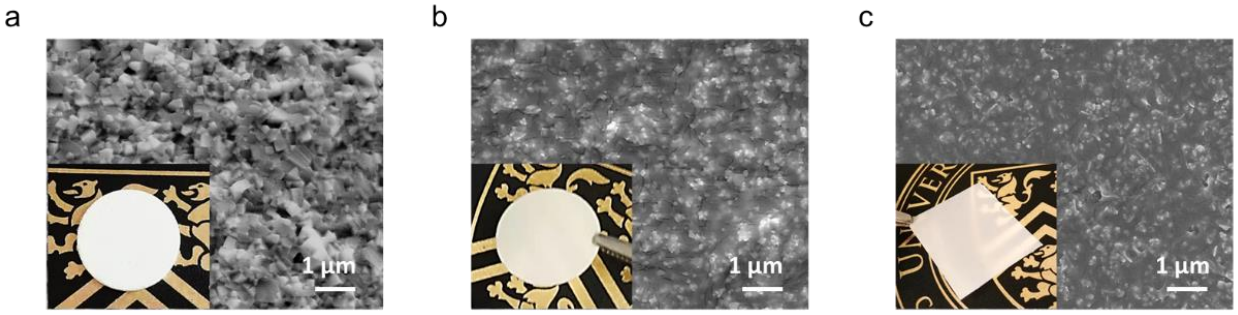

Figure 5.5 SEM and optical images (insets) of (a) LAGP pellet, (b) PL membrane and (c) PLE membrane with 30% EMITFSI. Reproduced with permission from *J. Electrochem. Soc*., 166, H205 (2019). Copyright 2019, The Electrochemical Society [110].

5.2 Electrochemical Characterization

5.2.1 Ionic Conductivity

Ionic liquid EMITFSI is mixed into PEO_{16}LiTFSI-LAGP at varying weight percentages relative to PEO ($y = m_{EMITFSI}/m_{PEO} \times 100\%$) to form PEO_{16}LiTFSI-LAGP-y EMITFSI (PLE) composite polymer electrolyte. The SS|PLE|SS cells are tested from 30 to 65°C. The Nyquist plots at 30°C, along with the proposed equivalent circuit is a shown in Figure 5.6. When broken down and separated, Arrhenius plot for σ_{LAGP}, $\sigma_{PE/GB}$, and σ_{Total} is presented in Figure 5.7.

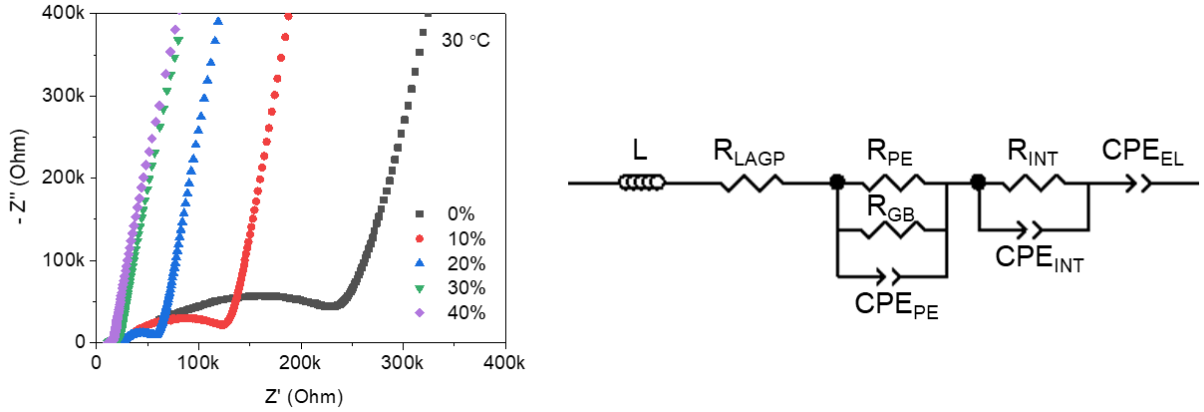

Figure 5.6 Nyquist plot and equivalent circuit for SS|PEO_{16}LiTFSI-LAGP-yEMITFSI|SS at 30°C. Reproduced with permission from *J. Electrochem. Soc*., 166, H205 (2019). Copyright 2019, The Electrochemical Society [110].

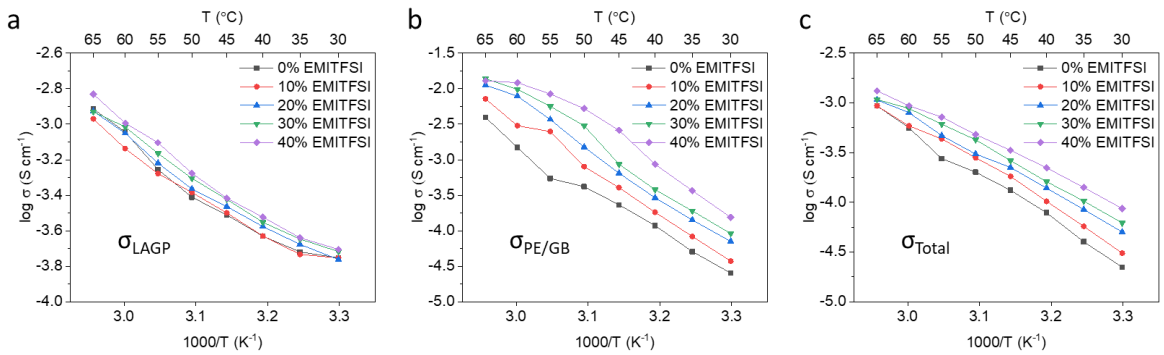

Figure 5.7 ionic conductivity attributed to a) LAGP, b) PEO/PEO-LAGP grain boundary, and c) total bulk conductivity of PLE electrolyte with different of EMITFSI weight content at different temperature. Reproduced with permission from *J. Electrochem. Soc*., 166, H205 (2019). Copyright 2019, The Electrochemical Society [110].

The Arrhenius plot for bulk LAGP conductivity again follows a relatively straight line as is the case for most solid ceramic electrolytes. σ_{LAGP} generally continuously increases with increasing EMITFSI with exception of 10% EMITFSI where it mostly overlaps with 0% and is within margin of error. However, the general increase in σ_{LAGP} can possibly be attributed to the clear improvement in $\sigma_{PE/GB}$. As previously shown in Figure 5.5, with increasing EMITFSI, gaps and cracks in the electrolyte may decrease. This coupled with the improved conductivity in the polymer phase suggests the boundary between LAGP-PEO may have become easier to overcome with increasing EMITFSI and allows for more utilization of bulk LAGP conduction and hence increase in σ_{LAGP}. Arrhenius plot for polymer/grain boundary shown in Figure 5.7b resembles a polymer electrolyte following VTF relation. However, with increasing EMITFSI content, the classic ionic conductivity transition point becomes less clear due to the plasticizing effect of EMITFSI and the decreased T_m shifts the transition point to lower temperatures.

Given EMITFSI's ability to enhance both bulk LAGP and polymer phase conduction, it is to no surprise that the total bulk ionic conductivities of the CPEs increase with increasing ionic liquid content as shown as in Figure 5.7c. This trend is in agreement with gel PEO-Ionic liquid electrolytes without active ceramic fillers[114]. At 40% EMITFSI, the ionic conductivity of the PLE is merely 3 times lower than a sintered LAGP pellet at 35°C and 6 times higher compared to without, as compared in Figure 5.8.

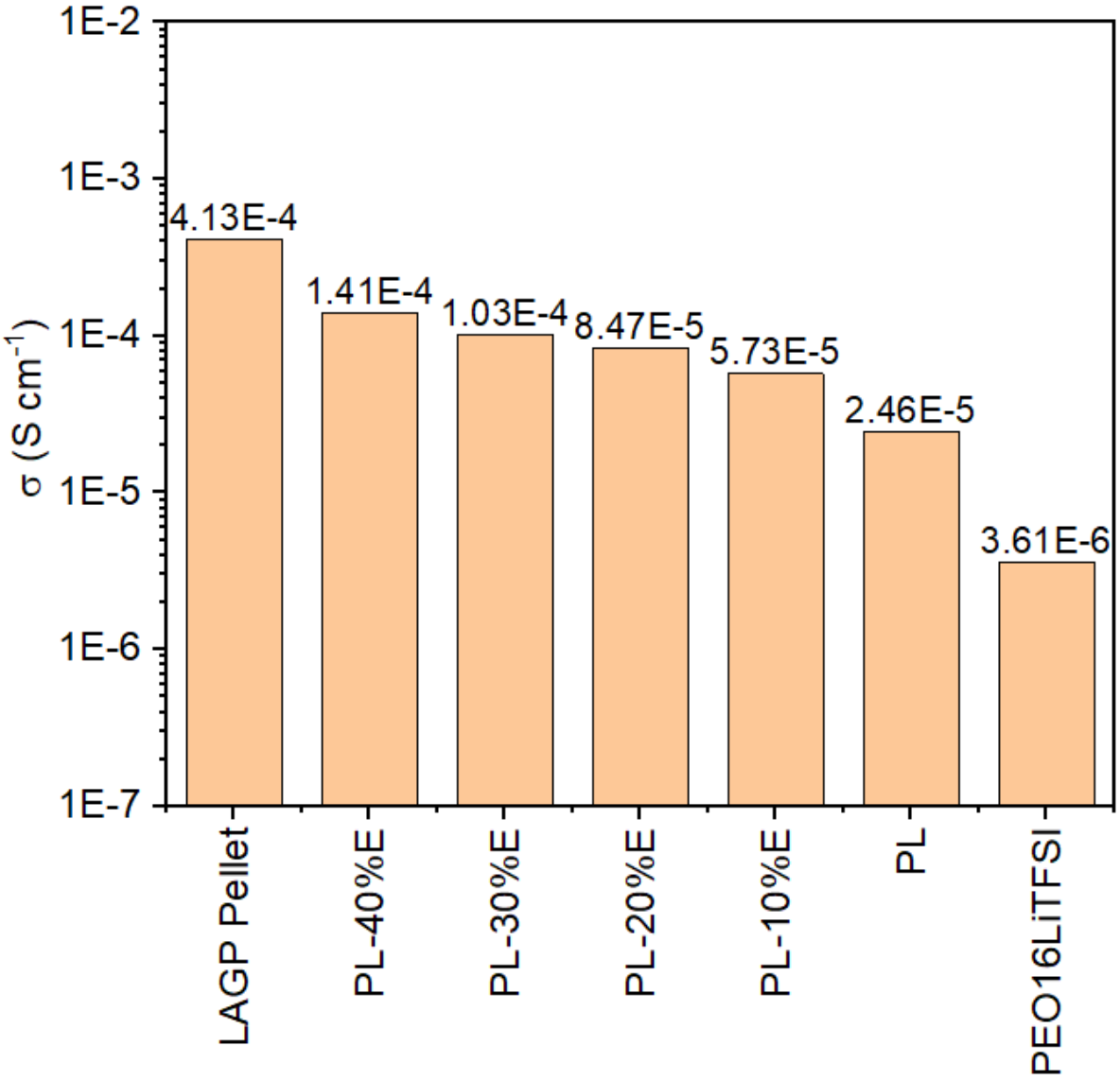

Figure 5.8. Ionic conductivity comparison at 35°C

5.2.2 Li^+ Transference Number

Despite EMITFSI seemingly is able to continuously improve the performance of this PLE in terms of ionic conductivity, the effective lithium ion conductivity needs to take into account the Li^+ transference number (t_{Li+}). This is due to ionic conductivity obtained through EIS accounts for impedance for all ionic transfer, including $TFSI^-$, EMI^+, and other possible side products ions produced through reactions against the electrodes. This results in ionic conductivities which appear higher than the actual ability of the

electrolyte to conduct Li+, so lithium ion conductivity (σ_{Li+}) is defined as the product between total ionic conductivity and Li^+ transference number, where $\sigma_{Li+} = \sigma_{Total} \times t_{Li+}$. LAGP is known to be a single ion conductor, transferring only Li^+ ions allows for $t_{Li+} \approx 1$ while ionic liquids such as EMITFSI have $t_{Li+} \approx 0.5$. Transference number is correlated to efficiency as well as rate capability. Thus it is important to investigate the impact of EMITFSI on the transference number of the composite polymer electrolyte PEO_{16}LiTFSI-LAGP-y EMITFSI.

EIS is performed on Li|CPE|Li cells at 50°C before and after 5 hours of polarization, and shown in Figure 5.9. Polarization of composite electrolytes is conducted at 50°C at 10 mV for 5 hours, the first 50 minutes of the measured current is shown in Figure 5.10.

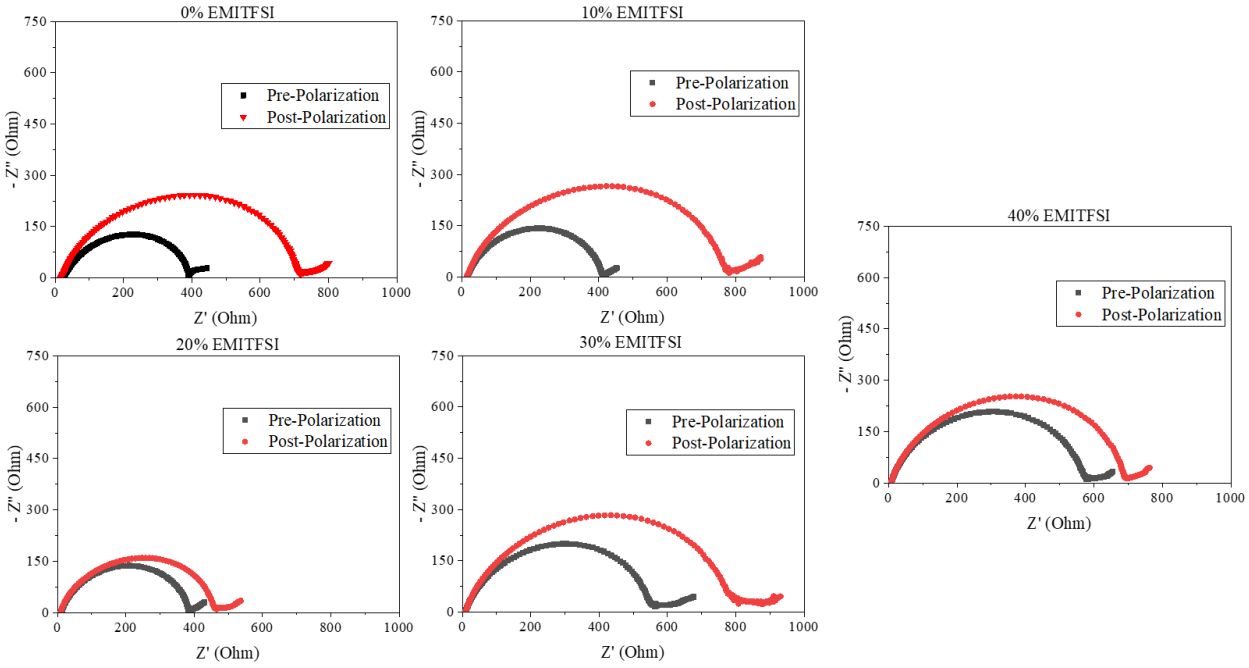

Figure 5.9. Impedance spectroscopy of Li|PLE|Li before and after polarization at 50°C. Reproduced with permission from *J. Electrochem. Soc*., 166, H205 (2019). Copyright 2019, The Electrochemical Society [110].

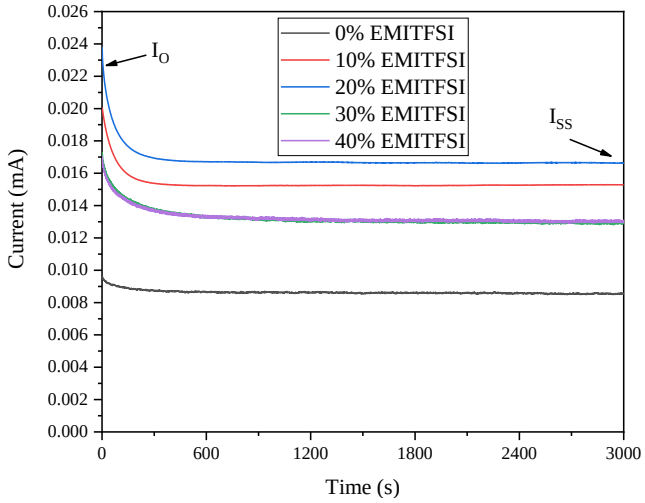

Figure 5.10. DC polarization of Li|PLE|Li at 50°C at 10 mV. Reproduced with permission from *J. Electrochem. Soc.*, 166, H205 (2019). Copyright 2019, The Electrochemical Society [110].

As shown in Table 5.2 the composite electrolyte without EMITFSI has a high lithium transference number of 0.88. The addition of 10% EMITFSI shows a decline to 0.77, followed by diminishing decline as further EMITFSI is added. It has been shown that the increase of EMITFSI concentration in PEO allows the anions to diffuse much quicker and easier than Li^+[115]. So although ionic conductivity increases with EMITFSI content, the contribution from anions also increases in proportion.

Table 5.2. Calculation of t_{Li+} utilizing Vincent-Evans equation. Reproduced with permission from *J. Electrochem. Soc.*, 166, H205 (2019). Copyright 2019, The Electrochemical Society [110].

Sample	ΔV (V)	$R_{B,o}$ (Ω)	$R_{B,SS}$(Ω)	I_o (A)	I_{SS} (A)	t_{Li+}	σ_{Li+} (S cm^{-1})
0% EMITFSI	0.01	20.989	17.111	9.64×10^{-6}	8.56×10^{-6}	**0.88**	**2.01×10^{-4}**
10% EMITFSI	0.01	15.148	13.900	1.96×10^{-5}	1.53×10^{-5}	**0.77**	**2.81×10^{-4}**
20% EMITFSI	0.01	10.763	8.890	2.38×10^{-5}	1.76×10^{-5}	**0.73**	**3.07×10^{-4}**
30% EMITFSI	0.01	9.043	9.002	1.73×10^{-5}	1.25×10^{-5}	**0.72**	**4.26×10^{-4}**
40% EMITFSI	0.01	7.846	7.561	1.71×10^{-5}	1.24×10^{-5}	**0.72**	**4.82×10^{-4}**

5.2.3 Stability testing (LSV)

Linear sweep voltammetry (LSV) is crucial to examine the stability of electrolyte. Al|CPE|Li cells were scanned from OCV to - 0.2 V and 6.5 V with aluminum current collector and lithium metal as working and counter electrode respectively and shown in Figure 5.11. As shown in the figure, PEO-LAGP composite without EMITFSI delivers anodic stability limit of around 4.2 V where oxidation of $TFSI^-$ is presumed to occur, while its cathodic stability limit is roughly 0 V. As EMITFSI is introduced into PEO-LAGP electrolyte, the cathodic stability limit was narrowed to around 1.5 V ascribed to the reduction of EMI^+ cation. Interestingly, the anodic limit of PLE electrolyte firstly expands to around 5.5 V and then decreases to around 4 V when a high EMITFSI content of 40% is added. The ability of EMITFSI to increase the anodic stability of PEO has been demonstrated. The decrease at 40% EMITFSI is likely due to the increase in oxidation reaction of $TFSI^-$ overcoming such effect and thus lowering the anodic stability. The overall stability windows for PLE electrolytes with less than 40% EMITFSI can reach around 4.0 V and cover the working voltage windows of most cathode materials. However, the relatively narrow stability limit of 40% EMITFSI sample may still cause unwanted decomposition of electrolyte during cycling and obstruct the electrochemical reversibility in the according cells.

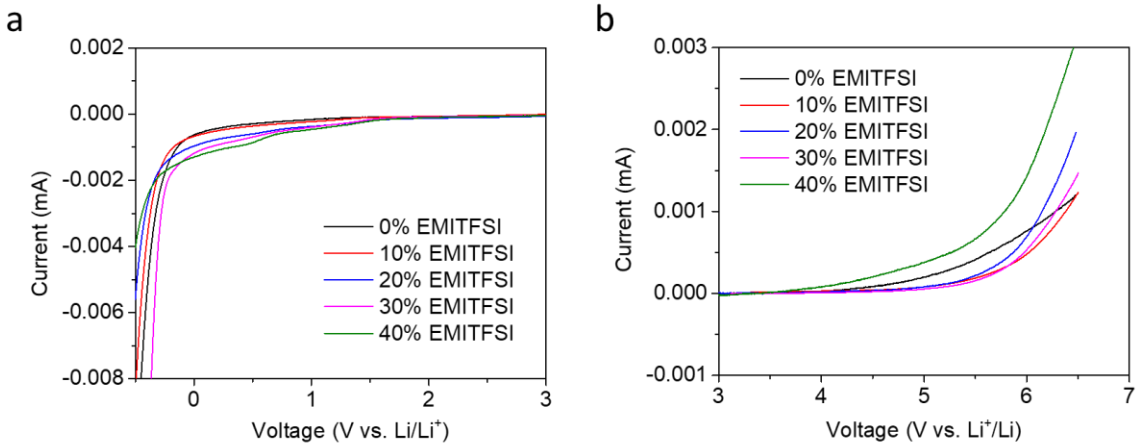

Figure 5.11. Linear sweep voltammetry of Al|PLE|Li cells with various EMITFSI content, scanned at 0.1 mV s^{-1}. Reproduced with permission from *J. Electrochem. Soc.*, 166, H205 (2019). Copyright 2019, The Electrochemical Society [110].

5.3 Galvanic Cycling

$LiFePO_4$|PLE|Li cells were fabricated into coin cells and tested through galvanic cycling. The main parameters of interest are:

1. Deliverable capacity and retention of discharge capacity over charge-discharge cycling
2. Rate capability
3. Coulombic efficiency

As shown in Figure 5.12, $LiFePO_4$|PLE|Li were cycled at 50°C, 48 mA g^{-1} (0.3C) for 125 cycles. Each sample contains 0%, 10%, 20%, 30%, and 40% EMITFSI. The highest initial discharge capacity of 146.71 mAh g^{-1} comes from 40% EMITFSI, likely due to its high ionic conductivity of 6.95×10^{-4} S cm^{-1}. However, 40% EMITFSI shows the largest loss in capacity, retaining 72.7% of its initial capacity over 125 cycles. 30% EMITFSI showed slightly lower initial capacity but retained its capacity better, with 74.9% retention over 125 cycles. CPE containing 20% EMITFSI showed good capacity retention of 79.6% and shares a similar initial discharge capacity compared to 10% EMITFSI.

All samples containing EMITFSI resulted in higher capacities over 125 cycles. This is consistent with ionic conductivity results obtained where $\sigma_{40\%\ EMITFSI} > \sigma_{30\%\ EMITFSI} > \sigma_{20\%\ EMITFSI} > \sigma_{10\%\ EMITFSI} > \sigma_{0\%\ EMITFSI}$. CPE containing 30% EMITFSI showed the most favourable deliverable capacity over 125 cycles.

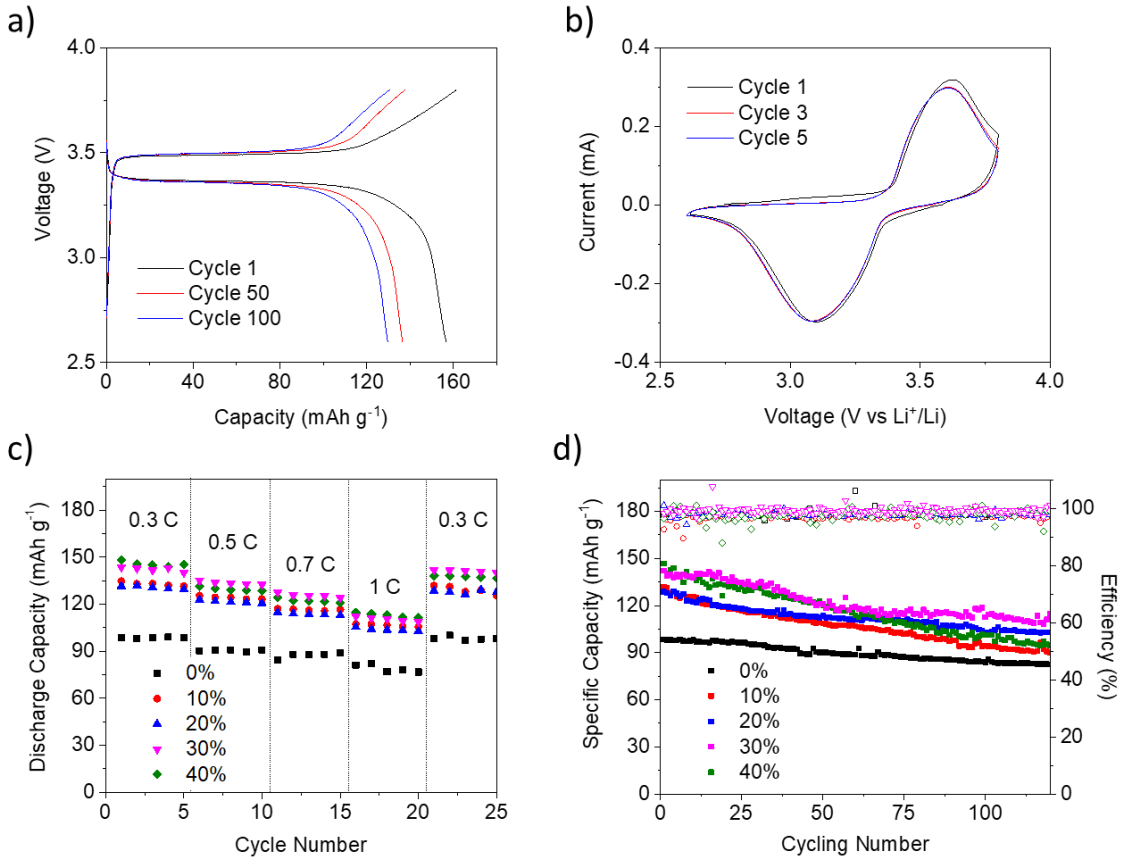

Figure 5.12 Discharge capacity of $LiFePO_4$|CPE|Li cells, where CPE contains various EMITFSI content, cycled at 50°C at current density of 48 mA g^{-1} (0.3 C). Reproduced with permission from *J. Electrochem. Soc*., 166, H205 (2019). Copyright 2019, The Electrochemical Society [110].

The charge/discharge profile is compiled below in Figure 5.13. The over-potential between the charge and discharge plateau increases continuously with EMITFSI content. The increasing over-potential is due to the decreasing t_{Li+}, where more energy is used to shuttle ions which do not participate in energy storage or discharge. At 40% EMITFSI, the over-potential clearly increases with cycle number. This can be ascribed to the instability of PL-40%E against lithium metal as demonstrated previously through LSV. The instability likely caused a continuous growth of SEI layer, requiring more and more energy to overcome, resulting in increasing over-potential as well as drastically decreased capacity.

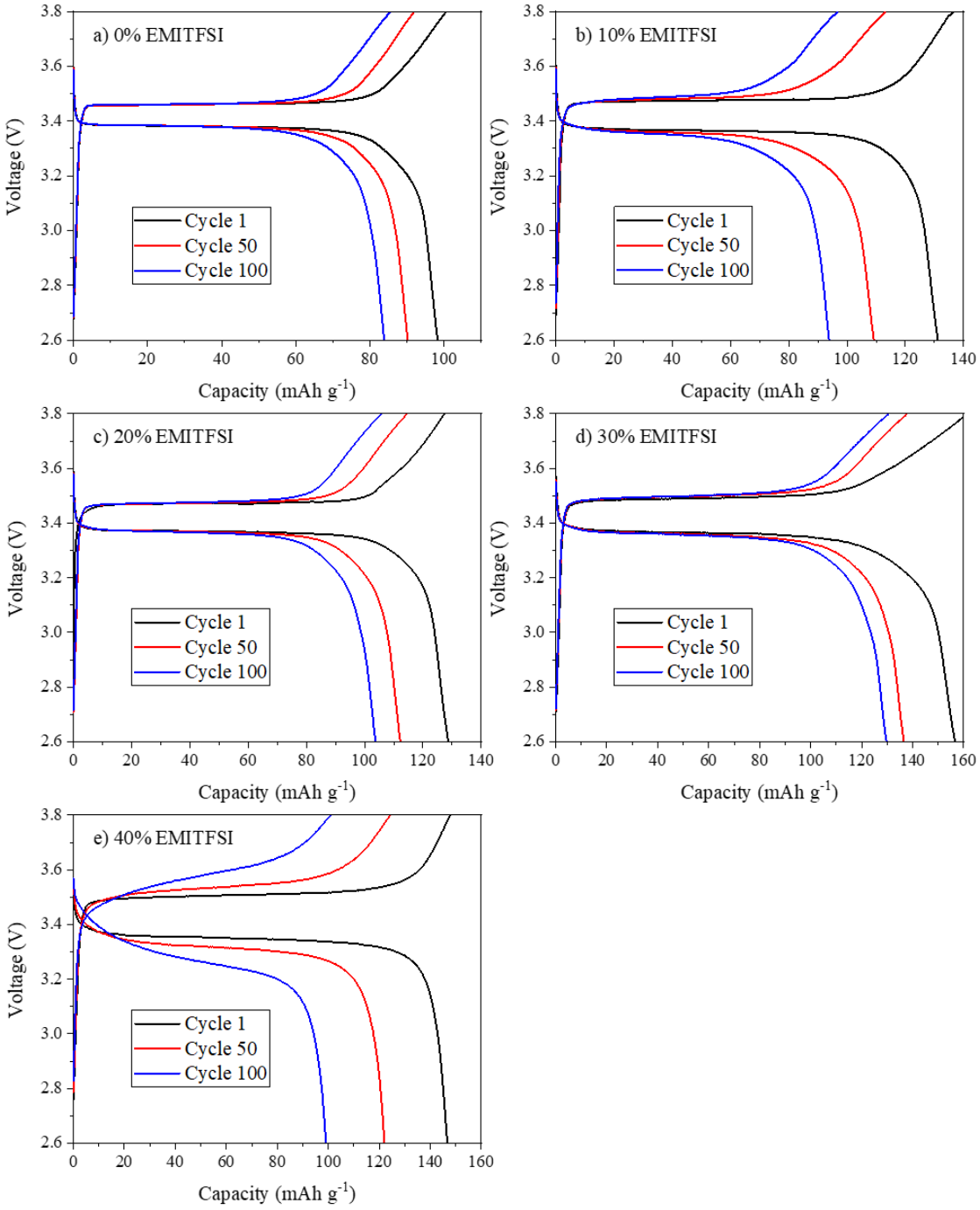

Figure 5.13 Charge-discharge profile of $LiFePO_4$|CPE|Li where the CPE contains, a) 0% EMITFSI, b) 10% EMITFSI, c) 20% EMITFSI, d) 30% EMITFSI, and e) 40% EMITFSI. Cycling performed at 50°C at current density of 48 mA g^{-1} (0.3 C). Reproduced with permission from *J. Electrochem. Soc*., 166, H205 (2019). Copyright 2019, The Electrochemical Society [110].

Impedance testing was performed on the full cells at the beginning of cycle 1 and 100 and plotted in Figure 5.14. The high frequency semi-circle is ascribed to lithium diffusion in the SEI layer. From 0-30% EMITFSI, this had minimal increase over 100 cycles. However, at 40% EMITFSI, the SEI resistance increased by over 100 times, in-line with the LSV results showing an unstable SEI layer. The second semicircle refers to charge transfer impedance at electrode-electrolyte interface, where the impedance increases more with higher EMITFSI content. Charge transfer impedance increased with EMITFSI content due to the lowering of t_{Li+}, where low t_{Li+} indicates shuttling of non-Li+ ions to the surface of the electrodes, impeding the charge transfer process. However, PL-30%E cell still shows the lowest total impedance by cycle 100 and is reflected in having the highest retained capacity and high rate capabilities.

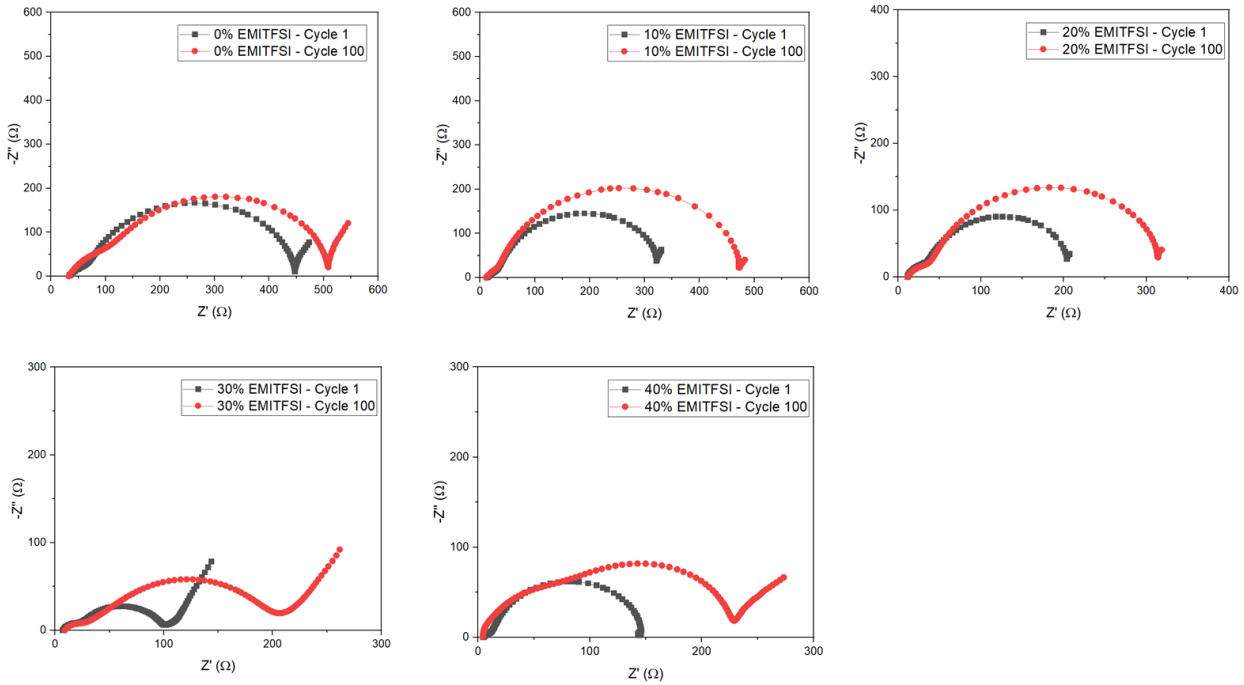

Figure 5.14. Nyquist plot of LFP|PEO_{16}LiTFSI-LAGP-yEMITFSI|Li at the beginning of cycle 1 and 100

5.3.1 Coulombic Efficiency

As shown in Figure 5.15 and Table 5.3, the average coulombic efficiencies of the CPE are compared with a conventional liquid electrolyte containing 1 M $LiPF_6$ in EC/DEC, soaked into a polypropylene membrane. Liquid electrolyte shows the lowest average coulombic efficiency of 94.07%, which is consistent with literature results which states organic solvents such as EC and DEC are thermodynamically unstable against lithium metal. Over time, with a low coulombic efficiency, the liquid electrolyte can be depleted due to parasitic reactions.

CPE with 30% EMITFSI showed the highest average coulombic efficiency of 99.19%, while 40% EMITFSI showing a quicker capacity fading is directly reflected in its lower coulombic efficiency of 97.85%.

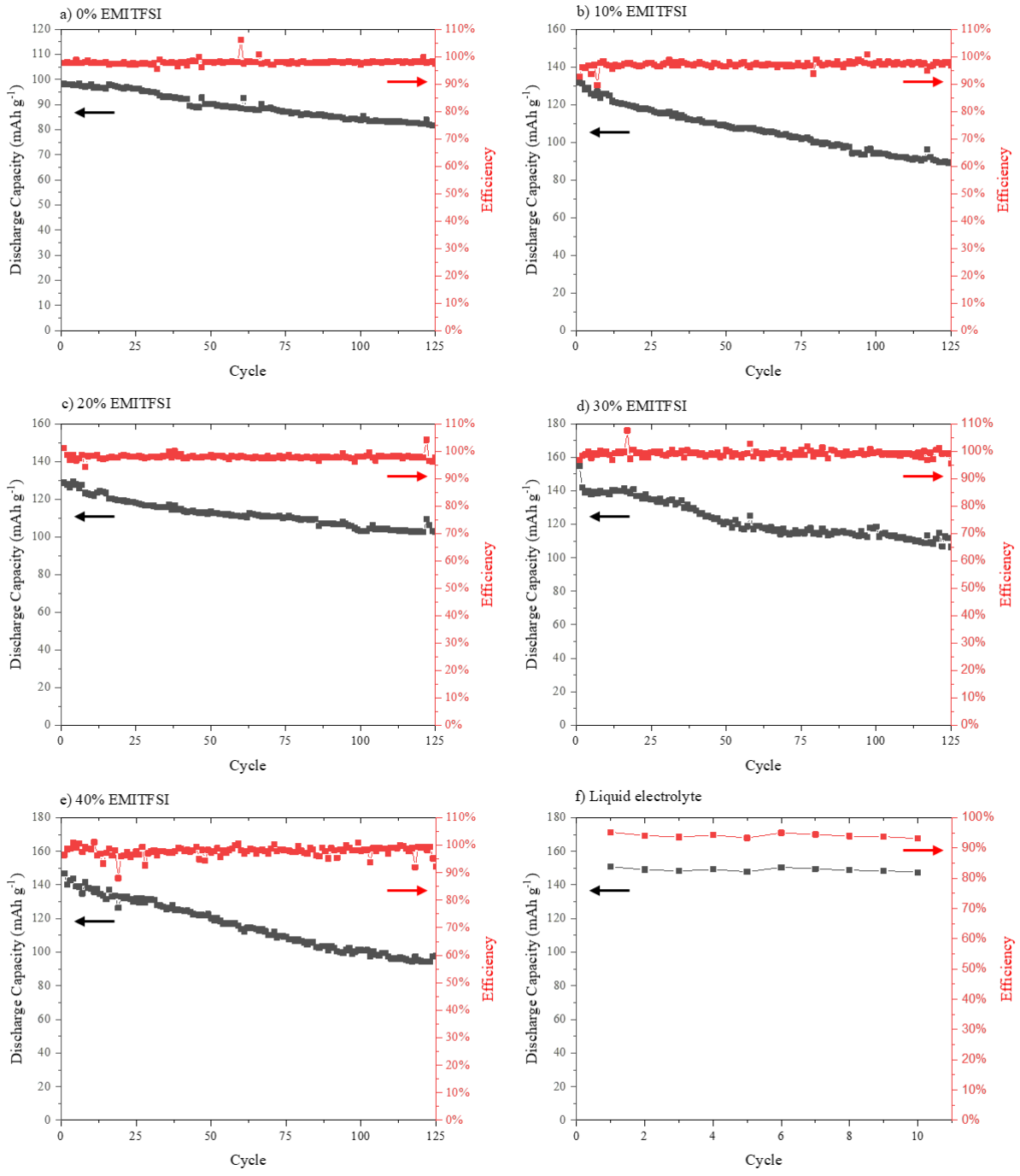

Figure 5.15 Discharge capacity and coulombic efficiency of $LiFePO_4$|CPE|Li with CPE containing a) 0% EMITFSI, b) 10% EMITFSI, c) 20% EMITFSI, d) 30% EMITFSI, and e) 40% EMITFSI cycled at 50°C, at current density of 48 mA g-1 (0.3 C). f) Discharge capacity and coulombic efficiency of $LiFePO_4$|LE|Li cell cycled at 50°C, at current density of 48 mA g^{-1} (0.3 C).

Table 5.3. Summary of coulombic efficiency for charge-discharge cycles performed at 50°C, at 48 mA g-1 (0.3 C)

Electrolyte		Coulombic Efficiency
PEO_{16}LiTFSI-LAGP +	0% EMITFSI	97.94%
	10% EMITFSI	97.11%
	20% EMITFSI	97.92%
	30% EMITFSI	99.19%
	40% EMITFSI	97.85%
Liquid Electrolyte ($LiPF_6$ with EC/DEC in PP)		94.07%

5.3.2 Post Cycling Evaluation

To evaluate the impact of lowered mechanical strength due to the addition of ionic liquid, it is important to verify any migration of the active cathode material LFP due to the weakening of the PEO binder. All the previous full cells were disassembled with the lithium anode removed. The cathode-electrolyte layers were then dipped into liquid nitrogen to freeze before cutting to reveal the cross section under SEM imaging. EDS for Fe and Ge were performed on the cross section as compiled in Figure 5.16. It is seen that despite operating at above melting point for EMITFSI-modified-PEO, the structural integrity is sufficient to trap the LFP in the cathode.

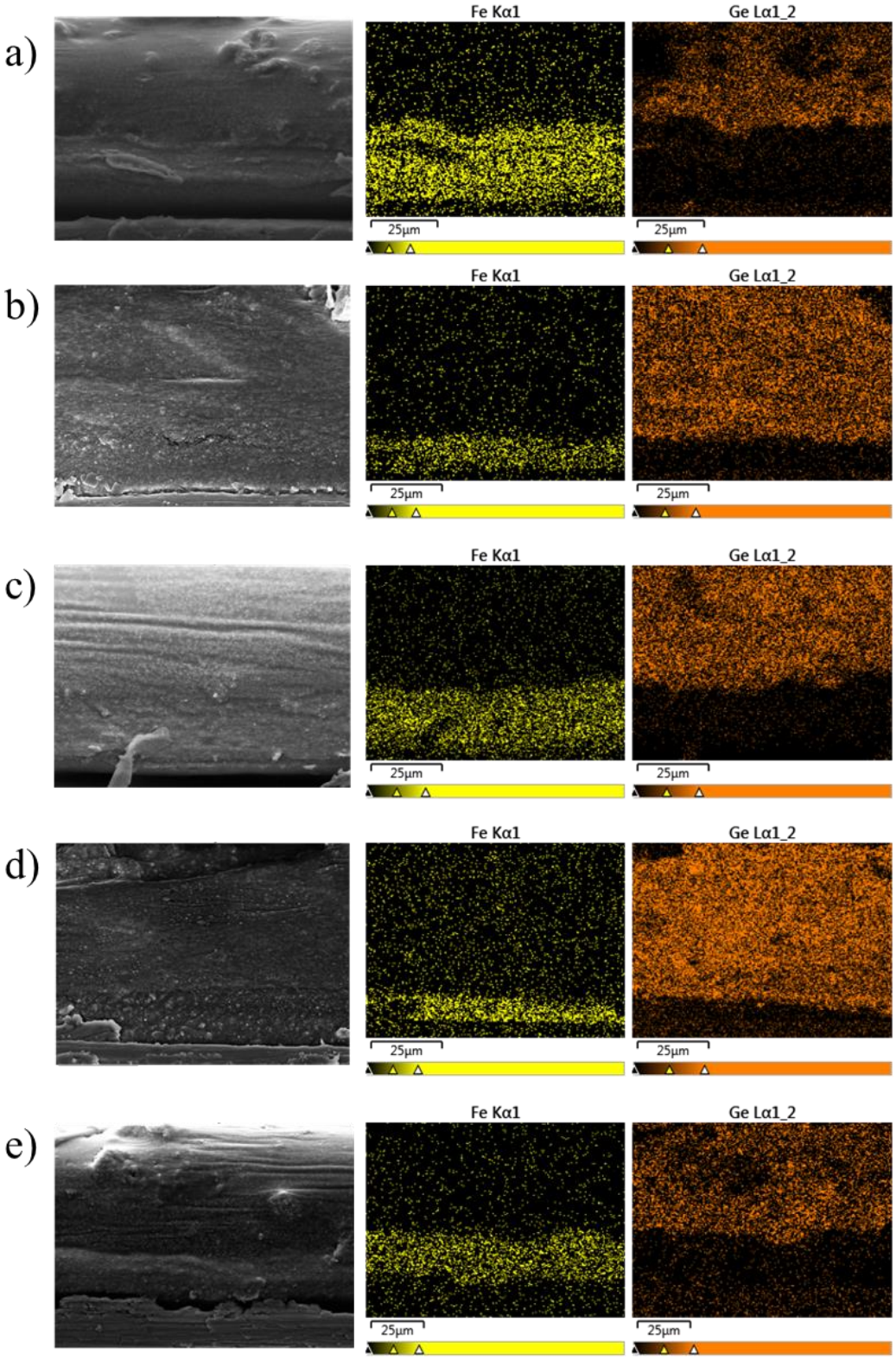

Figure 5.16 Cross-section SEM image and EDS mapping of $LiFePO_4$|CPE|Li cells with CPE containing a)

0% EMITFSI, b) 10% EMITFSI, c) 20% EMITFSI, d) 30% EMITFSI and e) 40% EMITFSI after cycling for > 125 cycles.

5.4 Conclusion

Upon the optimized LAGP loading in PEO electrolyte, further modification by addition of 30% liquid electrolyte EMITFSI relative to PEO weight, served to improve ionic conductivity by 4 times compared to without, to 1.03×10^{-4} S cm^{-1} at 35°C (4.26×10^{-4} S cm^{-1} at 50°C) and extend the electrochemical stability window of the composite electrolyte against lithium anode. With the optimized 30% EMITFSI, 139 mAh g^{-1} was achieved at a cycling rate of 0.3 C after the first discharge, 115 mAh g^{-1} after 125 cycles, and 112.2 mAh g^{-1} was delivered at 1 C. The decrease in t_{Li+} from 0.88 to 0.72 due to addition of EMITFSI is still largely favourable when compared to solid polymer electrolytes such as PEO-lithium salt which are typically below 0.5.

Chapter 6 Final Conclusion and Future Work

The benefits in switching from conventional LIB to solid state batteries lay in safety, energy and power density, and paving the path towards a wider selection of electrode material and battery design. The current obstacle to realizing a commercial future of solid state batteries, like most commodities, are performance and cost. This thesis delivers a composite ceramic-polymer electrolyte assisted by ionic liquid, which lowers cost by lowering LAGP loading, with high total ionic conductivity surpassing similar systems with even higher ceramic loading using an easily scalable layered casting method.

While PEO is one of the most predominant and well-studied solid polymer electrolyte due to its stability against lithium, ease of manipulation, and cheap cost, appreciable performance has generally required a working temperature of at least 60 to 70°C, which severely limits its practical uses in portable energy storage. By incorporating LAGP to provide mechanical integrity while plasticizing the PEO phase through ionic liquid EMITFSI, high performance was achieved at just 50°C, where ionic conductivity reached 4.26×10^{-4} S cm^{-1} with lithium transference number of 0.72. The battery delivered 139 mAh g^{-1} initially at a cycling rate of 0.3 C after the first discharge, and depreciated to 115 mAh g^{-1} after 125 cycles, with average coulombic efficiency of 99.19%. At 1C cycling rate, 112.2 mAh g^{-1} was delivered. This may help promote the development as well as mass production of high performing solid state lithium metal batteries for a safe and productive future.

However, while this work showed promising results for up to 125 cycles, the future of batteries has a much more stringent requirement for cycle life. The nature of capacity depreciation in this work is mostly due to the imperfect SEI layer formation with EMI^+ and $TFSI^-$ ions. One proven method to extend the cycle life is through atomic layer deposition (ALD) of an artificial SEI layer such as Al_2O_3. 5 cycles of ALD deposition of Al_2O_3 were coated onto the surface of PLE as an artificial interface against lithium metal. The results can be seen below in Figure 6.1, where it is obvious the capacity fading has decreased while initial deliverable capacity remains mostly unchanged. The Al_2O_3 was coated directly onto the surface of the PLE electrolyte instead of the conventional lithium metal surface. This was done in attempt to further stream-

line the production of the battery by eliminating the possibility of exposure of lithium metal to air or contaminants and causing oxidation. This preliminary work shows that it is possible to achieve similar lithium anode protection effects by directly depositing Al_2O_3 onto a polymer electrolyte through ALD.

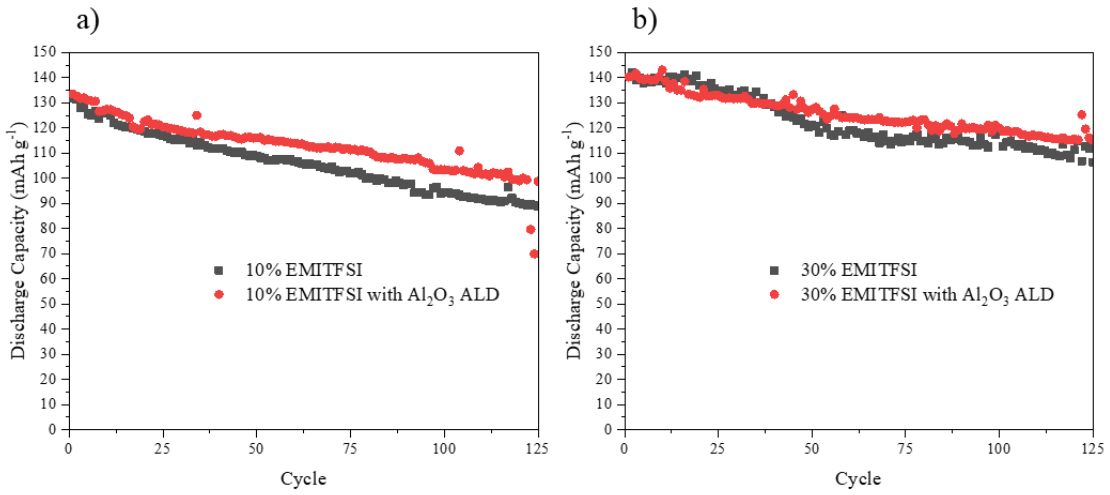

Figure 6.1 Full cell cycling comparison with and without Al_2O_3 ALD modification

Aside from surface modification to extend battery life cycle, the research and development into mass production of advance 3D structured electrolyte structure is also crucial to improving battery performance at near ambient temperature. However, in-lieu of a simple method to mass produce advance structured commercial solid electrolytes and malleable polymer electrolyte with high ambient temperature conductivity in the order of 10^{-3} S cm^{-1} or higher, layered structures of solid composite electrolytes is seemingly the current way to go.

References

[1] C. Wang *et al.*, "Suppression of Lithium Dendrite Formation by Using LAGP-PEO (LiTFSI) Composite Solid Electrolyte and Lithium Metal Anode Modified by PEO (LiTFSI) in All-Solid-State Lithium Batteries," *ACS Appl. Mater. Interfaces*, vol. 9, no. 15, pp. 13694–13702, 2017.

[2] J. O. Besenhard and H. P. Fritz, "Cathodic reduction of graphite in organic solutions of alkali and NR4 + salts," *Electroanal. Chem. Interracial Electrochem.*, vol. 53, pp. 329–333, 1974.

[3] J. O. Besenhard, "The electrochemical preparation and properties of ionic alkali metal-and NR4-graphite intercalation compounds in organic electrolytes," *Carbon N. Y.*, vol. 14, no. 2, pp. 111–115, 1976.

[4] J. Janek and W. G. Zeier, "A solid future for battery development," *Nat. Publ. Gr.*, vol. 1, no. September, pp. 1–4, 2016.

[5] X. Judez, G. G. Eshetu, C. Li, L. M. Rodriguez-Martinez, H. Zhang, and M. Armand, "Opportunities for Rechargeable Solid-State Batteries Based on Li-Intercalation Cathodes," *Joule*, vol. 2, no. 11, pp. 2208–2224, 2018.

[6] L. Gireaud, S. Grugeon, S. Laruelle, B. Yrieix, and J. M. Tarascon, "Lithium metal stripping/plating mechanisms studies: A metallurgical approach," *Electrochem. commun.*, vol. 8, no. 10, pp. 1639–1649, 2006.

[7] D. Aurbach, "The Study of Electrolyte Solutions Based on Ethylene and Diethyl Carbonates for Rechargeable Li Batteries," *J. Electrochem. Soc.*, vol. 142, no. 9, p. 2882, 1995.

[8] W. Xu *et al.*, "Lithium metal anodes for rechargeable batteries," *Energy Environ. Sci.*, vol. 7, no. 2, pp. 513–537, 2014.

[9] R. S. Thompson, D. J. Schroeder, C. M. López, S. Neuhold, and J. T. Vaughey, "Stabilization of lithium metal anodes using silane-based coatings," *Electrochem. commun.*, vol. 13, no. 12, pp. 1369–1372, 2011.

[10] J. t. T. Vaughey, G. Liu, and J.-G. Zhang, "Stabilizing the surface of lithium metal," *MRS Bull.*, vol. 39, no. 5, pp. 429–435, 2014.

[11] N. Nitta, F. Wu, J. T. Lee, and G. Yushin, "Li-ion battery materials: Present and future," *Mater. Today*, vol. 18, no. 5, pp. 252–264, 2015.

[12] J.-I. Yamaki, S.-I. Tobishima, K. Hayashi, K. Saito, Y. Nemoto, and M. Arakawa, "A consideration of the morphology of electrochemically deposited lithium in an organic electrolyte," *J. Power Sources*, vol. 74, pp. 219–227, 1998.

[13] D. Aurbach, E. Zinigrad, Y. Cohen, and H. Teller, "A short review of failure mechanisms of lithium metal and lithiated graphite anodes in liquid electrolyte solutions," *Solid State Ionics*, vol. 148, no. 3–4, pp. 405–416, 2002.

[14] I. Epelboin, "Behavior of Secondary Lithium and Aluminum-Lithium Electrodes in Propylene Carbonate," *J. Electrochem. Soc.*, vol. 127, no. 10, p. 2100, 1980.

[15] K. N. Wood *et al.*, "Dendrites and pits: Untangling the complex behavior of lithium metal anodes through operando video microscopy," *ACS Cent. Sci.*, vol. 2, no. 11, pp. 790–801, 2016.

[16] K. M. Diederichsen, E. J. McShane, and B. D. McCloskey, "Promising Routes to a High Li+Transference Number Electrolyte for Lithium Ion Batteries," *ACS Energy Lett.*, vol. 2, no. 11, pp. 2563–2575, 2017.

[17] A. R. Despic, J. Diggle, and J. O. Bockris, “Mechanism of the Formation of Zinc Dendrites,” *J. Electrochem. Soc.*, vol. 115, no. 5, pp. 507–508, 1968.

[18] K. Xu, “Nonaqueous liquid electrolytes for lithium-based rechargeable batteries,” *Chem. Rev.*, vol. 104, no. 10, pp. 4303–4417, 2004.

[19] W. D. Richards, L. J. Miara, Y. Wang, J. C. Kim, and G. Ceder, “Interface Stability in Solid-State Batteries,” *Chem. Mater.*, vol. 28, no. 1, pp. 266–273, 2016.

[20] B. Flamme *et al.*, “Guidelines to design organic electrolytes for lithium-ion batteries: Environmental impact, physicochemical and electrochemical properties,” *Green Chem.*, vol. 19, no. 8, pp. 1828–1849, 2017.

[21] D. E. Fenton, J. M. Parker, and P. V. Wright, “Complexes of alkali metal ions with poly(ethylene oxide),” *Polym. (United Kingdom)*, vol. 14, no. 11, p. 589, 1973.

[22] Z. Xue, D. He, and X. Xie, “Poly(ethylene oxide)-based electrolytes for lithium-ion batteries,” *J. Mater. Chem. A*, vol. 3, no. 38, pp. 19218–19253, 2015.

[23] D. Golodnitsky, E. Strauss, E. Peled, and S. Greenbaum, “Review—On Order and Disorder in Polymer Electrolytes,” *J. Electrochem. Soc.*, vol. 162, no. 14, pp. A2551–A2566, 2015.

[24] Z. Stoeva, I. Martin-Litas, E. Staunton, Y. G. Andreev, and P. G. Bruce, “Ionic conductivity in the crystalline polymer electrolytes PEO6:LiXF6, X = P, As, Sb,” *J. Am. Chem. Soc.*, vol. 125, no. 15, pp. 4619–4626, 2003.

[25] P. K. Singh, B. Bhattacharya, and R. K. Nagarale, “Effect of Nano-TiO2 Dispersion on PEO Polymer Electrolyte Property,” *Polymer (Guildf).*, pp. 1–5, 2008.

[26] G. X. Wang, L. Yang, J. Z. Wang, H. K. Liu, and S. X. Dou, “Enhancement of Ionic Conductivity of PEO Based Polymer Electrolyte by the Addition of Nanosize Ceramic Powders,” *J. Nanosci. Nanotechnol.*, vol. 5, no. 7, pp. 1135–1140, 2005.

[27] G. M. Hou, M. Q. Zhang, Y. F. Huang, and W. H. Ruan, “A TiO2/PEO composite incorporated with: In situ synthesized hyper-branched poly(amine-ester) and its application as a polymer electrolyte,” *RSC Adv.*, vol. 6, no. 86, pp. 83406–83411, 2016.

[28] L. Fan, C. W. Nan, and S. Zhao, “Effect of modified SiO2 on the properties of PEO-based polymer electrolytes,” *Solid State Ionics*, vol. 164, no. 1–2, pp. 81–86, 2003.

[29] R. J. Sengwa and S. Choudhary, “Dielectric and electrical properties of PEO–Al2O3nanocomposites,” *J. Alloys Compd.*, vol. 701, pp. 652–659, 2017.

[30] N. Lago, O. Garcia-Calvo, J. M. Lopezdelamo, T. Rojo, and M. Armand, “All-Solid-State Lithium-Ion Batteries with Grafted Ceramic Nanoparticles Dispersed in Solid Polymer Electrolytes,” *ChemSusChem*, vol. 8, no. 18, pp. 3039–3043, 2015.

[31] A. Sarnowska, I. Polska, L. Niedzicki, M. Marcinek, and A. Zalewska, “Electrochimica Acta Properties of poly (vinylidene fluoride- co -hexafluoropropylene) gel electrolytes containing modified inorganic Al 2 O 3 and TiO 2 filler , complexed with different lithium salts,” *Electrochim. Acta*, vol. 57, pp. 180–186, 2011.

[32] H. M. J. C. Pitawala, M. A. K. L. Dissanayake, V. A. Seneviratne, B. E. Mellander, and I. Albinson, “Effect of plasticizers (EC or PC) on the ionic conductivity and thermal properties of the (PEO) 9LiTf: Al 2O 3 nanocomposite polymer electrolyte system,” *J. Solid State Electrochem.*, vol. 12, no. 7–8, pp. 783–789, 2008.

[33] J. K. Lee, Y. J. Lee, W. S. Chae, and Y. M. Sung, “Enhanced ionic conductivity in PEO-LiClO4 hybrid electrolytes by structural modification,” *J. Electroceramics*, vol. 17, no. 2–4, pp. 941–944, 2006.

[34] H. Kasemägi, M. Klintenberg, A. Aabloo, and J. O. Thomas, “Molecular dynamics simulation of temperature and concentration dependence of the ‘filler’ effect for the LiCl/PEO/Al2O3-nanoparticle system,” *Electrochim. Acta*, vol. 48, no. 14-16 SPEC., pp. 2273–2278, 2003.

[35] C. C. Tambelli, A. C. Bloise, A. V. Rosário, E. C. Pereira, C. J. Magon, and J. P. Donoso, “Characterisation of PEO-Al2O3 composite polymer electrolytes,” *Electrochim. Acta*, vol. 47, no. 11, pp. 1677–1682, 2002.

[36] G. B. Appetecchi, S. Scaccia, and S. Passerini, “Investigation on the Stability of the Lithium-Polymer Electrolyte Interface,” *J. Electrochem. Soc.*, vol. 147, no. 12, p. 4448, 2002.

[37] E. Strauss, D. Golodnitsky, G. Ardel, and E. Peled, “Charge and mass transport properties of LiI-P(EO)n-Al2O3-based composite polymer electrolytes,” *Electrochim. Acta*, vol. 43, no. 10–11, pp. 1315–1320, 1998.

[38] X. L. Wang, A. Mei, M. Li, Y. H. Lin, and C. W. Nan, “Polymer composite electrolytes containing ionically active mesoporous SiO2 particles,” *J. Appl. Phys.*, vol. 102, no. 5, 2007.

[39] J. Syzdek, M. Armand, M. Marcinek, A. Zalewska, G. Zukowska, and W. Wieczorek, “Detailed studies on the fillers modification and their influence on composite, poly(oxyethylene)-based polymeric electrolytes,” *Electrochim. Acta*, vol. 55, no. 4, pp. 1314–1322, 2010.

[40] M. Kammoun, S. Berg, and H. Ardebili, “Flexible thin-film battery based on graphene-oxide embedded in solid polymer electrolyte,” *Nanoscale*, vol. 7, no. 41, pp. 17516–17522, 2015.

[41] S. Gomari, I. Ghasemi, and M. Esfandeh, “Effect of polyethylene glycol-grafted graphene on the non-isothermal crystallization kinetics of poly(ethylene oxide) and poly(ethylene oxide):lithium perchlorate electrolyte systems,” *Mater. Res. Bull.*, vol. 83, pp. 24–34, 2016.

[42] J. Shim, D. G. Kim, H. J. Kim, J. H. Lee, J. H. Baik, and J. C. Lee, “Novel composite polymer electrolytes containing poly(ethylene glycol)-grafted graphene oxide for all-solid-state lithium-ion battery applications,” *J. Mater. Chem. A*, vol. 2, no. 34, pp. 13873–13883, 2014.

[43] M. Kammoun, S. Berg, and H. Ardebili, “Flexible thin-film battery based on graphene-oxide embedded in solid polymer electrolyte,” *Nanoscale*, vol. 7, no. 41, pp. 17516–17522, 2015.

[44] X. Li, C. Zhang, and T. Meng, “Synergistic effects from graphene oxide nanosheets and TiO2 hierarchical structures enable robust and resilient electrodes for high-performance lithium-ion batteries,” *RSC Adv.*, vol. 6, no. 6, pp. 4321–4328, 2016.

[45] L. Cui, J. Gao, T. Xu, Y. Zhao, and L. Qu, “Polymer/Graphene Hybrids for Advanced Energy-Conversion and -Storage Materials,” *Chem. - An Asian J.*, vol. 11, no. 8, pp. 1151–1168, 2016.

[46] M. Yuan, J. Erdman, C. Tang, and H. Ardebili, “High performance solid polymer electrolyte with graphene oxide nanosheets,” *RSC Adv.*, vol. 4, no. 103, pp. 59637–59642, 2014.

[47] G. Feuillade and P. Perche, “Ion-conductive macromolecular gels and membranes.pdf,” vol. 5, pp. 63–69, 1975.

[48] F. B. Dias, L. Plomp, and J. B. J. Veldhuis, “Trends in polymer electrolytes for secondary lithium batteries,” *J. Power Sources*, vol. 88, no. 2, pp. 169–191, 2000.

[49] K. Karuppasamy *et al.*, “An enhanced electrochemical and cycling properties of novel boronic

Ionic liquid based ternary gel polymer electrolytes for rechargeable Li/LiCoO2 cells," *Sci. Rep.*, vol. 7, no. 1, pp. 1–11, 2017.

[50] L. Balo, H. Gupta, S. K. Singh, V. K. Singh, S. Kataria, and R. K. Singh, "Performance of EMIMFSI ionic liquid based gel polymer electrolyte in rechargeable lithium metal batteries," *J. Ind. Eng. Chem.*, vol. 65, pp. 137–145, 2018.

[51] M. Gouverneur, J. Kopp, L. Van Wüllen, and M. Schönhoff, "Direct determination of ionic transference numbers in ionic liquids by electrophoretic NMR," *Phys. Chem. Chem. Phys.*, vol. 17, no. 45, pp. 30680–30686, 2015.

[52] A. Unemoto *et al.*, "Development of bulk-type all-solid-state lithium-sulfur battery using LiBH4 electrolyte," *Appl. Phys. Lett.*, vol. 105, no. 8, 2014.

[53] A. Unemoto *et al.*, "Stable Interface Formation between TiS<inf>2</inf> and LiBH<inf>4</inf> in Bulk-Type All-Solid-State Lithium Batteries," *Chem. Mater.*, vol. 27, no. 15, pp. 5407–5416, 2015.

[54] S. Kim *et al.*, "Fast Lithium-Ion Conduction in Atom-Deficient closo-Type Complex Hydride Solid Electrolytes," *Chem. Mater.*, vol. 30, no. 2, pp. 386–391, 2018.

[55] M. Matsuo and S. I. Orimo, "Lithium fast-ionic conduction in complex hydrides: Review and prospects," *Adv. Energy Mater.*, vol. 1, no. 2, pp. 161–172, 2011.

[56] M. Latroche *et al.*, "Full-cell hydride-based solid-state Li batteries for energy storage," *Int. J. Hydrogen Energy*, vol. 44, no. 15, pp. 7875–7887, 2019.

[57] P. Hartwig, W. Weppner, and W. Wichelhaus, "Fast Ionic Lithium Conduction in Solid Lithium Nitride Chloride," *Mater. Res. Bull.*, vol. 14, pp. 493–498, 1979.

[58] T. Asano, A. Sakai, S. Ouchi, M. Sakaida, A. Miyazaki, and S. Hasegawa, "Solid Halide Electrolytes with High Lithium-Ion Conductivity for Application in 4 V Class Bulk-Type All-Solid-State Batteries," *Adv. Mater.*, vol. 30, no. 44, pp. 1–7, 2018.

[59] Y. Tomita, H. Matsushita, K. Kobayashi, Y. Maeda, and K. Yamada, "Substitution effect of ionic conductivity in lithium ion conductor, LI3INBR6 - xCLx," *Solid State Ionics*, vol. 179, no. 21–26, pp. 867–870, 2008.

[60] J. C. Bachman *et al.*, "Inorganic Solid-State Electrolytes for Lithium Batteries: Mechanisms and Properties Governing Ion Conduction," *Chem. Rev.*, vol. 116, no. 1, pp. 140–162, 2016.

[61] A. Manthiram, X. Yu, and S. Wang, "Lithium battery chemistries enabled by solid-state electrolytes," *Nat. Rev. Mater.*, vol. 2, no. 4, pp. 1–16, 2017.

[62] Y. Zhu, X. He, and Y. Mo, "Origin of Outstanding Stability in the Lithium Solid Electrolyte Materials: Insights from Thermodynamic Analyses Based on First-Principles Calculations," *ACS Appl. Mater. Interfaces*, vol. 7, no. 42, pp. 23685–23693, 2015.

[63] Y. Inaguma *et al.*, "High ionic conductivity in lithium lanthanum titanate," *Solid State Commun.*, vol. 86, no. 10, pp. 689–693, 1993.

[64] R. J. Chen, W. Liang, H. Q. Zhang, F. Wu, and L. Li, "Preparation and performance of novel LLTO thin film electrolytes for thin film lithium batteries," *Chinese Sci. Bull.*, vol. 57, no. 32, pp. 4199–4204, 2012.

[65] H. T. T. Le *et al.*, "Citrate gel synthesis of aluminum-doped lithium lanthanum titanate solid electrolyte for application in organic-type lithium-oxygen batteries," *J. Power Sources*, vol. 274,

pp. 1188–1199, 2015.

[66] H. Aono, E. Sugimoto, Y. Sadaoka, N. Imanaka, and G. Adachi, “Ionic Conductivity of the Lithium Titanium Phosphate (Li1+XMXTi2-X(PO4)3, M = Al, Sc, Y, and La) Systems,” *J. Electrochem. Soc.*, vol. 136, no. 2, pp. 590–591, 1989.

[67] Y. Yoon, J. Kim, C. Park, and D. Shin, “The relationship of structural and electrochemical properties of NASICON structure Li1.3Al0.3Ti1.7 (Po4)3 electrolytes by a sol-gel method,” *J. Ceram. Process. Res.*, vol. 14, no. 4, pp. 563–566, 2013.

[68] J. S. Thokchom and B. Kumar, “The effects of crystallization parameters on the ionic conductivity of a lithium aluminum germanium phosphate glass-ceramic,” *J. Power Sources*, vol. 195, no. 9, pp. 2870–2876, 2010.

[69] J. Awaka, N. Kijima, H. Hayakawa, and J. Akimoto, “Synthesis and structure analysis of tetragonal Li7La3Zr2O12 with the garnet-related type structure,” *J. Solid State Chem.*, vol. 182, no. 8, pp. 2046–2052, 2009.

[70] R. Murugan, V. Thangadurai, and W. Weppner, “Fast lithium ion conduction in garnet-type Li7La 3Zr2O12,” *Angew. Chemie - Int. Ed.*, vol. 46, no. 41, pp. 7778–7781, 2007.

[71] C. Bernuy-Lopez, W. Manalastas, J. M. Lopez Del Amo, A. Aguadero, F. Aguesse, and J. A. Kilner, “Atmosphere controlled processing of ga-substituted garnets for high li-ion conductivity ceramics,” *Chem. Mater.*, vol. 26, no. 12, pp. 3610–3617, 2014.

[72] Y. Deng *et al.*, “Structural and Mechanistic Insights into Fast Lithium-Ion Conduction in Li4SiO4-Li3PO4 Solid Electrolytes,” *J. Am. Chem. Soc.*, vol. 137, no. 28, pp. 9136–9145, 2015.

[73] P. G. Bruce and A. R. West, “Ionic Conductivity of LISICON Solid Solutions,” *Journal of Solid State Chemistry*, vol. 44. pp. 354–365, 1982.

[74] S. Taminato, T. Okumura, T. Takeuchi, and H. Kobayashi, “Fabrication and charge-discharge reaction of all solid-state lithium battery using Li4-2xGe1-xSxO4 electrolyte,” *Solid State Ionics*, vol. 326, no. June, pp. 52–57, 2018.

[75] M. A. K. L. Dissanayake, R. P. Gunawardane, A. R. West, G. K. R. Senadeera, P. W. S. K. Bandaranayake, and M. A. Careem, “Lithium ion conducting Li4-2xGe1-xSxO4 solid electrolytes,” *Solid State Ionics*, vol. 62, no. 3–4, pp. 217–223, 1993.

[76] X. Yu, “A Stable Thin-Film Lithium Electrolyte: Lithium Phosphorus Oxynitride,” *J. Electrochem. Soc.*, vol. 144, no. 2, p. 524, 1997.

[77] T. Fujibayashi, Y. Kubota, K. Iwabuchi, and N. Yoshii, “Highly conformal and high-ionic conductivity thin-film electrolyte for 3D-structured micro batteries: Characterization of LiPON film deposited by MOCVD method,” *AIP Adv.*, vol. 7, no. 8, 2017.

[78] S. Stramare, V. Thangadurai, and W. Weppner, “Lithium Lanthanum Titanates: A Review,” *Chem. Mater.*, vol. 15, no. 21, pp. 3974–3990, 2003.

[79] F. Aguesse *et al.*, “Microstructure and ionic conductivity of LLTO thin films: Influence of different substrates and excess lithium in the target,” *Solid State Ionics*, vol. 272, pp. 1–8, 2015.

[80] O. Bohnke, C. Bohnke, and J. L. J. Fourquet, “Mechanism of ionic conduction and electrochemical intercalation of lithium into the perovskite lanthanum lithium titanate,” *Solid State Ionics*, vol. 91, no. 1–2, pp. 21–31, 1996.

[81] J. B. Goodenough, H. Y. Hong, and J. A. Kafalas, “Fast Na+ - Ion Transport in Skeleton

Structures," *Mater. Res. Bull.*, vol. 11, no. 2, pp. 203–220, 1976.

[82] X. Xu, Z. Wen, X. Wu, X. Yang, and Z. Gu, "Lithium ion-conducting glass-ceramics of Li1.5Al 0.5Ge1.5(PO4)3-xLi2O (x=0.0-0.20) with good electrical and electrochemical properties," *J. Am. Ceram. Soc.*, vol. 90, no. 9, pp. 2802–2806, 2007.

[83] C. J. Leo, B. V. R. Chowdari, G. V. S. Rao, and J. L. Souquet, "Lithium conducting glass ceramic with Nasicon structure," *Mater. Res. Bull.*, vol. 37, no. 8, pp. 1419–1430, 2002.

[84] K. Hayamizu and S. Seki, "Long-range Li ion diffusion in NASICON-type Li1.5Al0.5Ge1.5(PO4)3 (LAGP) studied by 7Li pulsed-gradient spin-echo NMR," *Phys. Chem. Chem. Phys.*, vol. 19, no. 34, pp. 23483–23491, 2017.

[85] J. K. Feng, B. G. Yan, J. C. Liu, M. O. Lai, and L. Li, "All solid state lithium ion rechargeable batteries using NASICON structured electrolyte," *Mater. Technol.*, vol. 28, no. 5, pp. 276–279, 2013.

[86] H. Y. P. Hong, "Crystal structure and ionic conductivity of Li14Zn(GeO4)4 and other new Li+ superionic conductors," *Mater. Res. Bull.*, vol. 13, no. 2, pp. 117–124, 1978.

[87] J. Awaka, N. Kijima, H. Hayakawa, and J. Akimoto, "Synthesis and structure analysis of tetragonal Li7La3Zr2O12 with the garnet-related type structure," *J. Solid State Chem.*, vol. 182, no. 8, pp. 2046–2052, 2009.

[88] V. Thangadurai, S. Narayanan, and D. Pinzaru, "Garnet-type solid-state fast Li ion conductors for Li batteries: Critical review," *Chem. Soc. Rev.*, vol. 43, no. 13, pp. 4714–4727, 2014.

[89] C. Cao, Z.-B. Li, X.-L. Wang, X.-B. Zhao, and W.-Q. Han, "Recent Advances in Inorganic Solid Electrolytes for Lithium Batteries," *Front. Energy Res.*, vol. 2, no. June, pp. 1–10, 2014.

[90] Y. Li, J. T. Han, C. A. Wang, H. Xie, and J. B. Goodenough, "Optimizing Li^+ conductivity in a garnet framework," *J. Mater. Chem.*, vol. 22, no. 30, pp. 15357–15361, 2012.

[91] S. Sicolo and K. Albe, "First-principles calculations on structure and properties of amorphous Li5P4O8N3 (LiPON)," *J. Power Sources*, vol. 331, pp. 382–390, 2016.

[92] N. J. Dudney, "Solid-state thin-film rechargeable batteries," *Mater. Sci. Eng. B Solid-State Mater. Adv. Technol.*, vol. 116, no. 3 SPEC.ISS., pp. 245–249, 2005.

[93] H. Tak, T. Mun, C. Park, S. Wan, and H. Young, "Characteristics of lithium phosphorous oxynitride thin films deposited by metal-organic chemical vapor deposition technique," *J. Power Sources*, vol. 244, pp. 641–645, 2013.

[94] L. Le Van-jodin, F. Ducroquet, F. Sabary, and I. Chevalier, "Dielectric properties, conductivity and Li+ ion motion in LiPON thin films," *Solid State Ionics*, vol. 253, pp. 151–156, 2013.

[95] R. Koerver *et al.*, "Capacity Fade in Solid-State Batteries: Interphase Formation and Chemomechanical Processes in Nickel-Rich Layered Oxide Cathodes and Lithium Thiophosphate Solid Electrolytes," *Chem. Mater.*, vol. 29, no. 13, pp. 5574–5582, 2017.

[96] J. Zheng, P. Wang, H. Liu, and Y. Y. Hu, "Interface-Enabled Ion Conduction in Li 10 GeP 2 S 12 -Poly(ethylene Oxide) Hybrid Electrolytes," *ACS Appl. Energy Mater.*, vol. 2, no. 2, pp. 1452–1459, 2019.

[97] J. Lee, T. Howell, M. Rottmayer, J. Boeckl, and H. Huang, "Free-standing PEO/LiTFSI/LAGP composite electrolyte membranes for applications to flexible solid-state lithium-based batteries," *J. Electrochem. Soc.*, vol. 166, no. 2, pp. A416–A422, 2019.

[98] W. Wang, E. Yi, A. J. Fici, R. M. Laine, and J. Kieffer, “Lithium Ion Conducting Poly(ethylene oxide)-Based Solid Electrolytes Containing Active or Passive Ceramic Nanoparticles,” *J. Phys. Chem. C*, vol. 121, no. 5, pp. 2563–2573, 2017.

[99] J. Zheng and Y. Hu, “New Insights into the Compositional Dependence of Li-Ion Transport in Polymer − Ceramic Composite Electrolytes,” *ACS Appl. Mater. Interfaces*, vol. 10, pp. 4113–4120, 2018.

[100] W. Liu *et al.*, “Enhancing ionic conductivity in composite polymer electrolytes with well-aligned ceramic nanowires,” *Nat. Energy*, vol. 2, no. 5, pp. 1–7, 2017.

[101] J. Bae, Y. Li, F. Zhao, X. Zhou, Y. Ding, and G. Yu, “Designing 3D nanostructured garnet frameworks for enhancing ionic conductivity and flexibility in composite polymer electrolytes for lithium batteries,” *Energy Storage Mater.*, vol. 15, no. March, pp. 46–52, 2018.

[102] D. Golodnitsky, G. Ardel, and E. Peled, “Ion-transport phenomena in concentrated PEO-based composite polymer electrolytes,” *Solid State Ionics*, vol. 147, no. 1–2, pp. 141–155, 2002.

[103] S. Menkin *et al.*, “Evaluation of ion-transport in composite polymer-in-ceramic electrolytes. Case study of active and inert ceramics,” *Electrochim. Acta*, vol. 304, pp. 447–455, 2019.

[104] J. Zheng, H. Dang, X. Feng, P.-H. Chien, and Y.-Y. Hu, “Li-ion transport in a representative ceramic–polymer–plasticizer composite electrolyte: $Li_7La_3Zr_2O_{12}$ –polyethylene oxide–tetraethylene glycol dimethyl ether,” *J. Mater. Chem. A*, vol. 5, no. 35, pp. 18457–18463, 2017.

[105] K. M. Diederichsen, H. G. Buss, and B. D. McCloskey, “The Compensation Effect in the Vogel-Tammann-Fulcher (VTF) Equation for Polymer-Based Electrolytes,” *Macromolecules*, vol. 50, no. 10, pp. 3831–3840, 2017.

[106] Y.-J. Wang, Y. Pan, and D. Kim, “Conductivity studies on ceramic Li1.3Al0.3Ti1.7(PO4)3-filled PEO-based solid composite polymer electrolytes,” *J. Power Sources*, vol. 159, no. 1, pp. 690–701, Sep. 2006.

[107] M. Cordill, A. Llordes, J. M. Lopez del Amo, L. Buannic, F. Aguesse, and J. Zagórski, “Garnet-polymer composite electrolytes: new insights on local Li-ion dynamics and electrodeposition stability with Li metal anodes,” *ACS Appl. Energy Mater.*, 2019.

[108] Z. Zhang *et al.*, “An advanced construction strategy of all-solid-state lithium batteries with excellent interfacial compatibility and ultralong cycle life,” *J. Mater. Chem. A*, vol. 5, no. 32, pp. 16984–16993, 2017.

[109] J. Yang *et al.*, “High-performance solid composite polymer electrolyte for all solid-state lithium battery through facile microstructure regulation,” *Front. Chem.*, vol. 7, no. MAY, pp. 1–11, 2019.

[110] J. Ou, G. Li, and Z. Chen, “Improved composite solid electrolyte through ionic liquid-assisted polymer phase for solid-state lithium ion batteries,” *J. Electrochem. Soc.*, vol. 166, no. 10, pp. A1785–A1792, 2019.

[111] H. Hu, W. Yuan, L. Lu, H. Zhao, Z. Jia, and G. L. Baker, “Low glass transition temperature polymer electrolyte prepared from ionic liquid grafted polyethylene oxide,” *J. Polym. Sci. Part A Polym. Chem.*, vol. 52, no. 15, pp. 2104–2110, 2014.

[112] N. A. Stolwijk, C. Heddier, M. Reschke, M. Wiencierz, J. Bokeloh, and G. Wilde, “Salt-concentration dependence of the glass transition temperature in PEO-NaI and PEO-LiTFSI polymer electrolytes,” *Macromolecules*, vol. 46, no. 21, pp. 8580–8588, 2013.

[113] D. Golodnitsky, E. Strauss, E. Peled, and S. Greenbaum, “Review—On Order and Disorder in Polymer Electrolytes,” *J. Electrochem. Soc.*, vol. 162, no. 14, pp. A2551–A2566, 2015.

[114] A. R. Polu and H. Rhee, “Ionic liquid doped PEO-based solid polymer electrolytes for lithium-ion polymer batteries,” *Int. J. Hydrogen Energy*, vol. 42, no. 10, pp. 7212–7219, 2016.

[115] F. González, V. Gregorio, A. Rubio, L. Garrido, N. García, and P. Tiemblo, “Ionic liquid-based thermoplastic solid electrolytes processed by solvent-free procedures,” *Polymers (Basel).*, vol. 10, no. 2, 2018.